Master Thesis
TVVR 20/5019

Evaluation of Local Scour along Rönne Å at Ängelholm

Analysis of detailed bathymetric data in combination with HEC RAS modeling

Fainaz Inamdeen

Division of Water Resources Engineering
Department of Building and Environmental Technology
Lund University

Evaluation of Local Scour along Rönne Å at Ängelholm

Analysis of detailed bathymetric data in combination with HEC RAS modeling

By:
Fainaz Inamdeen

Master Thesis

Division of Water Resources Engineering
Department of Building & Environmental Technology
Lund University
Box 118
221 00 Lund, Sweden

Water Resources Engineering
TVVR-20/5019
ISSN 1101-9824

Lund 2020
www.tvrl.lth.se

Master Thesis
Division of Water Resources Engineering
Department of Building & Environmental Technology
Lund University

English title:	Evaluation of Local Scour along Rönne Å at Ängelholm. Analysis of detailed bathymetric data in combination with HEC RAS modeling.
Author:	Fainaz Inamdeen
Supervisors:	Prof. Magnus Larson Dr. Geraldine Thiere
Examiner:	Dr. Rolf Larsson
Language	English
Year:	2020
Keywords:	HEC RAS, Rönne å, Bend scour, Contraction scour, Abutment scour, HEC 18

ACKNOWLEDGEMENTS

I would like to take this opportunity to express my sincere gratitude to my supervisor Professor Magnus Larson at the Department of Water Resources Engineering, Lund University, for his valuable supervision, patience, guidance, and encouragement throughout this study.

Special gratitude to my co-supervisor Geraldine from Ängelholm municipality for her valuable assistance through providing and helping to acquire valuable data and suggestions.

I am very grateful to the Swedish Institute (SI) for the scholarship, giving me a great opportunity to study at LTH, Lund University by offering wonderful support. Additionally, I extend my warm gratitude to Sebastian Ståhl from Lunds Fontänhus for different support in Sweden.

Lastly, I'm profoundly grateful to my parents, family and friends for their moral support and encouragement throughout the time of my study in Sweden; without them, I would not have achieved this important milestone in my life.

A part of the present study was supported by the Swedish Transport Administration under contract TRV 2019/108845.

ABSTRACT

Riverbed scouring is an emerging problem aligned with higher frequent river discharges, experienced in a short period of time with shifting climate conditions. This problem brings a significant challenge to relevant authorities to safeguard river stability and hydraulic structures. This master thesis study is a preliminary investigation of the local scour problem along the Rönne å river stretch that falls in Ängelholm municipality, Skåne. The main objectives included a mapping of existing scour holes along the river reach with an evaluation of possible causes, building a hydraulic model for the river stretch, and estimating the potential scour risk of some existing bridges. HEC RAS one-dimensional model was selected to establish a hydrodynamic model for the downstream reach of about 12 km of the Rönne å. Bathymetry and geometry analyses revealed that the existing deep scour holes may have developed mainly by general scour mechanisms, such as bend scour and presence of hard non-erodible river bottom. The HEC RAS bridge scour analyses for six bridges disclosed that the bridges are more threatened by abutment scour than contraction or pier scour. The bridge Tegelbruksbron has the highest risk for abutment scour and Kristian II Bridge experiences the highest threat from contraction scour among the bridges investigated. The results are satisfactory for the initial assessment stage in bridge scour evaluation and useful for future investigations. The study further suggested for Ängelholm municipality to conduct a comprehensive sediment analysis along the riverbed to allow for more reliable interpretations and potential evaluation.

Keywords:
HEC RAS, Rönne å, Bend scour, Contraction scour, Abutment scour, River flow, HEC 18

TABLE OF CONTENTS

TABLE OF FIGURES

.

CHAPTER 1- INTRODUCTION

Bridges are identified as important components in road network adding many values to society. Most of the bridges are built across rivers and other water bodies. In the US alone, approximately 500 000 bridges of National Bridge Inventory (NIB) were constructed by crossing waterways (Arneson et al., 2012). Thus, river floods have a significant impact on bridge failures. Collapse of bridges causes significant direct and indirect economic losses to society in the form of reconstruction; interruptions to the transport of various essential goods and services for daily life. In some cases, the failure can lead to traditional heritage losses by damaging the ancient hydraulic structures. The riverbed erosion at bridge foundation (bridge scour) is a most influential way of bridge failure (Pizarro, Manfreda and Tubaldi, 2020). This complex threat to the bridge safety has initiated many research studies on bridge scour issues in the last couple of decades.

According to United States Federal Highway Administration (FHWA), the flood event in the upper Mississippi basin triggered 23 bridge failures in 1993 with an estimated loss of 15 million US dollars, and out of those, 19 failures were created by exceeding bridge scour. In New Zealand, the annual bridge scour damage costs were estimated to be around 36 million NZ dollars (Macky, 1990). It is predicted that 20% of bridges across Europe have the risk of failure due to potential bridge scour during the period 2040-2070 and estimated annual cost to mitigate bridge scour risk is approximately 541 million euros for the same period of 2040-2070 (Nemry and Demirel, 2012).

The geotechnical factors of the bed material, bridge geometry and hydraulic characteristics are key considerations on bridge scour developments. The evaluation of scour for existing bridges are always complicated and limited to a certain level due to lack of reliable data. However, FHWA urges to assess every single bridge over waterways to check its vulnerability to flood events for develop prudent measures when needed. In addition to bridge scouring, rivers may suffer from bend erosions and abrupt changes in river bottom conditions, which can exert influences on river stability. The hydraulic behavior of the river heavily influences the overall erosion problems and they are characterized through geology, geomorphological conditions and river flow conditions (Arneson et al., 2012). The dynamic and complex nature of riverbed scouring bring a huge challenge to authorities and decision makers.

1.1 BACKGROUND

The Rönne å (river) is the second largest river in the Skåne, flowing through Ängelholm municipality before meeting the sea at Skälderviken bay. It brings many benefits to the villages in the catchment such as to facilitate boat traffic routes, tourist attractions, salmon fishing, and farming, as well as providing many aesthetic values. This study was conducted in a Rönne å stretch belonging to the Ängelholm municipality. The Ängelholm city has a rich history of settlements along Rönne å since the 16th century, when the city was founded. Approximately sixteen bridges cross the river within the Ängelholm municipality boundaries, thus providing a smooth road network to conduct daily services through sustainable traffic management (Ängelholm municipality, 2020).

Ängelholm municipality has carried out many comprehensive studies on Rönne å during the period 2009-2020 to investigate various impacts and upcoming challenges, such as flooding and erosion. Several studies discovered that erosion of banks and river bottom is one of the key concerns to consider now and for the future.

In 2010, SWECO conducted a pilot study that discussed bank erosion in Rönne å, followed by several extended and more detailed studies on the river, listed below. Several of these studies focused on the erosion along Rönne å within the boundaries of Ängelholm municipality.

- 2010 - ”Översvämningar i Ängelholms kommun, En övergripande analys av möjliga hot längs Rönne å och kusten”, utförd av Ängelholms kommun
- 2010 -”Stranderosion i Ängelholms kommun, Inventering av nuvarande förhållande och rekommendationer för framtiden”, utförd av SWECO Environment AB
- 2010- ”Översiktlig analys av översvämningsrisk och erosion längs Rönne å i Ängelholms kommun”, utförd av SWECO Environment AB
- 2012- ”Bedömt framtida underhållsbehov för Ängelholms brobestånd med avseende på en 10-årsperiod”, utförd av Ramböll Sverige AB
- 2013- “Ängelholms kommun Erosionsutredning av Rönne å” , utförd av Norconsult AB

- 2020- “Bedömning av framtida utveckling av hålen i Rönne å vid sjukhusområdet i Ängelholm ur ett hydrodynamiskt perspektiv”, utförd av SWECO Environment AB
- 2020- “Djuphålor och observationer i batymetrin, Rapport, Rönne å” , utförd av MarCon Teknik AB

In 2019, Ängelholm municipality discovered that several large holes had developed in the river bottom close to the coastal outlet. In 2020, MarCon Teknik AB performed a thorough bathymetric survey by using multi-beam echo sounding technology, and identified that there similar uneven bottom holes exist along the river at a number of locations of different magnitudes. Also, it was observed that many holes had developed near bridge structures and river bends. These anomalies of the river bottom at bridges prompted Ängelholm municipality to conduct investigations on riverbed scouring to safeguard the bridges and surrounding areas in the river basin from possible damage.

This study is structured based on the hypothesis that development of the holes at bridge structures is due to bridge scouring, aiming at evaluating the scour characteristics by analyzing the geometric features. Furthermore, the study provides the incentive to investigate the potential bridge scour threat for future high flow scenarios in Rönne å.

1.2 OBJECTIVES

The purpose of the study is to determine the significance of local scour in the 12 km stretch of Rönne å at Ängelholm municipality, and to establish the mechanisms behind the scour development. The possible effects of the local scour on the bridges in Rönne å and on surrounding areas will also be analyzed together with an estimation of the scour potential using the HEC RAS hydraulic model.

The detailed objectives of the study are as follows:

1. Mapping existing scour holes along Rönne river reach with geometry analysis
2. Identifying possible causes for the scour hole development in the river
3. Building a hydraulic model for the river using HEC RAS

4. Estimating potential scour risk of some existing bridges using HEC RAS bridge scour analysis routine

1.3 PROCEDURE

The thesis was structured based on a comprehensive literature review, data collection, and a hydraulic modelling with flow simulations. Before addressing the objectives, the literature study was carried out on riverbed scour principles and analysis methods, including river hydraulics. Concurrently, existing studies regarding Rönne å at Ängelholm were reviewed to get more insight on the erosion problems. Furthermore, information about hydrological, geological and geomorphological features of the river, as well as bridge geometry, were gathered and analyzed to gain an understanding of the current scour issues.

The relevant flow data for the detailed study were obtained through SMHI's vattenweb.se. The riverbed characteristics and bridge geometry information were obtained through past reports that were performed at Rönne å by different consultancy firms in previous years. The river bathymetry data for the study reach was obtained with the help of the SCALGO Live GIS tool, the data was produced through a bathymetric survey, which was used to support hydraulic modelling and visual representation of existing scour hole development. Then, a scour hole mapping was done by identifying existing scour holes with relevant geometry analysis.

HEC RAS software was used to perform the numerical modelling for bridge scour analysis. In HEC RAS, the bridge scour analysis was performed by combining a one-dimensional steady flow hydraulic model and a bridge scour calculation option. The RAS Mapper (a function in HEC RAS) was used to construct relevant river geometry for steady flow analysis using the river bathymetric data obtained from SCALGO Live. The river flows for several return years were estimated by a flood frequency analysis using modelled daily flow data, obtained through SMHI's S-Hype model. Before bridge scour analysis the hydraulic model was tested and calibrated to obtain reliable hydraulic characteristics for the bridge scour model. Finally, the bridge scour simulations were performed for certain bridges in Ängelholm by HEC RAS to predict expected scour development for predicted river flows. Finally, the

results were compared and interpreted with river survey data to draw conclusions about the scour development.

1.4 REPORT CONTENT

The main content of the report starts from Chapter 2, explaining the basic mechanisms and theory of bridge scour including main components such as contraction scour, pier scour, and abutment scour. Furthermore, it includes factors that can affect the scour development and available methods to estimate scour depth. Chapter 3 summarizes scouring at river bends and downstream hard bottom in a river during higher flow periods. Chapter 4 gives an overview of the studied river reach of Rönne å, including information about geography, geology and geomorphology, climate, and flow characteristics in the study area. Chapter 5 gives an overview of the bridge scour model used by HEC-RAS by explaining basic functions and equations used for model development. Chapter 6 summarizes the data used in this study that combine river flow, river bathymetry, bridge geometry, and geotechnical characteristics of the bed material. Chapter 7 includes the identification of potential scour holes through geometric analysis. Chapter 8 provides output details of bridge scour obtained from the HEC RAS simulations, and Chapter 9 provides interpretations and evaluations of local scour analysis based on the output from the HEC RAS modelling and visual bathymetry interpretation. Finally, Chapter 10 finishes the study with some conclusions.

CHAPTER 2- BRIDGE SCOUR

2.1 GENERAL

Water flow over a sediment bed often initiates sediment motion in river bed through a complex interactive process between the flow and the sediment. Gradients in the sediment transport cause local erosion, typically termed scour. The scour can occur in general along the river bed or around man-made hydraulic structures (Arneson et al., 2012). The erosion occurs due to more sediment being transported downstream compared to what is supplied from upstream to the eroding location. The scour development in the river bed can occur because of natural mechanisms, such as meandering, bending, river confluences, and tidal inlet flows; such scour is typically denoted "general scour". In comparison, "local scour" refers to scour development around structures due to water flow obstructions (Namaee and Sui, 2019). Both the local scour and the general scour are directly dependent upon the properties of the water flow and the shear stresses exerted on the river bed. In addition, for the local scour, the interaction between the flow and the structure becomes significant and complex vortex systems develop that can locally enhance the sediment transport (Pizarro, Manfreda, and Tubaldi, 2020). This chapter summarizes the fundamentals of bridge scour and discusses the important components affecting the scour.

Bridge scour refers to the lowering of the river bed elevation at a bridge foundation due to river flows through the bridge opening with sufficient velocity. It consists of both general and local scour. Overall, the change in the river bed elevation is more significant adjacent to the abutments and piers (FDOT Manual, 2015). There are many geotechnical, hydrologic, and hydrodynamic factors that affect bridge scour rates. Increasing bridge scour can severely affect bridge stability and lead to bridge failures. The bridge scour is a significant threat to bridge safety and a large cause for bridge failures around the world. Many countries regard bridge scour as a serious issue, because the risk of loss is huge to society in many aspects (Pizarro, Manfreda, and Tubaldi, 2020). Scour evaluation is a dominant feature in the design of new bridges as well as in the evaluation of safety concerning existing bridges. Many countries (e.g., America, Australia, and the UK) follow their own bridge scour manuals, which include common basic scour concepts. The *"Evaluating Scour at Bridges –HEC 18"* of U.S. Federal Highway Administration

(FHWA) is a good example for the code of practice in bridge scour analysis. According to HEC 18, the total bridge scour is estimated considering long-term aggradation and degradation of the river bed, contraction scour at the bridge, and local scour at the piers and/or abutments.

Aggradation and degradation refer to changes in the river bed elevation over the long term, due to natural or man-induced causes that may impact the river where the bridge is located. Aggradation involves deposition of sediments at the river bed around the bridge, where the material is eroded and transported from the river upstream of the bridge. Degradation refers to an eroding river bed over the long term influenced by the limited supply of sediments from areas upstream of the bridge. In the assessment when a river is aggraded, the aggradation is not be considered in the total scour evaluation, and local scour and contraction scour need to be calculated using the existing bed elevation as base elevation. However, if a river is degraded the long-term degradation needs to be considered in the total scour, in addition to contraction and local scour at the bridge (Arneson et al., 2012).

There are several factors and situations that affect long-term bed elevation changes; for example, changes in land use in the river basin due to urbanization and deforestation, dam and reservoir construction that obstruct river flows, sand mining in the upstream river bed, diversion channels into and out from the main river, natural lowering of the river fluvial system, tidal currents and floods in coastal streams, and sediment control structures (Arneson et al., 2012). The above changes generally work at a slow rate to achieve a new long-term equilibrium striving towards vertical stability of the river bed.

2.2 CONTRACTION SCOUR

Contraction scour refers to erosion of material from the bed and the river banks associated with a velocity increase due to a decrease in flow cross-sectional area. In general, it could occur across all or most of the channel width resulting from the reduction in flow cross section by a natural constriction of the river or man-made structures such as bridges and embankments (See Figure 2.2.). Furthermore, in some cases the embankments and abutments can force overbank flows through bridge openings, enhancing the contraction scour. Other influences such as ice formation in the river, natural berms along the banks due to sediment deposits, debris blockages at bridge openings,

vegetative cover in the channel or floodplain, and pressure flows can also increase the contraction scour (Zhang et al., 2013).

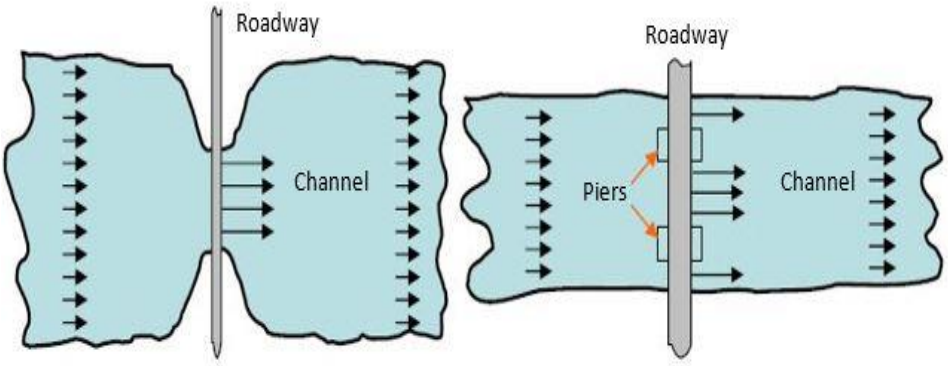

Figure 2.1.: The two contracted cross-sections by man-made structures (FDOT Manual, 2015).

It should be understood that contraction scour differs from long-term degradation and local scour. The reduction of the flow cross-sectional area leads to increase in flow velocity and bed shear stress following the continuity equation. This increase in velocity enhance the erosive forces of the flow under bridge openings and promotes the removal of more bed material than the sediment transport upstream of the constriction. In the river streams, the contraction scour lowers the bed elevation until the flow area increases, implying a decrease in velocity and shear stress, until equilibrium is reached when the rate of contraction scour for a particular situation approaches zero. In coastal rivers with tides, the cross-sectional area growth can increase the discharge, and in tidal inlets, the contraction scour may increase without meeting equilibrium conditions.

The contraction scour is generally classified as live-bed or clear-water scour (Arneson et al., 2012; this terminology is also applicable to other types of scour). Live-bed contraction scour occurs when the bed material is being transported to the bridge contraction from the upstream reach. The scour increases until the amount of bed material transported into the contraction is equal or greater than an amount of bed material transported from the contraction; then, equilibrium condition has developed. As scour develops, the shear stress and velocity of the flow in the constriction decrease, while the flow

area increases. It can be expected that maximum live-bed scour occurs when the shear stress falls to the point where bed material transported into contraction equals to the bed material transported from the contraction (Arneson et al., 2012).

Clear-water scour occurs when no bed material is being transported to bridge contraction from the upstream reach. The presence of the contraction initiates sediment transport, inducing the local scour. The clear-water scour increases until the flow velocity or the bed shear stress in the contraction equal to the critical velocity or the critical shear stress of mean particle size of the bed material, and an equilibrium condition develops. It can be expected that maximum live-bed scour depth occur when the shear stress at the bed drops to the critical shear stress of the bed material (Arneson et al., 2012).

HEC-18 circular suggests that typical clear-water scour occurs at coarse-bed material streams, low gradient streams during low flows, armored riverbeds where the only locations that stream forces are possible to penetrate the armor layers are at bridge piers and/or abutments, and vegetated river overbank areas.

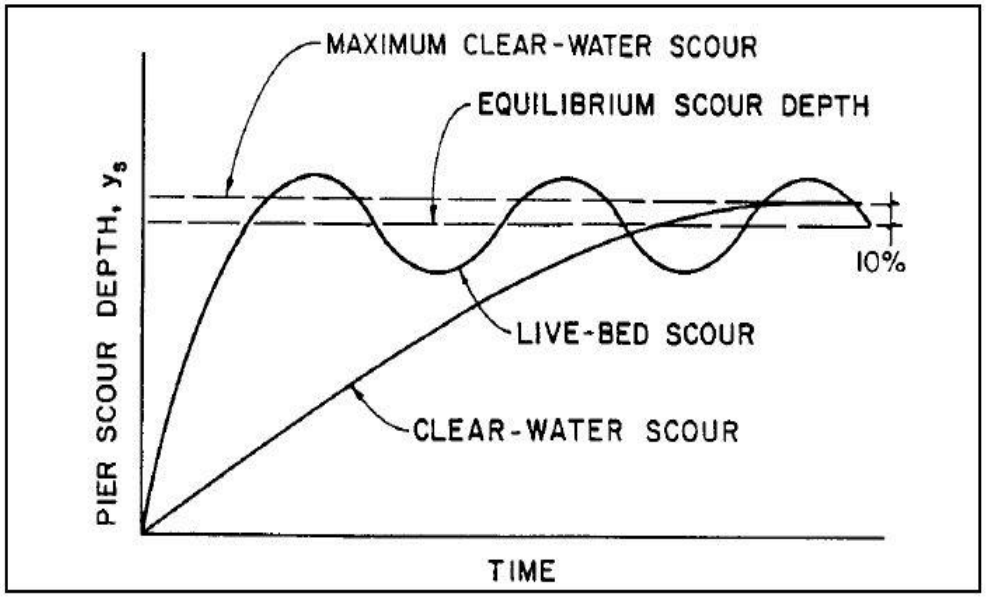

Figure 2.2.: Scour depth growing with time at a sand bed (HEC-18, FHWA).

During some parts of flood events, the bed material may be subjected to live-bed scour at higher discharges and then clear-water scour for lower discharges. Generally, clear-water scour takes more time to reach the maximum scour than live-bed scour, because of clear-water scour is most probably related to coarser river bed material. Thus, it may require several flood events to reach the maximum limit in clear-water scour. Because of the cyclic nature due to cuts at higher flows and fillings at lower flows by upstream transport, the live-bed scour typically oscillates up and down around its equilibrium limit (Arneson et al., 2012). The above figure 2.2 describes the clear-water and live-bed scour growth in a sand bed with time.

There are various methods available to predict contraction scour such as hydraulic geometry equations to understand changes in river geometry, numerical sediment transport models couple with various sediment transport equations, and contraction scour equations (Zhang et al., 2013). The Laursen contraction scour equations are the most widely used equations and often the basis for contraction scour estimations. According to Laursen (1960), the flow velocity is compared with the critical velocity of the bed material to decide whether contraction scour is live-bed or clear-water scour. The Laursen equations are used in the HEC-18 manual and the HEC RAS bridge scour models, including many assumptions and limitations, which are further discussed under Chapter 5.

2.3 PIER SCOUR

Pier scour refers to the erosion of material from the river bed around the bridge piers due to the acceleration of flow and formation of three-dimensional complex vortex flows (secondary flows). Figure 2.3 shows an example of pier scour formation. According to Melville (1975), the flow generates a complex system around the piers that consists of down-flow and surface roller at the upstream pier nose. Moreover, it develops horseshoe vortices at the upstream side of the pier near the bed and wake vortices at the downstream wake region of the pier, see figure 2.4.

The basic mechanism of a pier scour can be explained by considering the secondary flows mentioned in figure 2.4. When the flow approaches the upstream end of the piers, the flow velocity goes to zero due to stagnation. So according to Bernoulli's concept, the flow velocity reduction increases the water surface level and forms surface rollers, and while a part of the stagnation

flow induces a down-flow. Because the flow velocity in the stagnation points decreases from the surface to the bed, the dynamic pressure also decreases towards the bed, creating a gradient that generates the down-flow.

Figure 2.3.: Local scour formation at a pier (Zhang et al., 2013).

When the down-flow approaches the sediment bed, another stagnation point forms at the bed. The stagnation pressure gradient initiates complex horseshoe vortex systems on the leading edge of the structure. When down-flow hits the bottom, it loosens the bed material and the horseshoe vortex transports the loosened bed material away from the piers (Melville, 1975).

In addition, Melville (1975) found that after scouring is initiated, more down-flow occurs, increasing the size and strength of the horseshoe vortex. With the growth of the vortex, the hole enlarges and vortex moves further down into the hole. Furthermore, he found that when an increase in the cross-sectional area of the scour hole reduces the strength of the horseshoe vortex, the material transport rate is weakened and equilibrium is approached. The hole development is almost vertical with very sharp slopes at the initial stage. When it approaches equilibrium, it develops laterally and maintains a slope angle corresponding to the shape of an inverted cone in the bed.

Wake vortices are created due to flow separation downstream the pier. The wake vortices also remove material from the river bed and possibly develop large holes at downstream end of the pier; furthermore, the wake vortices cause the bed material to remain in suspension that was carried from upstream into the wake region.

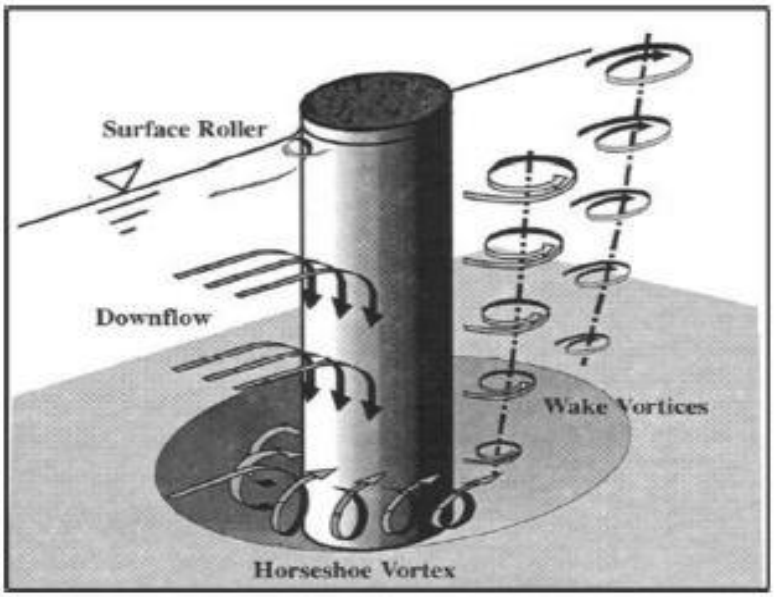

Figure 2.4.: Formation of vortex flows around a cylindrical pier (after Melville and Coleman, 2000)

According to Rambabu et al. (2003), in non-cohesive soils, the gravity forces and submerged density of the bed material are the main resistance forces against scouring. In contrast, in cohesive soils, the net attractive surface force of bonding particles primarily controls the resistance to scouring. More geotechnical considerations on the scour process are discussed in section 2.5. Eventually, pier scour also can be classified as live-bed scour and clear-water scour as discussed in section 2.2.1. For live bed scour, the scour reaches an equilibrium when the amount of outflow bed material from pier base region equals the amount of inflow bed material to the region. For clear-water scour the scour reaches an equilibrium when the horseshoe vortex, together with the other vortex systems, decreases and the flow initiates shear stresses equal to the critical shear stress of the bed material at the bottom of the scour hole.

There are many empirical and semi-empirical equations available to estimate pier scour. The semi-empirical equations were developed from extensive laboratory studies together with basic sediment transport concepts. The most common equations were developed by Melville and Sutherland, Laursen, Colorado State University (CSU), Jain and Fischer, Neill, Ahmad, Molinas and Hosny, and Briaud et al. The FHWA developed the HEC-18 equation based on CSU, with the addition of coefficients for the effect of bed forms, size of the bed material, and wide piers, to estimate scour depth in alluvial sand-bed channels. Also, it was recommended to use it with a clay reduction factor to estimate scour depth in cohesive soil. In general, HEC-18 equation overestimates the scour depth in cohesive sediments (Arneson et al., 2012).

There are several factors that can affect the pier scour condition including:

- Flow velocity

  The scour depth increases when the flow velocity increases. It can affect both supercritical (Fr > 1) and subcritical (Fr < 1) flows (Arneson et al., 2012).

- Flow depth

  The scour depth increases when the depth of the flow increases. The magnitude of the increase can be higher than 2 times or more for the piers (Arneson et al. 2012). However, Briaud et al. (2011) stated that for shallow depth conditions, the rate of scouring is faster than in deep water and the time it takes to reach the equilibrium limit is lower than for deep water condition.

- Pier width

  Generally, the scour depth increases when pier width increases but there is a certain limit for this increase. There is a strong correlation between pier width and flow depth with regard to pier scour morphology (Melville and Coleman, 2000).

- Pier length

  Generally, the scour depth is not heavily influenced by pier length when the flow is perpendicular to the pier width. In case the pier is skewed to the flow, the pier length also have an impact through the

effective pier width and significantly influences the scour depth. (Arneson et al., 2012).

- Bed material characteristics

  The size, gradation, and cohesion of the bed material can affect scour depth significantly. The resistance force against erosion depends on the soil characteristics. The size of the bed material defines whether the scour is clear-water or live-bed scour. Furthermore, cohesive forces heavily influence the time it takes to reach maximum scour for a certain flood events (Arneson et al., 2012). Ansari et al. (2002) found that antecedent moisture content of the soil can affect the behavior of the scouring. More information is discussed in section 2.5.

- Angle of attack

  The angle of attack of the flow to the pier has a significant effect on the scour depth. As pointed out under pier length, a skewed angle makes significant impact on the effective pier width (Arneson et al., 2012).

- Shape of the pier

  The shape of the nose of a pier can markedly influence the scour depth. This is because the strength of the vortex system is influenced by pier nose shape (Melville, 1997). Shen et al. (1969) concluded that blunt-nosed piers have higher strength horseshoe vortices and maximum scour occurs at pier noses. In contrast, the sharp-nosed piers have higher strength of wake vortices and the maximum scour occurs downstream of the piers. According to HEC-18, the shape effect is much lower when the angle of attack of the flow exceeds five degrees.

- Bed configuration

  The bed configuration can have an effect on flow velocity and sediment transport thus affecting the scour behavior. The bed configuration is characterized by plane beds to antidunes, and the particular configuration depends on the characteristics of the bed material and hydraulic properties of the flow (Arneson et al., 2012).

- Ice and debris flows

Flow blockages due to ice and debris can increase the effective width of the piers and change the effective shape of piers. In addition, they can change flow depths. HEC-18 includes equations for an estimate of the pier scour when debris effects are present.

2.4 ABUTMENT SCOUR

Abutment scour refers to erosion of bed material from the main-channel bed and floodplains around the bridge abutment due to conveyance of the approach flow by the formation of three-dimensional complex vortex flows (secondary flows). Figure 2.5 shows an example of an abutment scour incident on a major highway in the U.S.

Figure 2.5.: Local scour formation at bed around an abutment of a waterway bridge (Ettema et al., 2004)

The basic mechanism of abutment scour can be explained by studying the flow field formation as illustrated in figure 2.6. The waterway crossing conditions at bridges lead to very complex flow phenomena due to the flow-boundary interactions (Ettema et al., 2004). The waterway crossings involve the main channel, floodplains, and embankments. Further, the sloping flood plains assist in the conveyance of larger flows through a bridge to enhance the sediment removal.

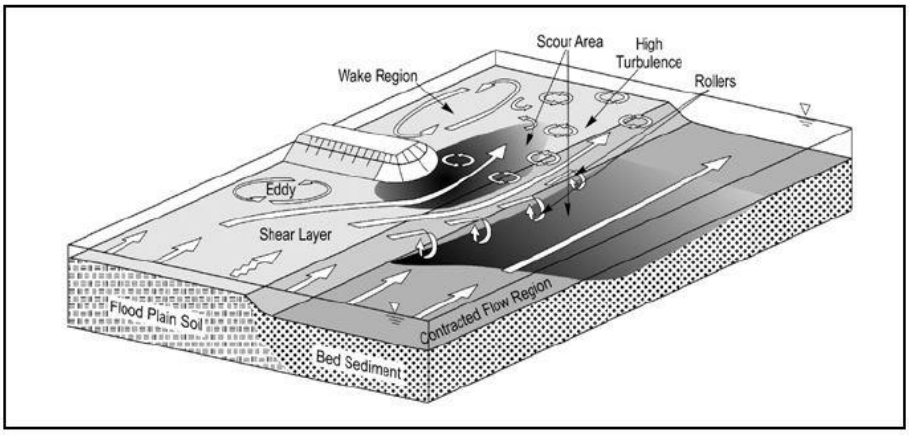

Figure 2.6.: The near-field flow with complex vortices at a bridge abutment (Arneson et al., 2012).

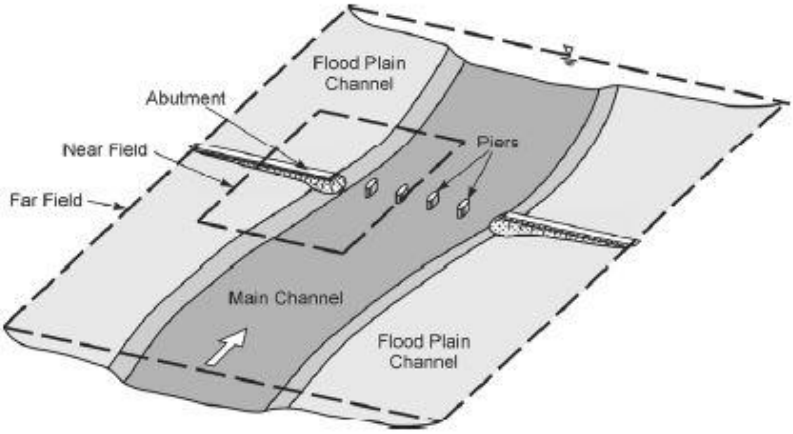

Figure 2.7.: Illustration of far-field and near-field flow zones (Ettema, Yoon, Nakato and Muste, 2004)

The near-field flow is formed at the floodplains and the main channel around abutments, and causes more influences on the scouring behavior than the far field. However, the far-field flow can make a significant impact on the near-field flow. An overview of a near-field and a far-field flow is presented in figure 2.7. In the near-field flow, the waterway is narrowing due to the bridge abutment and its embankment. Because the flow width contracts, the flow velocity accelerates through the contraction and generates macro-turbulence

eddies and a three-dimensional vortex flow system by flow separation at the base of the abutment (Ettema et al., 2004). The flow contraction and turbulence formation are complicated by the varying shape of the channel. Furthermore, the two flow features are difficult to separate and its dominancy depends on the extent of flow contraction and the characteristics of the abutment (Arneson et al., 2012). The basic mechanism of the vortex system is quite similar to the pier scour condition as explained in section 2.3.

As shown in figure 2.6, a flow-separation region forms immediately downstream of the abutment where wake vortices appear. Just upstream of the abutment or flow-separation point, small eddies may develop. The size and strength of the upstream eddies depend on the stagnation length and alignment of the abutment. The downfall vortices and wake vortices influence the abutment scouring similarly to pier scouring (Ettema et al., 2004).

As for the pier scour equations, there are many equations available to predict abutment scour. Liu et al., Laursen, Froehlich, and Melville developed equations based purely on laboratory studies. In HEC 18 circular, FHWA recommended the Froehlich equation and the HIRE equation developed by Richardson, Simons, and Julien in 1990. The Froehlich equation was developed using dimensional analysis together with regression analysis based on laboratory data. It is more recommended for live-bed scour situations and when projected abutment length to the flow depth is less than or equals 25. The HIRE equation was developed based on field data from the U.S. Army Corps of Engineers and is recommended to be used when projected abutment length to the flow depth is greater than 25.

There are several factors can affect the abutment scour condition including:

- Bed material characteristics

  The bed materials of the main channel, floodplain, and embankment often have different characteristics due to their formation from different alluvial sediments, and hence the erosion behavior is not similar for these areas. In general, the main channel bed is formed by more non-cohesive sediments like sands and gravel. The floodplain is formed by more cohesive sediments like silt and clay. The earth-fill embankments are formed by compacted soils from the floodplain or elsewhere and its compactness gives specific shear strength to withstand erosion (Arneson et al., 2012). The main channel bed is more erosion-prone than floodplains, which

generally contain more cohesive soils and vegetation cover. Furthermore, the geotechnical complexity gives limitations and restrictions to estimate abutment scouring from site to site (Ettema et al., 2004).

- Abutment Length

The effect of abutment length on bridge scour is varying depending on the specific reference. According to HEC-18, laboratory studies showed that the scour depth increases for an increase in the projected length of an abutment or embankment into the flow, because of the flow interception directly related to abutment length. However, Arneson et al. (2012) stated, based on field cases, due to ineffective flow occurrences, the length of active flow (live flow) obstructed by the abutment is a more important influence parameter in bridge estimation and in many abutment scour equations. Figure 2.8 shows the live flow zones compared to whole abutment length.

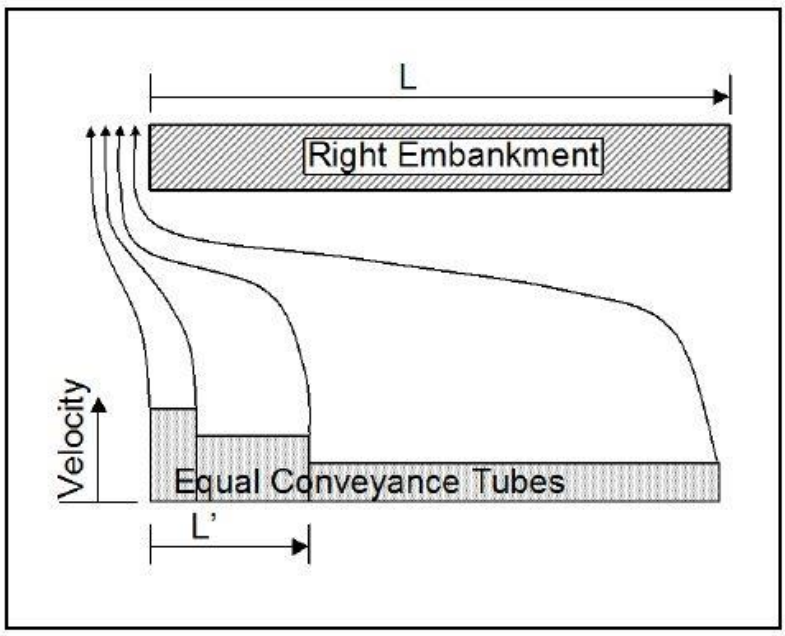

Figure 2.8.: Length of active or live flow for abutment scour estimation (Arneson et al, 2012)

➢ Abutment Location

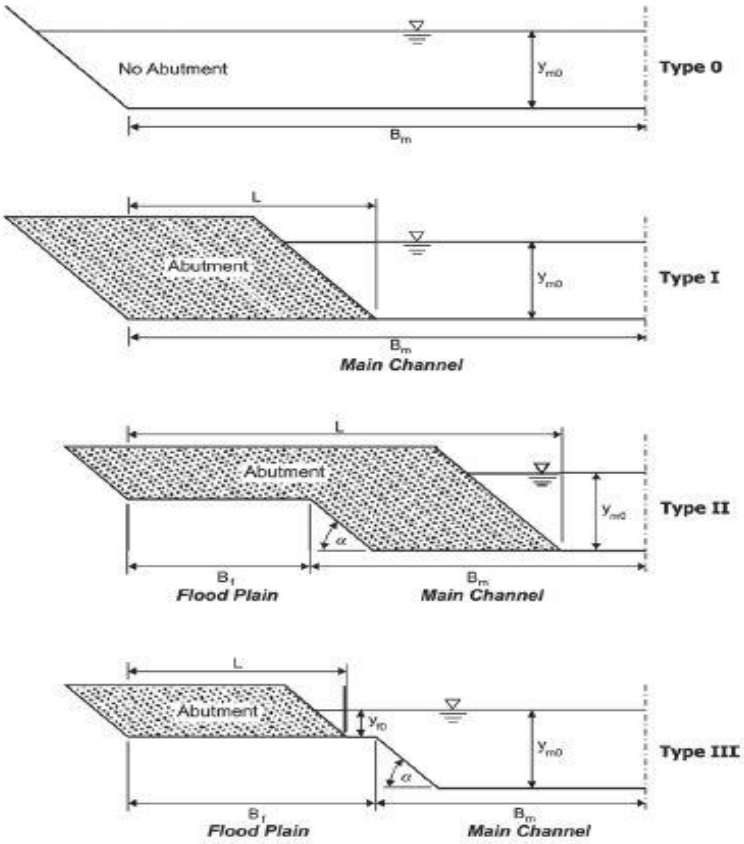

Figure 2.9.: Basic abutment lay-outs (Ettema et al., 2004)

The abutment location in the waterway could affect the flow field and influence scour behaviors. The amount of overbank flow intercept and return to the bridge opening at the abutment may differ because of different abutment layouts. According to Ettema et al. (2004), the common abutment location layouts for spill-through abutments can be classified as seen in figure 2.9. HEC-18 suggests that more severe abutment scour can develop when large intercepted overbank flow returns to the bridge opening directly compared to gradually returns of overbank flow to the bridge opening.

- Abutment Skew

  The angle of attack of the flow to the abutment has a significant effect on scour depth. If an abutment skewed towards downstream, the depth of the scour hole would decrease. In contrast, if an abutment skewed towards upstream, the depth of scour hole would increase, and scour equations should have a parameter to correct scour depth for skew angles (Arneson et al., 2012).

- Abutment shapes

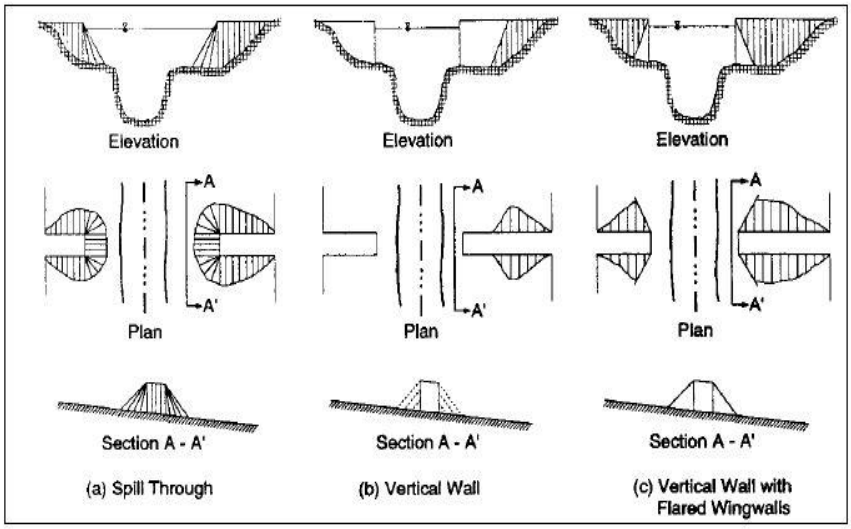

Figure 2.10.: The most common abutment shapes (Arneson et al., 2012)

The magnitude of abutment scour is significantly influenced by abutment shapes (Ettema et al., 2004). Generally, there are three shapes of abutments and these are wing-wall, spill-through, and vertical-wall abutments. Figure 2.10 illustrates the common abutment shapes. According to Melville and Coleman (2000), the slope feature and riprap nature of spill-through abutments induce less scour depth than other shapes of abutments. Furthermore, HEC-18 states that the scour depth is about two times higher for vertical-wall abutments as compared to spill-through abutments. Similarly, the scour depth at wing-wall abutments is 20 percent lower compared to vertical-wall abutments.

2.5 GEOTECHNICAL CONSIDERATIONS FOR BRIDGE SCOUR

The geotechnical properties of sediments at channel beds and banks significantly influence scouring behavior. The sediment-water interaction determines to what extent the hydraulic forces can be erosive against resistance properties of sediments in a river. Geotechnical properties are the main concern behind the development of scour equations and methods (Arneson et al., 2012). The shear strength of the soil is often considered as a good predictor of the critical shear stress. The critical shear stress directly affects the threshold amount and rate of the sediment transport. The sediment motion starts when the shear stress by water flows at the bed equals or exceeds the critical shear stress of the sediments (Soulsby, 1997). Based on what influences the shear strength, the soil can be classified as cohesive and non-cohesive soil.

In cohesive soil like clay and silts, the cohesion property of the soil defines the shear strength of the soil. The cohesion denotes the attraction forces between particles. The cohesive soils are very fine and the particle size is less than 0.06 mm. In pure cohesive soil, the internal resistance or friction between particles is assumed as zero, and cohesion is the only factor causing shear strength. Due to this cohesion nature, erosion often takes place by block by block compare to individual particles and generally bring more resistance to transport (erosion). Thus, scour estimation in cohesive soils brings more complex phenomena to be considered. The threshold limit for cohesive soil particles never correlates with particle size compared to non-cohesive soils (Kimiaghalam et al., 2016).

In contrast, the non-cohesive soils like sand and gravel are often considered to be coarse with self-weight characteristics. The attractive forces between particles assumed negligible and internal friction or resistance between particles due to sliding and rolling define the shear strength of the soil. This nature brings particle by particle removal when erosion takes place. In non-cohesive soil, the shear strength (critical shear stress) increases with particle sizes, so fine sand is more erodible than coarse sand (Kimiaghalam et al., 2016).

In addition, it is very import to understand that in reality the site conditions often are more complicated with a combination of cohesive and non-cohesive soils. Hence, in the field the shear strength must be determined by both internal friction and attractive forces between sediment particles. The scour in cohesive

soil is time-depended because the rate of erosion increases in a very slow manner due to cohesion property, whereas in non-cohesive soils the maximum scour can be reached rapidly during a single flood event without time-dependent shear strength (Arneson et al., 2012).

As shown in Figure 2.11, Briaud et al. (2011) developed a general relationship for how the erosion rate varies with flow velocity, Unified Soil Classification System (USCS), and some other geotechnical properties when threshold limit for erosion was set (when exceed the critical shear stress).

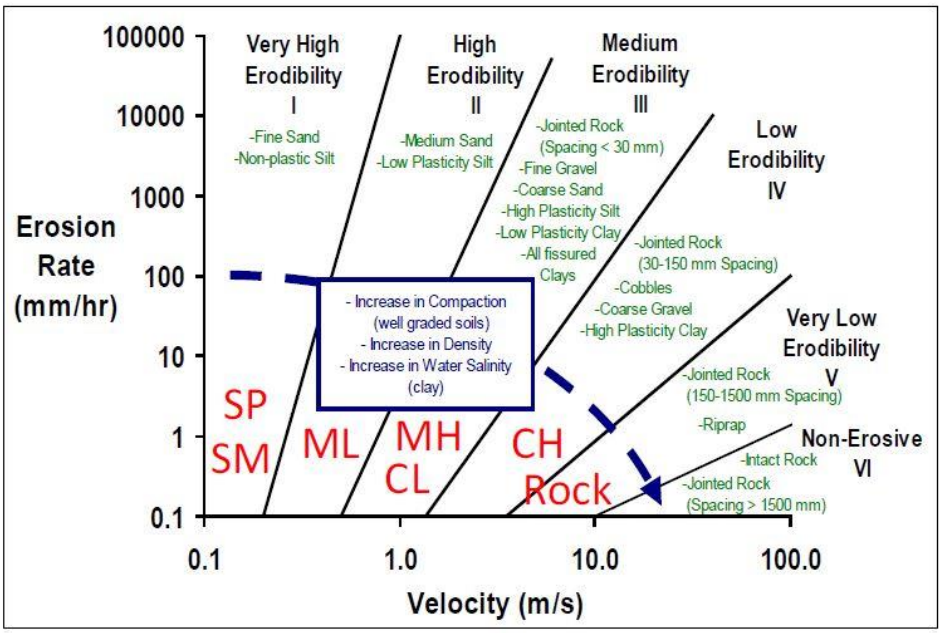

Figure 2.11.: Relationship between erosion rate and flow velocity for different bed materials (Briaud et al., 2011)

2.6 SCOUR EVALUATION OF BRIDGES

Scour evaluation is a very important in bridge construction and analysis, but often involves a complex investigation to determine the vulnerability of a particular bridge to scour. The evaluation and assessment for prudent measures are needed to be directed by an experienced interdisciplinary team of hydraulic, geotechnical, and structural engineers (Arneson et al., 2012). Generally, a

comprehensive investigation needs to be performed in several stages. According to Kirby (2015), the stages may be classified as:

- Screening: The screening of bridges that are subjected to the water flow impact by setting priorities along with initial risks.
- Initial assessment: The estimation of scour depths and review current protection measures available for identified bridges. Moreover, the estimation of potential scour depths is performed based on hydrologic and hydraulic variables. The initial scour depth estimation can be used to categorize bridges as low to high risk bridges.
- Detailed assessment: After the initial assessment, a detailed scour assessment should be done for high-scour risk bridges. Through more detailed studies, further evaluation is performed of potential risks and the possibility to design scour countermeasures for protection.
- Re-assessment: In this stage, periodic inspection and monitoring are carried out to ensure and identify changes of in the scour for a certain time interval.

2.7 SCOUR ESTIMATION METHODS

The estimation of bridge scour is widely practiced by using a wide range of methods and formulas; still, a universally recognized method to estimate scour depth and rate of scour has not been developed due to complex nature of scour (Zhang et al., 2013). Many equations were proposed in the past in various studies, as mentioned above in the different sections of this chapter. This section briefly summarizes a few widely used prediction methods. Reliable and robust estimations are crucial in assessment and decision making regarding scour, since underestimation can lead to bridge failures. In contrast, an overestimation may have economic consequences and lead to prevention measures that are not necessary. It is important to note that there are other equations available for scour estimations not covered in the following review.

➢ HEC-18 Method

HEC-18 is a widely used method in the US transportation department and it was developed by FHWA through different research studies. The latest, fifth version, was released in 2012. The scour estimation equations are more or less empirical and semi-empirical, and were developed based on laboratory studies with uniform, non-cohesive soils. Thus, this method has no consideration of

the variability and heterogeneity of riverbed material. Thus, it is mostly reliable to use for uniform non-cohesive soil conditions (Arneson et al., 2012). Nevertheless, the bed soils at bridges often have varying grain sizes with various cohesive properties. This is the main drawback of the HEC-18 method and it typically overestimates the scour depth in cohesive material. Also, this method is based on a single flood event without taking flood duration into account and provides restrictions to estimate the rate of scour. Thus, it is limited to conservative estimations, but it is still a popular method (Zhang et al., 2013). A one-dimensional hydraulic model such as WSPRO or HEC-RAS can be used to find hydraulic characteristics for the HEC-18 method, and HEC-RAS modeling has a bridge scour analysis option that is developed based on HEC-18 method equations.

- SRICOS-EFA Method

The SRICOS-EFA (Scour Rate in Cohesive Soil-Erosion Function Apparatus) method was developed by Briaud, Chen, and fellow students at Texas A&M University in the 1990s by considering various field data samples of coarse-grain, fine-grain soils, cohesive and non-cohesive soils, and layered soils. This method also includes time effects and thus give an estimation of scour rates. This is the advantage of the method apart from being applicable in cohesive soils. However, the requirement of in-situ sampling and laboratory testing creates practical and economic limitations on its usage.

- Simplified SRICOS Method

The constraints from in-situ sampling and laboratory testing made Briaud et al develop the Simplified SRICO-EFA method in 2009. The soil characteristics and erodibility for a particular site are obtained from pre-classified charts based on previous research. This method is useful for screening stages, and the time-bound scour estimation feature provides a tool for estimation of future development scour depth within the bridge life period (Zhang et al., 2013).

- NCHRP Method

In 2010, Wagner et al. prepared an NCHRP Document (project 20-14) and a method that developed the HEC-18 approach through funding from FHWA and AASHTO. The main advantage of this method is that it can utilize real-time hydraulic data from flood events for scour depth calculations. Moreover, the simulated hydraulic data can also be used for calculations, which allows

for comparing results from simulated discharges with real-time flow data. The limitations are mainly due to constraints regarding instrumentation and real-time monitoring. This method cannot calculate the rate of scour (Arneson et al., 2012).

- The FDOT Method

This method was developed by Florida Department of Transportation (FDOT) in 2005. The method is very similar to the HEC-18 approach, but the local scour prediction is performed by Sheppard equations. It includes the ratio of pier width to sediment diameter in estimating scour depth.

- ABSCOUR Method

This method was developed by Maryland State Highway Administration (MD SHA) in 2007 and is similar to the HEC 18 method. However, the method is using the MDSHA equations for estimating abutment scour based on research and development by Chang and Davis.

CHAPTER 3- GENERAL SCOUR

3.1 BEND SCOUR

Bend scour refers to the removal of sediment material from the bank toe, resulting from river flow through meander bends. The sediment removal happens due to formation of helical flows (a spiral shape flow) that pile up water at the concave side of the bend and produce complex currents moving towards the inside of the meander bends (point bar). Furthermore, these secondary currents exert higher shear stress on the concave side of the banks and develop erosion. Therefore, the erosion at the outer bank is a dominant feature in bends and thus requires proper measures to counteract the bend scour or erosion (Shafai-Bejestan, Mahmoodi and Soozepour, 2016). Figure 3.1 illustrates a plan view of a typical bend including higher shear stress locations. Three empirical methods by Thorne (1993), Maynord (1997), and Watanabe et al. (1990) are available to estimate bend scour with some limitations (Ghodsian and Mousavi, 2004).

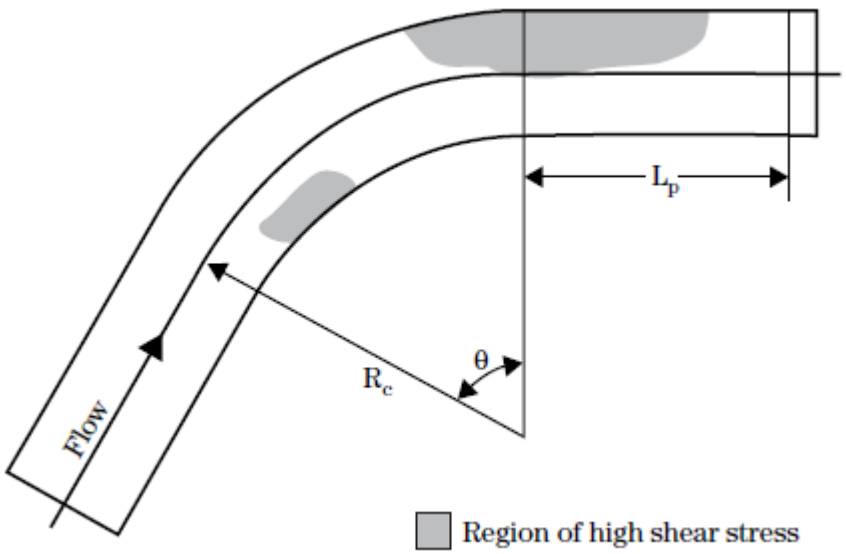

Figure 3.1: A typical plan view of a bend with potential higher shear stress area (Technical 14B, USDA)

3.2 RIFFLE-POOL SEQUENCES

Riffle-Pool sequences refer to typical bedform undulations that appear in meander bends. The pools are positioned on the concave side of the bend where erosion often takes place due the occurrence of higher shear stress and higher flow velocity. The riffles are positioned where sedimentation (deposition) takes place at downstream points of bends, See figure 3.2. The geomorphological changes and the riffle-pool characteristics of a particular meander bend are influenced by hydraulic and bend characteristics. The main parameters are river discharge, sediment characteristics, planform, the radius of curvature, and sinuosity (Salmela et al., 2020). During low discharge, the riffles erode and deposition occurs in the pools. However, next effective flood can cause river bed scouring and develop pool at the same locations in the meander bends. Furthermore, previous runoff events can influence the present characteristics of riffle-pool sequences to a certain extent (Keller, E.A., 1971).

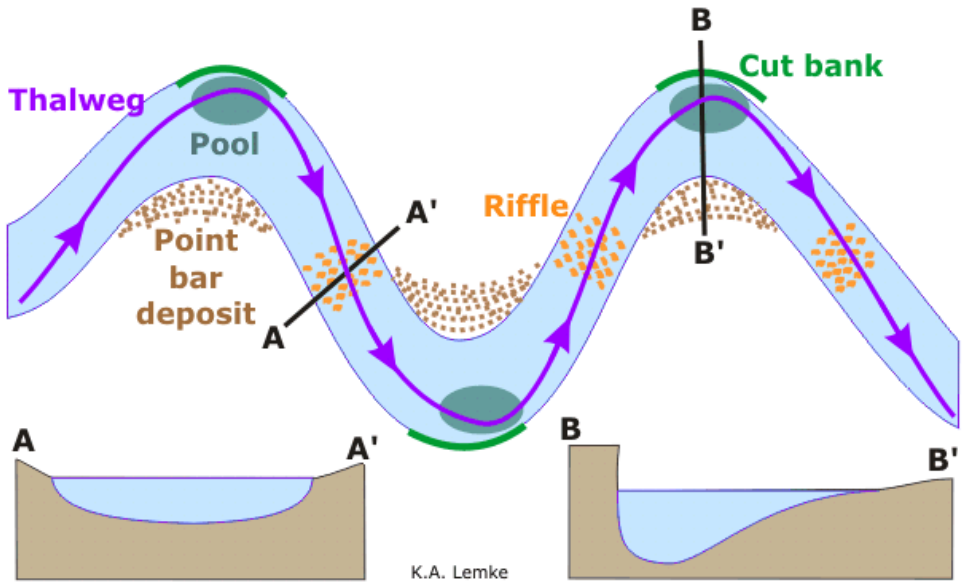

Figure 3.2: A typical view of riffle-pool sequences in meander bends (K.A. Lemke)

3.3 LOCAL SCOUR DOWNSTREAM OF HARD RIVER BOTTOM

A literature review on this topic was not directly involved in the current study, but due to lack of literature studies available on scour hole development downstream of the non-erodible bottom (hard bottom), it was decided to review similar topics. This could give insights on scour hole development downstream hard bottom, since such holes are significant in the studied river. Sung (2016) carried out a laboratory study of local scouring downstream of a riverbed protection for low Froude number flows (subcritical flows). He developed a conceptual model based on the geometric shape of the hole, see figure 3.3. Furthermore, he was able to explain the formation of the scour hole shape from the initial phase to equilibrium conditions. The laboratory results justified his conceptual model by a showing a similar geometric hole shape.

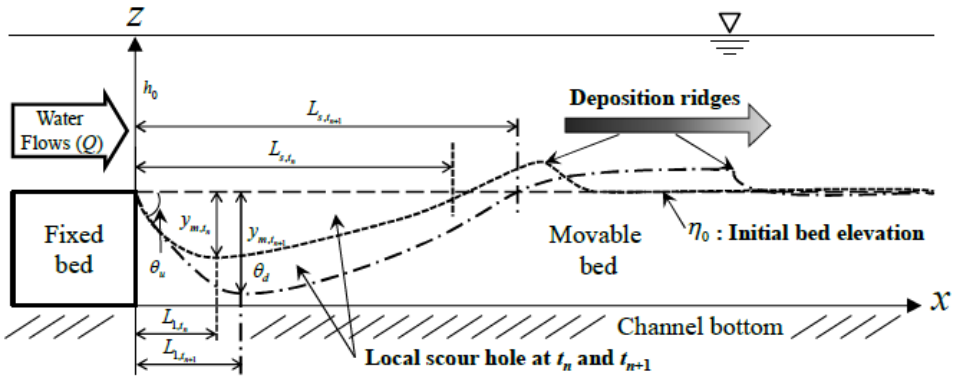

Q: water discharge from the upstream of the flume (m/s^3)
h_0: water depth at the tailgate of the flume (m)
η_0: initial bed elevation (m)
L_s: total length of scour hole (m)
y_m: maximum scour depth (m)
L_1: longitudinal distance from the longitudinal transition (x= 0) to the location of y_m (m)
θ_u: upstream scour slope (degree)
θ_d: downstream scour slope (degree)
t_n: time step (hour)

Figure 3.3: A schematic geometric shape of a scour hole downstream of a fixed bed (Park, 2016)

Sung (2016) concluded that the shape of the scour hole is characterized by flow duration, and the upstream slope of the hole reaches an equilibrium faster than

any other section. He found that the eroded particles aggregate along the downstream part of the hole, and scouring rates are greater in finer sediments than in coarser sediments downstream of the fixed bed. In addition, Sung (2016) determined that the surface properties of the bed protection, upstream flow conditions, and sediment properties downstream the protection can significantly affect the local scouring.

CHAPTER 4- RÖNNE Å AT ÄNGELHOLM

4.1 GENERAL

The Rönne å river basin is situated in South Sweden (Northwest Skåne) and is characterized by a total catchment area of about 1 922 km^2. The Rönne å starts from Skåne's second-largest lake called Lake Ringsjön at an elevation of +54 m (RH 2000) and the total length of the river is around 83 km. The river flows through many municipalities in Skåne and finally through Ängelholm municipality to meet the coast in the bay of Skälderviken. For the current study, a 12-km river reach from the coastal outlet and upstream was considered. Figure 4.1 shows the location of the river in Sweden, including a map of the studied river reach.

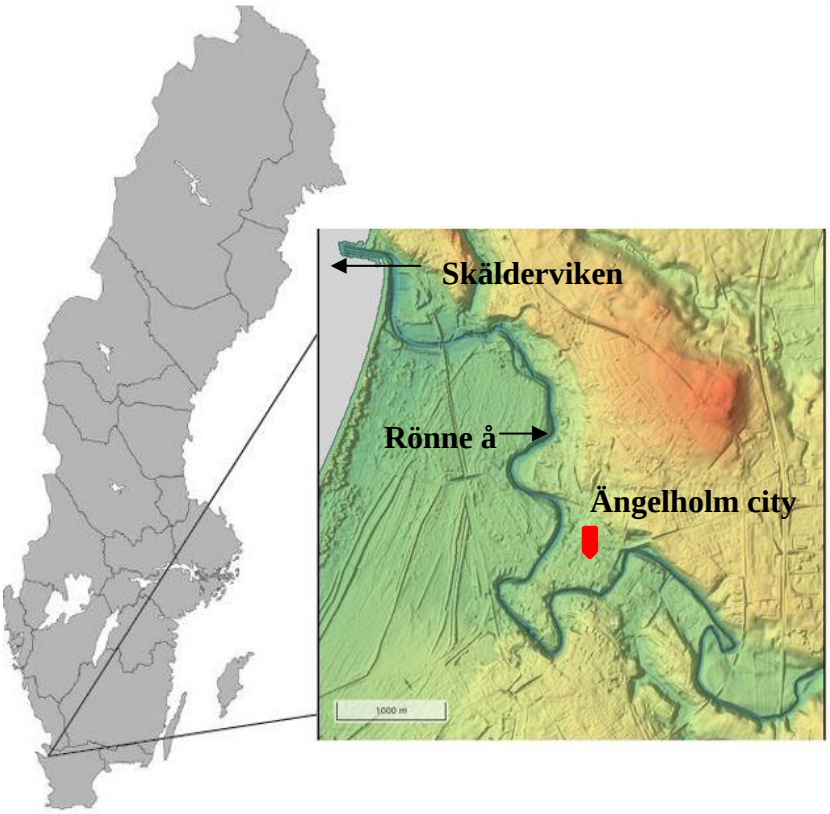

Figure 4.1: The map shows studied river reach of Rönne å at Ängelholm Municipality and its geographical location in Sweden, obtained from SCALGO Live

According to SMHI, the main catchment is divided into 52 sub-catchments based on the main river and its tributaries. Since the studied river stretch is the downstream 12 km, there are only three catchments with a total area of about 37.5 km^2 adding water to the river, as shown in figure 4.2.

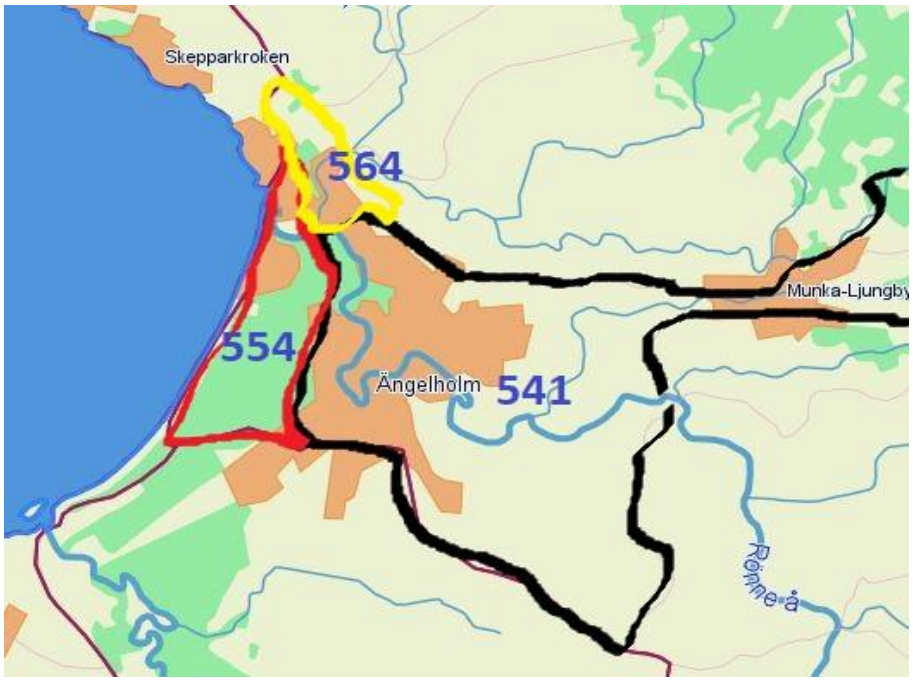

Figure 4.2: The sub catchments of Rönne å basin aligned to the study area at Ängelholm municipality (Vattenatlas.se)

The sub-catchments 541 and 554 directly contribute to the flow in Rönne å and sub-catchment 564 contributes to flow in Rössjöholmsån river, which has a confluence with the downstream part of Rönne å (the sub-catchment numbers used are the same in subsequent chapters). Land use of the catchments in Ängelholm is mainly characterized by urban and cultivation. According to SGU (Geological Survey of Sweden), the bedrocks of the catchments are platform sedimentary rocks, including clay, shale, sandstone, and coal lithological features. The main soil types of the floodplain upstream of the studied river reach mainly consist of young fluvial sand, midstream mainly of

postglacial find sand, and downstream of young fluvial sand again; see Appendix 1 for the complete geological map from SGU. There are 16 bridges crossing Rönne å in Ängelholm municipality.

4.2 CLIMATOLOGY AND HYDROLOGY

There are many small streams and tributaries contributing to the total flow in Rönne å before it reaches Skälderviken outlet on the west coast. In 2016, SMHI simulated the flows by using the S-Hype model, dividing the total catchment into various sub-catchments. Since the study is limited to a 12-km length of river reach, the flows through sub-catchment number 541, 564, and 554 (see figure 4.2 above) are considered to this study. The flow from catchment 554 represents the cumulative total river flow of Rönne å from upstream the studied river reach.

According to SMHI model outputs, the corrected maximum, minimum, and average flow of the main river for the 2004 -2019 period is 207 m^3/s, 2.4 m^3/s, and 23.1 m^3/s, respectively. Due to various climatic conditions through the years, the annual average river flow may change dramatically between the years, see figure 4.3. Furthermore, according to the SMHI simulation model the average water temperature is 9.6 °C. More details regarding river flows are discussed in chapter 6, section 6.1.

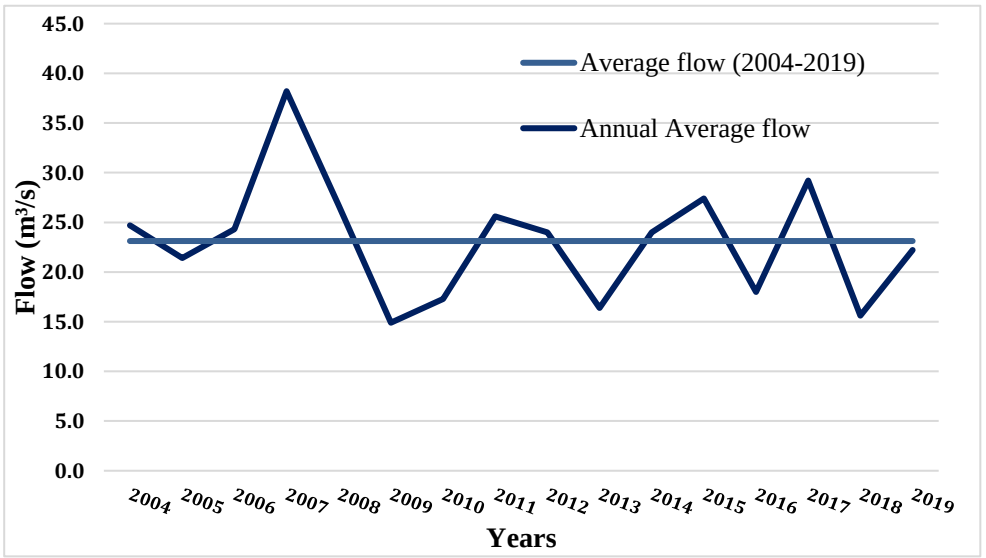

Figure 4.3: The annual average river flow for years 2004-2019

4.3 RIVER HYDRAULICS

The roughness characteristics may differ significantly over a cross-section due to thick vegetation in overbanks with large trees, see figure 4.4. The different roughness conditions imply different frictional resistances against the water flow. In general, a river with higher roughness causes a higher energy loss compared to a river with lower roughness (Brunner, 2016).

Figure 4.4: A typical river section showing various roughness condition in the overbanks (Gränsjö, 2020)

Apart from surface roughness, the irregularities in shape and size of the Rönne å sections can influence on the frictional energy loss. Strong northwest wind forces and other meteorological effects influence the water level in the Rönne å. Hence, the water level variation at Skälderviken outlet have significant impact on flow velocity and cause backwater effects.

4.4 GEOMORPHOLOGY AND SEDIMENT TRANSPORT

The Rönne å flows through Ängelholm in a unique V-shaped valley with a gentle longitudinal bottom slope. The general river width is 30-40 m and the average river cross-sectional area about 160 m^2. The channel meanders in

many places, with the highest sinuosity of 2.8 at the upstream location of the studied river reach, as shown in figure 4.1. Braiding features can be seen in some places, especially in the downstream section after river Rössjöholmsån confluences with Rönne å about 1.7 km from the coastal outlet. The downstream part of the river is mainly characterized by sand deposition of fluvial system and the formation of deltas (Almström, 2010). According to SMHI's S-Hype model results for the 2004-2019 period, Rönne å transports annually an average of 8 963 tons sediments from entire catchments, with an average concentration of 11.7 mg/l. Most of this material is wash load originating from the catchment surface and not from the river itself.

4.5 RIVER BANK EROSION AND SCOUR

The riverbank erosion of Rönne å has been a serious challenge for Ängelholm municipality in the last decade and has initiated several studies regarding erosion in past years, as mentioned under chapter 1. The erosion occurs when more sediment is transported downstream than coming from upstream to the banks in a particular area. The erosion is very significant at steep river sections and outer bend curves, where the water velocities are high in the Rönne å.

Figure 4.5: An example of typical erosion problems at Ängelholm causing trees to fall into the river (Almström, 2010).

According to the Swedish Geotechnical Institute (SGI), the wave generation and rapid drawdown of water by boat transport can also enhance erosion at the overbanks in Ängelholm (Almström, 2010). Also, it has been established that the river reach at the central and upper part of Ängelholm has more erosion issues compared to the lower part of the city. In some places, some measures have been taken to stabilize the banks and prevent erosion where steep slopes are common; especially in central Ängelholm, some private landowners have been using rubble packing, placing concrete walls and sheet piles to protect lands from riverbank erosion. The erosion already had led to landslides in some private lots. The other great threat from erosion is that trees fall into the river from banks, causing interruption to boat traffic and blockage problems at bridges and narrow passages for the river flow. Figure 4.5 illustrates an example of a tree falling due to bank erosion at Rönne å.

The recent bathymetry and topography survey by MarCon Teknik AB (MTE) along the Rönne å river reach shows that the erosion is not only limited to banks. There are many uneven bottom holes prominent along the riverbed. For example, downstream of the Carl XV Bridge, the riverbed has a 7.5-m deep inverted cone-shaped hole with an approximately 40-m longitudinal surface extension. This problem initiates another challenge to Ängelholm municipality to check the potential development of these scour holes for future scenarios and forecast the threats to bridge foundations.

CHAPTER 5- HEC RAS MODEL

5.1 GENERAL

The Hydrologic Engineering Center's River Analysis System, generally known as HEC-RAS is an open-source computer-aided program developed by the US Army Corps of Engineers. This software was developed to be employed for various useful river analysis such as one-dimensional steady flow, one and two-dimensional unsteady flow, sediment transport, water temperature and water quality, and bridge scour. For instance, the current model study is performed by a 1D steady flow analysis with bridge scour computations. In HEC RAS, the bridge scour analysis is performed based on a method outlined in HEC 18 circular by FHWA in 2001. It should be noted although the HEC 18 latest updated version was released in 2012, HEC RAS uses procedures that are outlined in the older version and has still not been updated. Thus, performing HEC RAS bridge scour analysis requires careful evaluation and good interpretation of the computed results (Brunner, 2016).

As mentioned in chapter 2, the hydraulic characteristics are one of the key parameters for bridge scour estimation. Therefore, to develop bridge scour analysis, at first HEC RAS is required to develop a one-dimensional hydraulic model using geometric data and steady flow data of the river. Through a steady flow analysis, the relevant hydraulic data are obtained to perform scour calculations at the bridge locations. HEC RAS computes the contraction scour, pier scour, and abutment scour as separate components. This chapter summarizes information that are important for understanding the bridge scour analysis in HEC RAS.

5.2 1D HYDRAULIC MODEL ANALYSIS

The hydraulic characteristics for bridge scour analysis are determined by the water-surface profile (flow depth) and energy grade lines (energy loss) resulting from solving steady-state flow equations. HEC RAS performs 1-D, steady-state, gradually-varied flow analysis based on following assumptions: 1. the flow is steady, hence hydraulic characteristics not dependent on time duration; 2. The flow is one-dimensional and only the velocity component in the main flow direction is taken into consideration; 3. the river channel has smaller slopes, less than 0.1 (Brunner, 2016).

5.2.1 GOVERNING EQUATIONS

The 1-D steady flow analysis includes fundamental hydraulic equations such as the continuity equation, energy equation, momentum equation, and flow resistance equation. The energy equation is applicable when gradually varied flow conditions prevail. In contrast, when rapidly varied flow conditions, such as hydraulic jumps, bridge constrictions, and river junctions, the momentum equation is applied to estimate water surface elevations.

- **The Continuity Equation**

$$Q = A_1V_1 = A_2V_2 \quad (1)$$

where: A_1, A_2 = Cross-sectional area normal to the direction of flow at river sections (m^2)
V_1 , V_2 = Average velocities at cross sections (m/s)
Q = River discharge (m^3/s)

- **The Energy Equation**

In HEC RAS, the energy equation is used to determine water surface profile at cross sections by solving it with a standard step iterative procedure (see figure 5.1).

$$Z_2 + Y_2 + \frac{\propto_2 V_2^2}{2g} = Z_1 + Y_1 + \frac{\propto_1 V_1^2}{2g} + h_e \quad (2)$$

where: Z_1 , Z_2 = Elevation of the main channel inverts (m)
Y_1 , Y_2 = Depth of water at cross sections (m)
V_1 , V_2 = Average velocities at cross sections (m/s)
$\propto_1, \propto_2$ = Velocity weighting coefficients
g = Gravitational acceleration (m/s^2)
h_e = Energy head loss (m) (generally friction loss + minor loss)

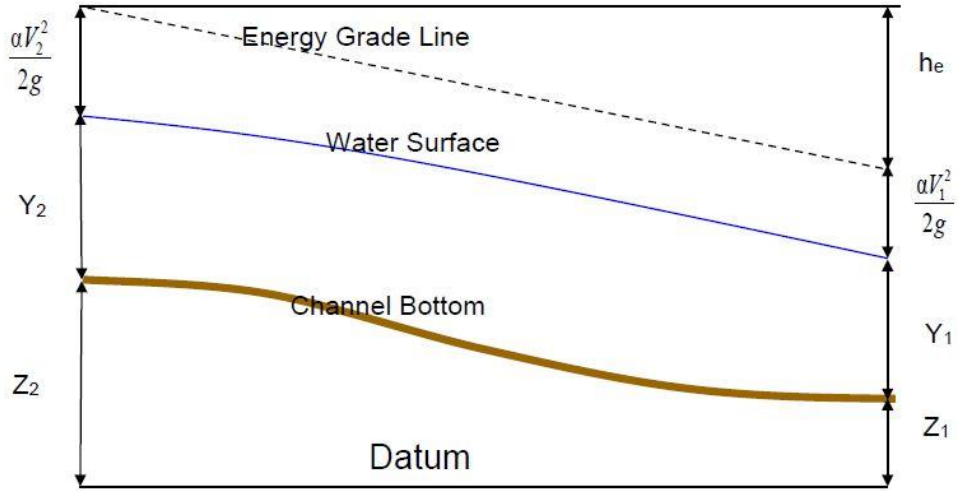

Figure 5.1.: The graphical representation of the energy equation (Brunner, 2016).

- **Flow Resistance Equation**

Flow resistance equation for HEC RAS analyses is given form of the Manning's equation

$$Q = KS_f{}^{1/2} \tag{3}$$

where: Q = River discharge (m^3/s)
K = Channel conveyance (m^3/s)
S_f = Friction slope (m/m)

$$K = \frac{1}{n} AR^{2/3} = \frac{1}{n} A\left[\frac{A}{P}\right]^{2/3} \tag{4}$$

where: A = Cross-sectional area normal to the direction of flow (m^2)
n = Manning's roughness coefficient
P = wetted perimeter (m)
R = hydraulic radius (m)

- **The Momentum Equation**

In HEC RAS, usage of the momentum equation is not a default option. However, it can be applied for hydraulic jumps, stream junctions, and bridges when expecting rapidly varied flow conditions. The momentum equation is derived by applying Newton's second law of motion to a body of water between two river cross-sections (see figure 5.2).

$$P_2 - P_1 + W_x - F_f = Q\ \rho\ \Delta V_x \qquad (5)$$

where: P_1, P_2= Hydraulic pressure force at cross-sections (N)
W_x = Gravitational force of water in the flow direction (N)
F_f = Frictional force due to external friction (N)
Q = River discharge (m^3/s)
ρ = Density of the water (kg/m^3)
ΔV_x = Change in velocity in the flow direction (m/s)

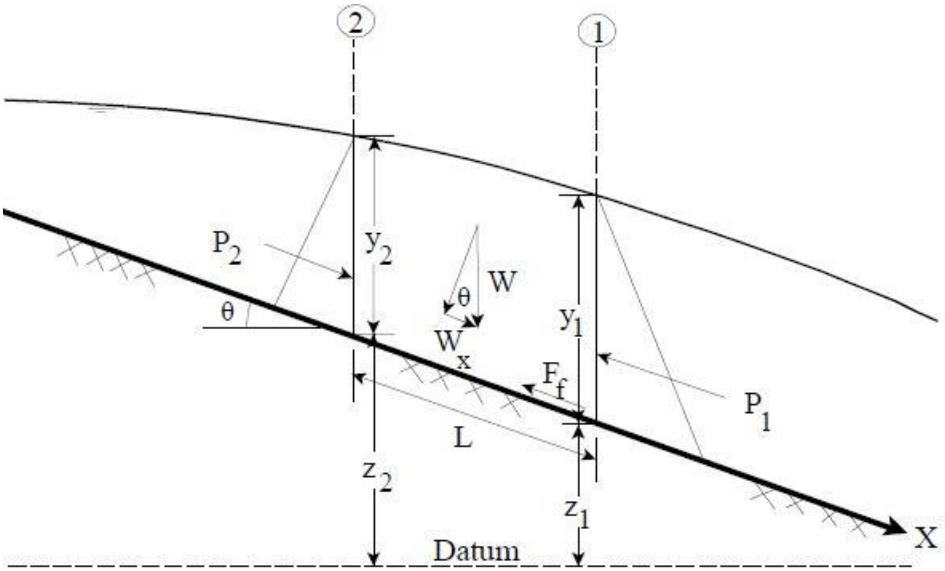

Figure 5.2.: The graphical representation of the momentum equation (Brunner, 2016).

5.2.2 MODELLING ENERGY LOSSES

For the 1D steady-state gradually varied flow analysis the total energy loss in the river channel is a result of bed friction and contraction and expansion losses. In reality there are other factors that can create energy losses, such as formation of turbulence including eddies, spirals, and secondary currents at river constrictions and bends.

- **Friction loss**

Friction loss is an energy loss along a river reach due to roughness elements of the channel boundaries.

$$h_f = \bar{S_f}\,\Delta x \tag{6}$$

where: h_f = Energy loss due to friction (m)
$\bar{S_f}$ = Average friction slope between two adjacent cross sections (m/m)
Δx = Incremental channel length between cross sections (m)

Average friction slope is calculated based on by rearranging friction equation as below. It is known as the average conveyance method and this is the default option in HEC RAS (Brunner, 2016).

$$\bar{S_f} = \left[\frac{Q_1 + Q_2}{K_1 + K_2}\right]^2 \tag{7}$$

where: Q_1, Q_2 = River discharges at cross sections (m^3/s)
K_1, K_2 = channel conveyance at cross sections (m^3/s)

- **Expansion and contraction losses**

Expansion and contraction losses is generally referred to as minor losses due to changes in the cross-sectional area. In HEC RAS, the program assumes expansion loss when the velocity head of the upstream is greater than the downstream velocity head. In contrast, a contraction loss is

assumed when the downstream velocity head is greater than the upstream velocity head.

$$h_e = C\left(\frac{\propto_2 \bar{V}_2^2}{2g} - \frac{\propto_1 \bar{V}_1^2}{2g}\right) \quad (8)$$

where: h_m = Energy loss due to expansion or contraction (m)
C = Coefficient of expansion or contraction
$\propto_{\mathbf{1}}, \propto_{\mathbf{2}}$ = Velocity weighting coefficients
$\bar{V}_1, \bar{V}_2$ = Average velocities at cross sections (m/s)
g = Gravitational acceleration (m/s^2)

HEC RAS reference manual version 5.0 suggests some typical values for expansion and contraction coefficients in a subcritical flow as given table 5.1 below.

Table 5.1.: The expansion and contraction coefficients for subcritical flow (Brunner, 2016)

	Expansion	Contraction
No Transition Loss Computed	0.0	0.0
Gradual Transitions	0.3	0.1
Typical Bridge Sections	0.5	0.3
Abrupt Transitions	0.8	0.6

5.2.3 MODELLING BRIDGES

The modelling of bridges is a unique procedure in HEC RAS to evaluate the proper energy losses at bridges. The procedure involves placing cross-sections, defining ineffective flow areas, inserting bridge geometry, and evaluating energy losses around bridges. Figure 5.3 shows a basic cross-section plan layout combining four cross-sections. HEC RAS computes energy losses based on three zones as described in the following. Furthermore, HEC RAS uses different methods based on the flow characteristics. Nevertheless, in this section, the methods are explained for low flow and subcritical flow

conditions. The low flow refers to the fact that the water surface is always below the low chord of the bridge opening.

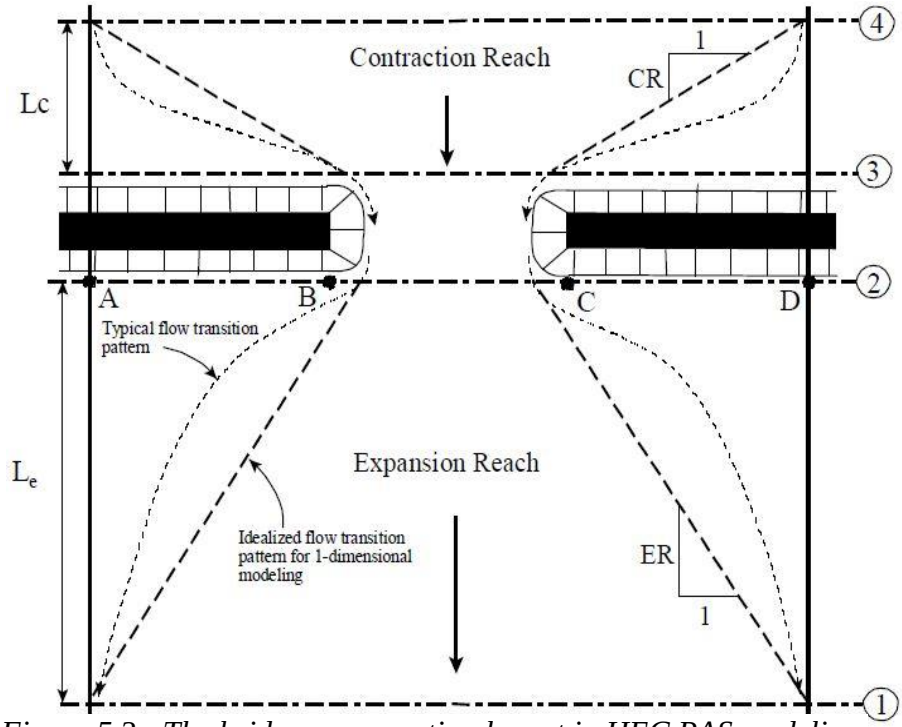

Figure 5.3.: The bridge cross section layout in HEC RAS modeling (Brunner, 2016)

- **Zone 1:** The energy loss immediately downstream of the bridge (cross-sections 2 to 1) by an expansion of the flow and it is calculated as friction and expansion losses by equations given above.

- **Zone 2:** The energy loss immediately upstream of the bridge (cross-sections 4 to 3) by a contraction of the flow and it is calculated as friction and contraction losses by equations given above.

- **Zone 3:** The energy loss at the bridge structure (cross-sections 3 to 2) and it can be calculated based on four different methods.

    1. Energy Equation (standard step method)

The bridge is considered similar to a natural river in this method while using increased wetted perimeter inside the bridge structure where water is in contact with bridge walls.

2. Momentum Balance Method

This method is based on a momentum balance inside the bridge cross-section. Hence the frictional force and drag force on piers are main components in the calculation. So this method requires proper roughness and drag coefficients.

3. Yarnell Equation

This equation was developed by Yarnell in 1934 and can be used to predict water elevation changes between downstream and upstream of the bridge. This equation requires the Yarnell pier shape coefficient, the pier obstructed area, and the velocity of the water.

4. FHWA WSPRO Method

The WSPRO method was developed by the Federal Highway Administration (FHWA) and uses the energy equation to compute the water surface profile across cross-sections 4 to 1, including cross-sections 3 to 2.

5.3 COMPUTING CONTRACTION SCOUR

In HEC RAS, the contraction scour at a bridge is calculated using a modified version of the Laursen (1960) equation for live-bed scour and the Laursen (1963) equation for clear-water scour conditions. Furthermore, a condition is specified for clear-water scour, implying that the critical velocity of the bed material is larger than the average velocity at the approach section upstream of the bridge (Vc > V). It is assumed that live-bed scour prevails when the critical velocity of the bed material is less than the average velocity at the approach section (Vc < V). The following equation from Laursen is used to determine the critical velocity of the bed material.

$$V_C = K_u \, y_1^{1/6} \, D_{50}^{1/3} \qquad (9)$$

where: Vc = Critical velocity above which material of size D_{50} and smaller will be transported (m/s)

y_1 = Average depth of flow in the main channel or overbank area at the approach section (m)

D_{50} = Bed material particle size in a mixture of which 50% are smaller (m)

Ku = 6.19 (S.I. Units)

5.3.1 LIVE-BED CONTRACTION SCOUR EQUATION

$$y_2 = y_1 \left[\frac{Q_2}{Q_1}\right]^{6/7} \left[\frac{W_1}{W_2}\right]^{K_1} \quad (10)$$

$$y_s = y_2 - y_0 \quad (11)$$

where: y_s = Average depth of contraction scour (m).

y_2 = Average depth after scour form in the contracted section, (m). This is taken as the section inside the bridge at the upstream section in HEC-RAS model.

y_1 = Average depth in the main channel /floodplain at the approach section (m).

y_0 = Average depth in the main channel or floodplain at the contracted section before scour (m).

Q_1 = Flow in the main channel or floodplain at the approach section, which is moving sediments (m^3/s).

Q_2 = Flow in the main channel or floodplain at the contracted section, which is moving sediments, (m3/s).

W_1 = Bottom width in the main channel or floodplain at the approach section (m). This is approximated as the top width of the active flow area in HEC-RAS.

W_2 = Bottom width of the main channel or floodplain at the contracted section minus pier widths (m). This is approximated as the top width of the active flow area.

K_1 = Exponent for mode of bed material transport (calculated from table below)

Table 5.2.: The exponent for mode of transport of bed material (Brunner, 2016)

V* /ω	K_1	Mode of bed material transport
< 0.50	0.59	Mostly contact bed material discharge
0.50 to 2.0	0.64	Some suspended bed material discharge
> 2.0	0.69	Mostly suspended bed material discharge

where: $V^* = (g\ y_1\ S_1)^{1/2}$ shear velocity in the main channel or floodplain at the upstream approach section (m/s).

ω = Fall velocity of bed material based on D_{50} and temperature (T) (m/s). (based on the graph below)

g = Acceleration of gravity (m/s2).

S_1 = Slope of the energy grade line at the upstream approach section in the channel (m/m).

The fall velocity is determined based on the water temperature in the channel by predefined curves shown in the HEC 18 manual. See figure 5.4.

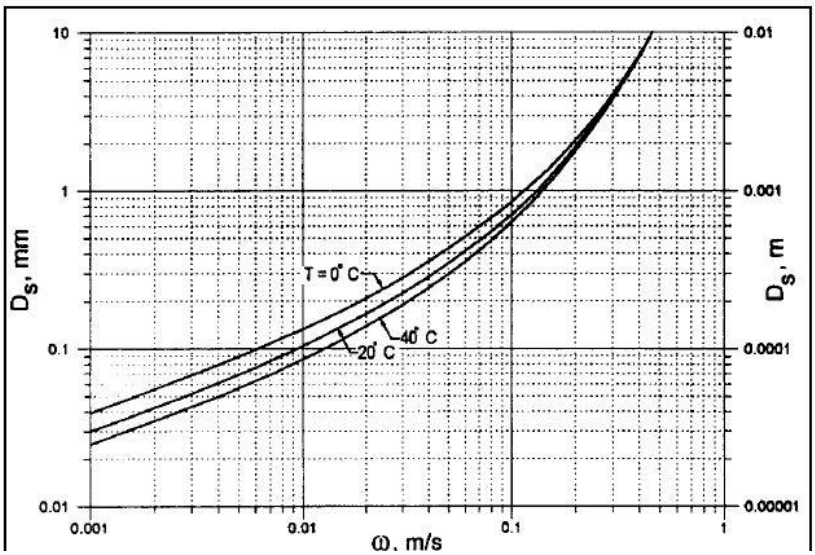

Figure 5.4.: Fall velocity of sand-sized particles with relationship of water temperature (Arneson et al., 2012)

5.3.2 CLEAR-WATER CONTRACTION SCOUR EQUATION

$$y_2 = \left[\frac{Q_2^2}{C D_m^{2/3} W_2^2}\right]^{3/7} \quad (12)$$

$$y_s = y_2 - y_0 \quad (13)$$

where: D_m = (1.25 *D_{50}) Diameter of the smallest non-transportable particle in the bed material in the contracted section (m).
D_{50} = Median diameter of the bed material (m).
C = 40 for metric units.

Note: other notations are similar as explained for the live-bed scour equation.

Note: In HEC RAS bridge scour analysis, all the parameters needed for equations are acquired directly from the 1D steady flow analysis by the hydraulic model, except the correction factor K_1 and bed material size D_{50}. The factor K_1 is calculated based on a given water temperature (T). HEC RAS also provides an option to users if they want to amend values of acquired parameters for particular cases.

5.4 COMPUTING PIER SCOUR

HEC RAS uses HEC-18 pier equation (CSU equation) to estimate pier scour depth by considering factors that affect the scour depth. This equation is used for live-bed scour and clear-water scour conditions and is considered as default equation in HEC RAS. In addition, HEC RAS provides the Froehlich equation for comparing the results.

5.4.1 HEC-18 PIER EQUATION (CSU EQUATION)

$$y_s = 2.0\, K_1\, K_2\, K_3\, K_4\, a^{0.65}\, y_1^{0.35}\, Fr_1^{0.43} \quad (14)$$

where: y_s = Depth of pier scour (m)
K_1 = Correction factor for pier nose shape (see table 5.3)
K_2 = Correction factor for angle of attack of flow (by an equation, see below)
K_3 = Correction factor for bed condition (see table 5.4)
K_4 = Correction factor for armoring of bed material (by combination of equation as below)

a = Pier width (m)

y_1 = Flow depth directly upstream of the pier (m). This is taken from the flow distribution output for the cross section just upstream from the bridge by the hydraulic model.

Fr_1 = Froude Number directly upstream of the pier. This is taken from the flow distribution output for the cross-section just upstream from the bridge by the hydraulic model.

- **Correction Factor K_1**

Table 5.3.: The correction factor for shape of pier nose (Brunner, 2016)

Shape of Pier Nose	**K_1**
(a) Square nose	1.1
(b) Round nose	1.0
(c) Circular cylinder	1.0
(d) Group of cylinders	1.0
(e) Sharp nose (triangular)	0.9

- **Correction Factor K_2**

$$K_2 = \left(\cos\theta + \frac{L}{a}\sin\theta\right)^{0.65} \qquad (15)$$

where: L = Length of the pier along the flow line (m)

θ = Angle of attack of the flow, with respect to the pier (°)

a = Pier width (m)

Note: When L/a is greater than 12, the software uses L/a = 12 as a maximum value in equation (15) above. When the angle of attack of the flow is greater than 5 degrees, K_2 dominates and K_1 should be set to 1.0 and HEC RAS automatically corrects for it.

- **Correction Factor K_3**

Table 5.4.: The correction factor for bed condition (Brunner, 2016)

Bed condition	Dune height (ft)	K3
Clear-water scour	N/A	1.1
Plane bed and antidunes	N/A	1.1
Small dunes	10 > H ≥ 2	1.1
Medium dunes	30 > H ≥10	1.1 to 1.2
Large dunes	H ≥30	1.3

- **Correction Factor K_4**

This correction factor is determined based on bed material of armoring. This factor decreases scour depth when the bed materials that have a D50 ≥ 0.002 m and a D95 ≥ 0.020m. This factor can be calculated by the following equations developed by J. S. Jones (Brunner, 2016).

$$K_4 = 0.4\, V_R^{0.15} \tag{16}$$

where:

$$V_R = \left[\frac{V_1 - V_{i50}}{V_{c50} - V_{i95}}\right] \tag{17}$$

$$V_{i50} = 0.645 \left[\frac{D_{50}}{a}\right]^{0.053} V_{c50} \tag{18}$$

$$V_{i95} = 0.645 \left[\frac{D_{95}}{a}\right]^{0.053} V_{c95} \tag{19}$$

$$V_{c50} = K_u\, y^{1/6}\, D_{50}^{1/3} \tag{20}$$

$$V_{c95} = K_u\, y^{1/6}\, D_{95}^{1/3} \tag{21}$$

where: V_R = Velocity ratio

V_1 = Average velocity in the main channel or overbank area at the cross section just upstream of the bridge (m/s)

V_{i50} = Approach velocity required to initiate scour at the pier for material size D_{50} (m/s)

V_{i95} = Approach velocity required to initiate scour at the pier for material size D_{95} (m/s)

V_{c50} = Critical velocity for D_{50} bed material size (m/s)

V_{c95} = Critical velocity for D_{95} bed material size (m/s)

a = Pier width (m)

y = Depth of water just upstream of the pier (m)

K_u = 6.19 (S.I. Units)

Note: The minimum value on K_4 is 0.4, for the applications.

5.4.2 THE FROEHLICH PIER EQUATION

$$y_s = 0.32\,\phi\,(a')^{0.62}\,y_1^{0.47}\,Fr_1^{0.22}\,D_{50}^{-0.09} + a \qquad (22)$$

where: ϕ = Correction factor for pier nose shapes: ϕ = 1.3 for square nose piers; ϕ = 1.0 for rounded nose piers; and ϕ = 0.7 for sharp nose (triangular) piers.

a' = Projected pier width with respect to the angle of the flow (m)

Note: other notations are similar to what is used in the HEC-18 (eq. 21) equation above.

Note: Generally the Froehlich equation is used to predict maximum pier scour for design purposes. It includes the pier width (a) as a factor of safety and HEC RAS always includes the pier width in the equation. When estimating scour depth for a particular flood event, it is recommended to subtract the pier width value manually.

Note: Based on HEC-18, HEC RAS limits the maximum pier scour depth as per the following conditions for round nose piers aligned with the flow. This is applicable to both equations mentioned above.

$y_s \leq 2.4$ times the pier width (a) for $Fr_1 \leq 0.8$

$y_s \leq$ 3.0 times the pier width (a) for $Fr_1 > 0.8$

In HEC RAS pier scour depth analysis, all the parameters needed for the equations are acquired directly from the 1D steady flow analysis by the hydraulic model, except the correction factors K_1 and K_3 and the bed material fraction size D_{95}. Furthermore, HEC RAS provides an option to users, if they want to amend values of acquired parameters for particular cases.

5.5 COMPUTING ABUTMENT SCOUR

HEC RAS uses two equations based on the HEC-18 report recommendations to predict the abutment scour depth. The HIRE equation is used when the ratio between wetted embankment length (L) and approach flow depth (y_1) is greater than 25. Similarly, when the ratio is less than or equal to 25, an equation by Froehlich is used in HEC RAS analysis.

5.5.1 THE HIRE EQUATION

$$y_s = 4\, y_1 \left(\frac{K_1}{0.55}\right) K_2\, Fr_1^{0.33} \qquad (23)$$

where: y_s = Scour depth (m)

y_1 = Depth of flow at the toe of the abutment on the overbank or in the main channel (m), is taken at the cross section just upstream side of the bridge.

K_1 = Correction factor for abutment shapes, (See table 5.5 below)

$K_2 = (\theta/90)^{0.13}$ correction factor for angle of attack (θ) of flow with abutment. $\theta = 90$ when abutments are perpendicular to the flow, $\theta < 90$ if embankment points towards downstream, and $\theta > 90$ if embankment points towards upstream. (See figure 5.5 below)

Fr_1 = Froude number based on flow velocity and depth adjacent and just upstream of the abutment toe.

Table 5.5.: The correction factor for abutment shapes (Brunner, 2016)

Description	K1
Vertical-wall Abutment	1.00

Vertical-wall Abutment with wing walls	0.82
Spill-through Abutment	0.55

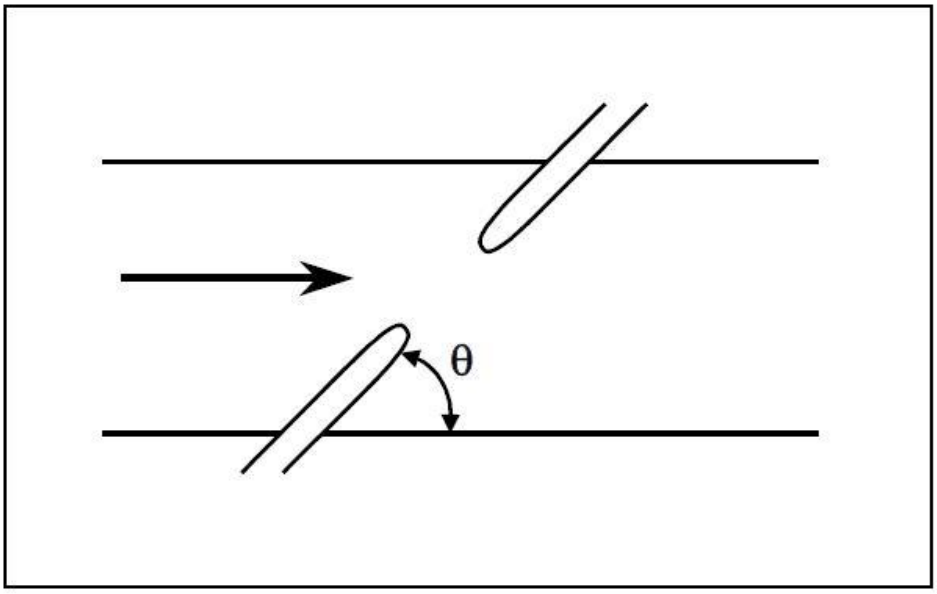

Figure 5.5.: Skew Angle of abutment to the flow direction for correction factor K_2 (Arneson et al., 2012)

5.5.2 FROEHLICH'S ABUTMENT EQUATION

$$y_s = 2.27\, K_1\, K_2\, (L')^{0.43}\, y_a^{0.57} Fr^{0.61} + y_a \qquad (24)$$

where: L′ = Length of abutment (embankment) projected perpendicular to flow (m)

y_a = Average depth of flow on the floodplain at the approach section (m)

Fr = Froude number of the floodplain flow at the approach section, $Fr = Ve / (g\, y_a)^{1/2}$

Ve = Average velocity of the approach flow Ve = Qe /Ae (m/s)

Qe = Flow obstructed by the abutment and embankment at the approach section (m^3/s)

Ae = Flow area of the approach section obstructed by the abutment and embankment (m^2)

Note: other notations are similar as explained under equation (23).

Note: In general, the Froehlich equation is used to predict maximum abutment scour depth for design purposes. Therefore, the average depth (y_a) of flow is included as a factor of safety and HEC RAS always includes the average depth in the equation. When estimating scour depth for a particular flood event, it is recommended to subtract the average depth (y_a) manually.

In HEC RAS abutment scour depth prediction, all the parameters needed for equations are acquired directly from the 1D steady flow analysis by the hydraulic model, except the abutment shape and the skew angle correction factors. Furthermore, HEC RAS provides an option to users if they want to amend values of acquired parameters for particular cases.

5.6 LIMITATION OF HEC RAS BRIDGE SCOUR ANALYSIS

The HEC RAS bridge scour analysis has all the limitations that the HEC 18 scour manual specifies. Hence, it is more reasonable, and basically limited to, the application for uniform, non-stratified, and non-cohesive bed material. However, in reality, the conditions are often more complex. Furthermore, the hydraulic characteristics for the scour depth equations are derived from a 1D hydraulic model with steady flow conditions prevailing; but in the case of realistic bridge cross sections, the flow distribution is unsteady due to various roughness patterns and obstructions. The degree of uncertainty in the empirical equation should also be factored in when evaluating the HEC RAS model predictions. Time-varying scour depth analysis and scour rate predictions are not possible to perform through HEC RAS analysis.

CHAPTER 6- DATA EMPLOYED AND ANALYSIS

The input data are crucial in all hydrological modelling and the accuracy of data significantly impact the trustworthiness of the model output. Generally, data acquisition and validation are the biggest challenges for comprehensive studies. Often there is a need to obtain data from various sources and uncertainties may differ among the sources. This chapter summarizes the background of the data used for the local scour analysis. Figure 6.1 illustrates, the various data employed in the current study at different stages.

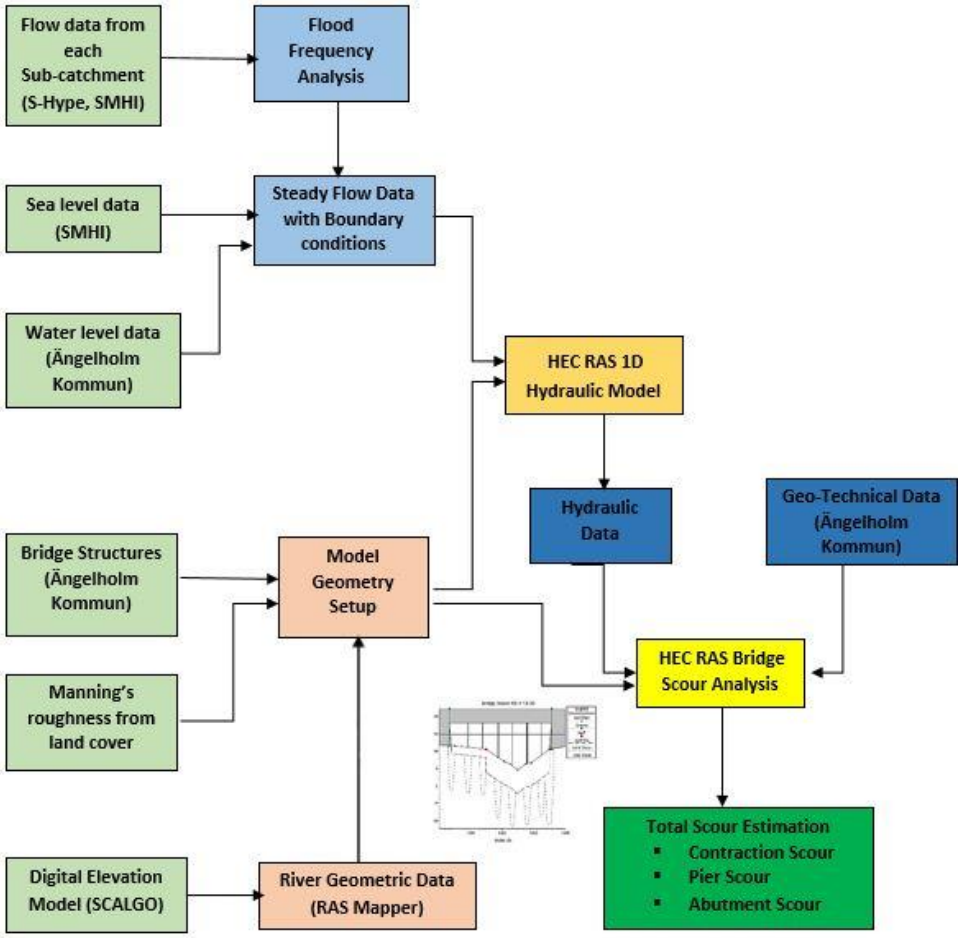

Figure 6.1: The flow chart of data usage at different stages in the scour analysis

6.1 WATER LEVEL

Since the studied river reach was close to the sea, it can be assumed that the water level in the sea could significantly affect the water level along the river, especially when the flow is low. The effect will be much higher in the downstream part of the river compared to upstream. The occurrences of strong winds change the water level frequently at the Skälderviken outlet, especially from the north-west, and minor tidal influences can also be observed (around 0.1 m). There were no continuous measurements at the Skälderviken outlet of water level variations; such information was vital for setting up the right boundary conditions for the analysis.

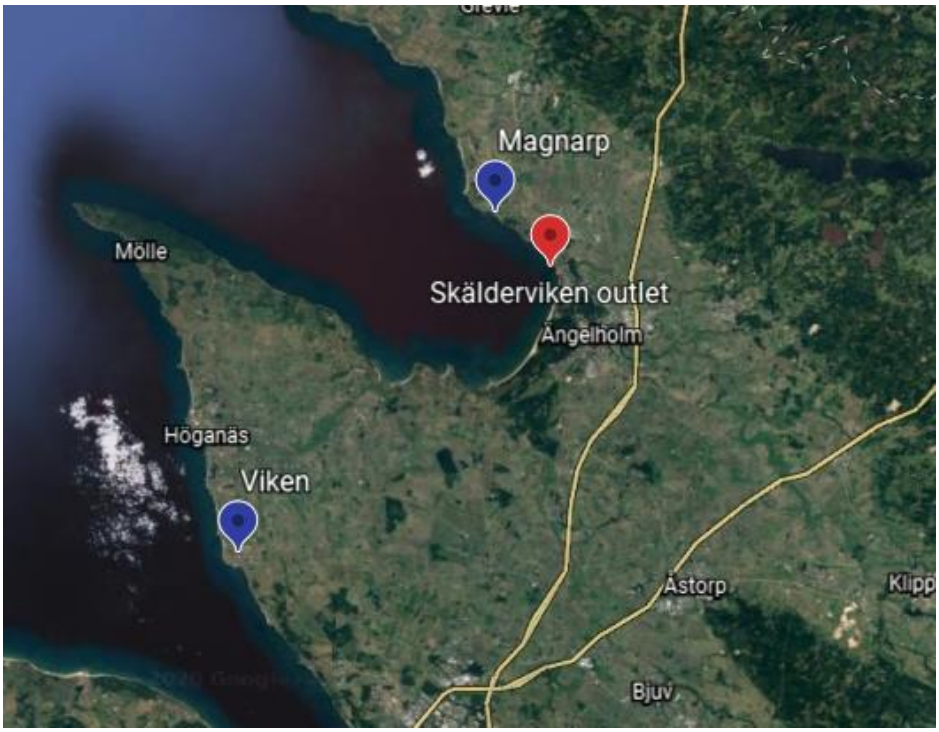

Figure 6.2.: The locations of the SMHI sea level measurement stations near the study area (Google Earth, 2020)

The closest active SMHI station to find sea level data was Viken station, located 20 km south of Skälderviken. Furthermore, there was a non-active SMHI station at Magnarp, which was around 4 km to the north of Skälderviken outlet, see figure 6.2. The water level data for Viken station was acquired

through the SMHI website for the period of 2010-2019 and was used for the analysis, see figure 6.3. The shorter series of measurements from the SMHI station at Magnarp (2011- 2014) was used for model calibration purposes, since it was much close to Skälderviken, see figure 6.4. Also, there were two measurement stations in the river called Pyttebron and Invallningen where water levels were recorded during certain periods by Ängelholm municipality. The Pyttebron station was around 4.6 km upstream from the coastal outlet, whereas Invallningen was just 1 km upstream of the coastal outlet. Because of the more upstream location, the Pyttebron measurements were less influenced by the sea level variations, also showing the effects of the flow; thus, more useful in the calibration and validation. In addition, the measurements at Invallningen exhibited quality as well as reliability issues.

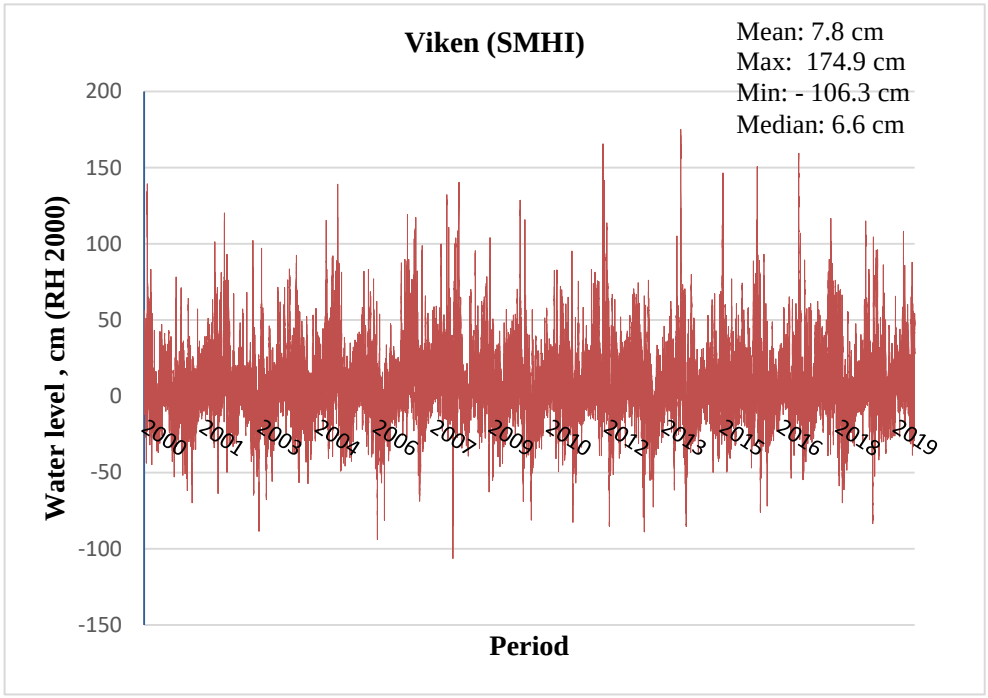

Figure 6.3: The sea level measurements for the Viken station by SMHI for the period of 2010 - 2019

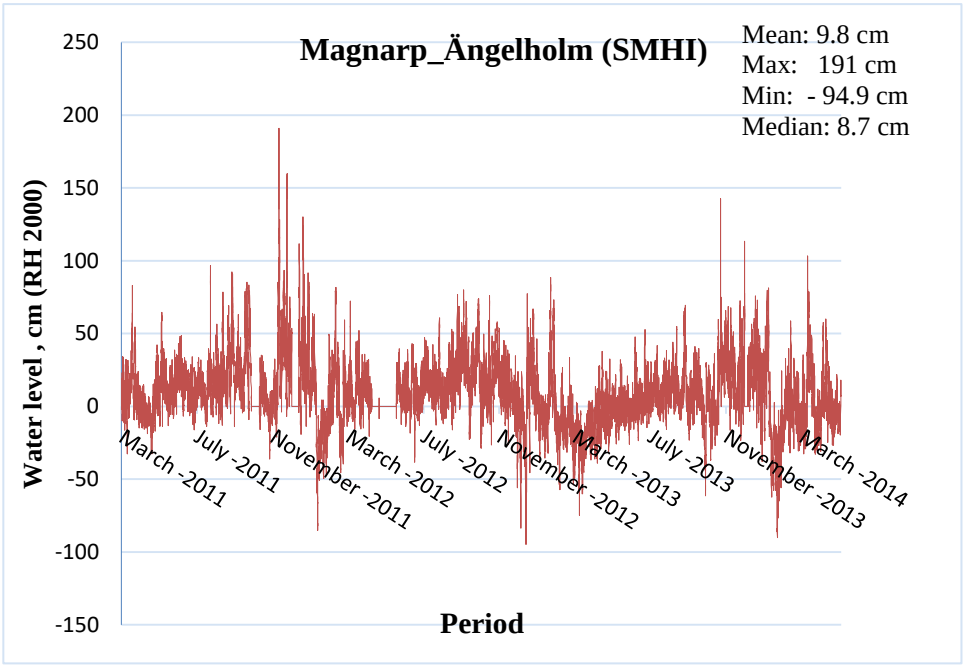

Figure 6.4: The sea level measurements for the Magnarp station by SMHI for the period of 2011 - 2014

6.2 RIVER FLOW

The bridge scour analysis using HEC RAS requires representative flow data for satisfactory model representation and calculation. According to HEC 18, bridge scour analysis is generally performed for 25, 50, 100, and 200 years return flood magnitudes. In this study, bridge scour analysis was carried out also for 2 and 10 years return flood frequencies to consider more current and less extreme erosion problems in the river section. The flow data for the study were derived from vattenwebb.smhi.se. The flow data were produced through the S-HYPE simulation model by SMHI in 2016 with a 25% average model uncertainty (SMHI, 2016). Since there were no measurement stations close to the study area, the flow values were obtained only through S-Hype model simulations. The closest station (Forsmöllan) was around 32 km upstream of the studied river reach. Therefore, these measurements cannot represent to the downstream reach and its flows.

As mentioned under section 4.1, the flow data were acquired for sub-catchments 541, 564, and 554. Table 6.1 shows the average and maximum flows (corrected values) for 2004-2019 for each river reach based on the sub-catchment flows.

Table 6.1: The flow data for river reaches, obtained through SMHI's S-HYPE model

River Reach	**564**		**541**		**554**	
Year	Annual average flow [m³/s]	Annual maximum flow [m³/s]	Annual average flow [m³/s]	Annual maximum flow [m³/s]	Annual average flow [m³/s]	Annual maximum flow [m³/s]
2004	4.83	29.7	19.8	112	24.7	140
2005	3.64	20.4	17.7	101	21.4	118
2006	4.29	20.5	20.0	115	24.3	133
2007	6.22	39.2	31.9	169	38.2	207
2008	4.85	25.9	21.8	59.1	26.7	69.9
2009	2.63	11.7	12.2	39.9	14.9	47.7
2010	3.79	22.6	13.4	64.9	17.3	78
2011	4.89	32.4	20.6	98.9	25.6	118
2012	5.33	29.2	18.6	94.0	24	114
2013	3.38	17.0	12.9	57.8	16.4	72.3
2014	4.05	21.1	19.9	89.2	24	105
2015	5.00	21.5	22.3	92.0	27.4	109
2016	2.92	16.1	15.0	62.2	18	77.5
2017	5.61	26.0	23.5	91.1	29.2	110
2018	2.41	19.0	13.2	67.1	15.6	82
2019	4.52	24.3	17.6	84.0	22.2	106

Note: All values were corrected in the S-Hype model by SMHI

Figure 6.5 shows the typical trend of river flood changes over the year with respect to the average flow for the year 2019, clearly displaying the seasonal variations. The maximum, minimum, and average flows of the main river for the 2004 -2019 period are 207 m^3/s, 2.4 m^3/s, and 23.1 m^3/s respectively.

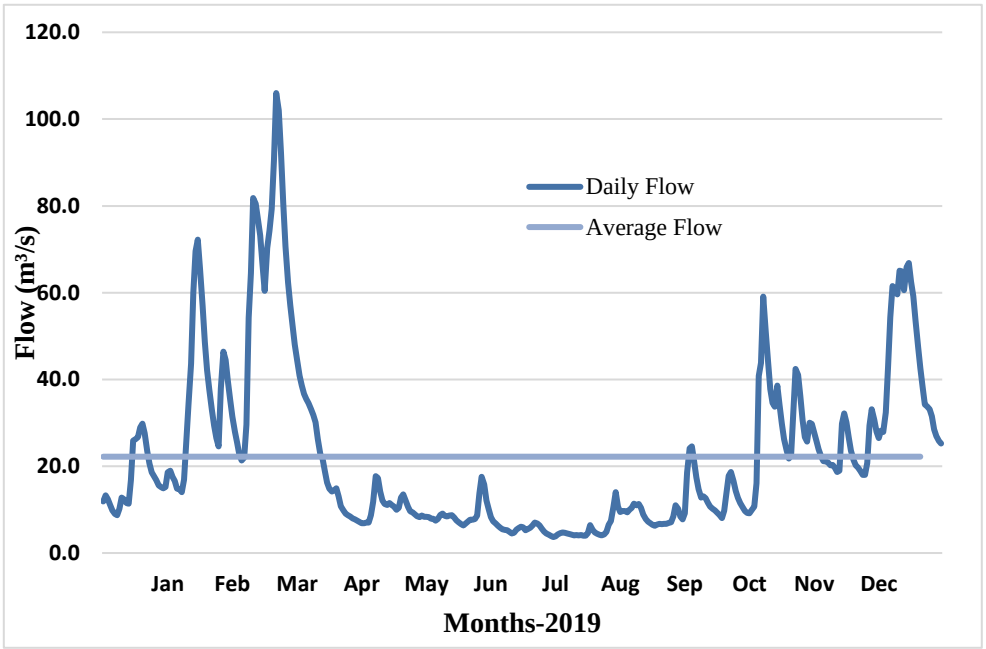

Figure 6.5: The river flow variations during year 2019 (Data from S-Hype model)

6.3 FLOOD FREQUENCY ANALYSIS (FFA)

Flood frequency analysis was done using the Gumbel distribution with Flood Frequency Factor using the Powell Method. Generally, when two rivers confluence as in the current study, one needs to develop a joint probability distribution for the annual maximum discharge pair on the river confluence, by using a copula function such as Gumbel-Hougard copula to the given flood events (Gilja, Ocvirk and Kuspilić, 2018). However, in this study for simplification, it was assumed that the two upstream reaches (541 and 564) have the same return simultaneous probability for a given extreme event. Thus, downstream (554) discharges were calculated by adding upstream (541 and 564) reach discharges for a given return period, since 564 reach contributed less to Rönne å river compared to the main reach.

For further justification, the flood frequency was performed for sub-catchment 554 too by using discharge flows obtained by the S-Hype model, and the error percentages were below 6% for several return periods. The flood frequency analysis results are given in Table 6.2. The complete flood frequency analysis method and data are given in Appendix 1.

Table 6.2: The predicted river flows for various return periods and comparisons between different approaches

Flood Frequency	Reach 541	Reach 564	Reach 554- by adding	Reach 554- by FFA	Error	Error %
QT2 (m^3/s)	82.3	22.4	104.7	99.4	5.3	5.4
QT10 (m^3/s)	127.1	32.4	159.5	153.7	5.8	3.8
QT25 (m^3/s)	149.6	37.4	187.0	181.0	6.1	3.4
QT50 (m^3/s)	166.3	41.2	207.5	201.2	6.3	3.1
QT100 (m^3/s)	182.9	44.9	227.8	221.3	6.4	2.9
QT200 (m^3/s)	199.4	48.6	248.0	241.4	6.6	2.7

In 2016, SMHI conducted a detailed flood mapping along Rönne å on behalf of Ängelholm municipality. The study was carried out for different scenarios. The value for a 100-year return period, in today's climate, combination with 25 years seawater levels in Skälderviken was 207 m^3/s. This is close to the 50-year return period flood according to FFA in the current study. The difference might be due to the S-Hype model uncertainties and/or statistical variations. However, in 2007 the maximum flood was noteworthy with 207 m^3/s and therefore the likelihood of occurrence of maximum flows again can be expected to be higher than before. Further, the FFA results indicated that the floods for 50-, 100-, and 200-year return period have a gentle increment as per Gumbel distribution**.** The flood exceedance probabilities for the above-mentioned return periods are calculated and given in Appendix 1.

6.4 BATHYMETRY AND TOPOGRAPHY

The river bathymetric data and topographic data were obtained through SCALGO Live. The data were produced by a river survey carried out from

October 2019 to April 2020 by MarCon Teknik AB (MTE) on behalf of Ängelholm municipality. The multibeam echo sounding technology was used for underwater bathymetry survey and LiDAR (Light Detection and Ranging) technology used for survey river slopes and bridges. They survey was performed along a 12-km river stretch from Skälderviken outlet to E6 bridge. The measurements were taken using the *SWEREF 99* (Swedish reference frame 1999) coordinate system. Furthermore, the elevation and depth data used in the present study were obtained based on the RH 2000 reference elevation plane with 1x1 m finer spatial resolution.

According to SGU, most of the river deposits are superimposed with fine sand over the bedrocks of sandstones and claystones. The latest MTE investigation (2020) concludes that some places in the river have exposed hard bottom layers with sandstones and clay stones. It is hypothesized as the reason for the development of deep scour holes in the bed in places where no built structures are located close to the holes.

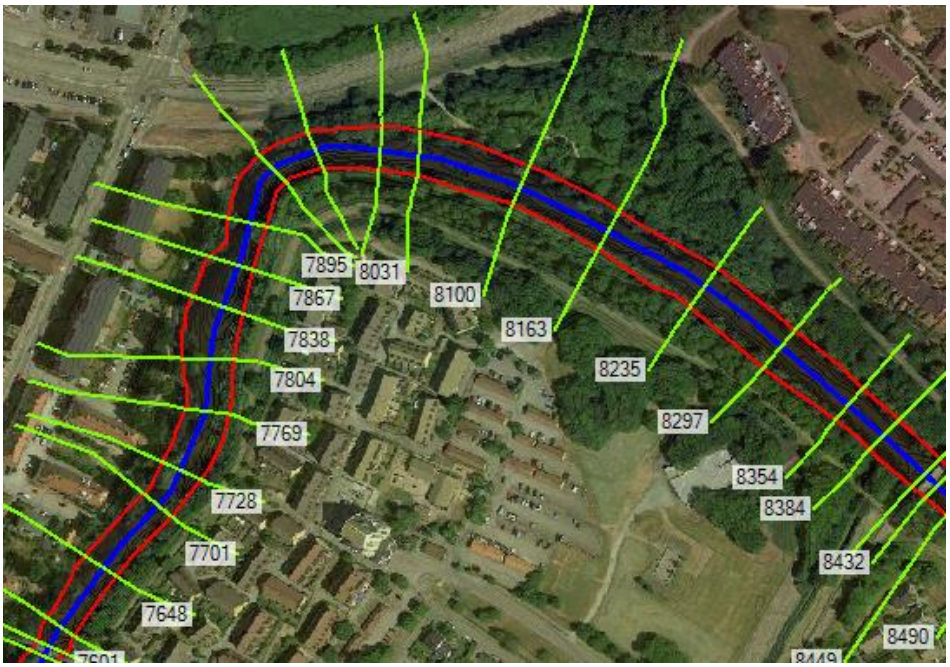

Figure 6.6.: A general view of constructed cross sections in part of Rönne å for model analysis (HEC RAS model)

For the HEC RAS model requirements, the river reach was divided into a number of cross-sections with the help of the RAS Mapper. There were 75 cross-sections drawn along the study reach considering meandering and river constrictions, natural or due to bridge structures. Figure 6.5 shows, a general view of the drawing of cross sections, and they were named with reference to the measuring distance (in meter) from the downstream end. Hence, the most upstream cross section is XS-11760 and the most downstream cross section XS-38 at Skälderviken outlet.

6.5 BOUNDARY CONDITIONS

Since the water flow is subcritical everywhere in Rönne å river, the HEC RAS model operates only with the downstream boundary conditions. The setup of the boundary condition may vary depending on the purpose of the study. To find maximum scour development, the boundary condition was the water level observation or estimation at Skälderviken outlet. To estimate water levels of the interest for Ängelholm municipality for flooding purposes, the average and the maximum sea levels were used as boundary conditions, see table 6.3.

Table 6.3.: The sea level used as boundary condition for different purposes.

Sea level	Data source	Purpose
-1.06 m	Min from Viken 2010-2019 data series (SMHI)	To find hydraulics characteristics for maximum scour potential
1.75 m	Max from Viken 2010-2019 data series (SMHI)	To find maximum levels for flooding purposes
0.08 m	Average from Viken 2010-2019 data series (SMHI)	To find average water levels in the river for flood management
0.36 , 0.5, 0.34 & 0.061 m	From Magnarp 2011-2014 data series (SMHI) for some representative flows	To calibrate the hydraulic model

6.6 BRIDGE STRUCTURES

There are 16 bridges crossing Rönne å river at various locations in Ängelholm municipality and most of them are located in the mid-part of the river stretch, see figure 6.6. Some bridges were built in the 1920s and still serve the municipality well.

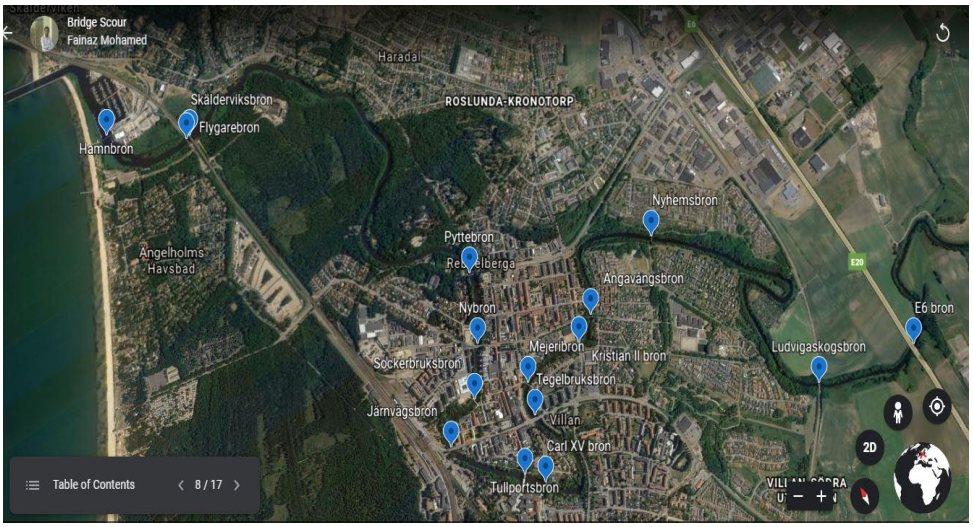

Figure 6.7.: The bridges crossing Rönne å in Ängelholm (Google Earth, 2020).

Most of the bridges cross the river perpendicularly, although some bridges are skewed to flow direction and expected to be more vulnerable to erosion conditions, for example Tegelbruksbron. The bridge geometric data were crucial in the present study; however, in some cases only a limited amount of bridge data were available. A general summary for the bridges are presented in table 6.4.

Table 6.4: Basic information about the bridges crossing Rönne å in Ängelholm

Location	Bridge name	Length	Year of construction	Construction Material
KP 0+970 m	Hamnbron	81 m	1970	Steel in combination with precast concrete

KP 1+575 m	Flygarebron	89.6 m	2010	Wood
KP 1+600 m	Skälderviksbron		2009	Reinforced concrete
KP 4+625 m	Pyttebron	45 m	1921	Steel
KP 5+000 m	Nybron	51.7 m	1971	Reinforced concrete
KP 5+275 m	Sockerbruksbron	34 m	1983	Reinforced concrete
KP 5+600 m	Järnvägsbron	45.7 m	1927	Reinforced concrete
KP 6+025 m	Tullportsbron	127.4 m	2015	Steel
KP 6+175 m	Carl XV bro	28 m	2005	Steel
KP 6+825 m	Tegelbruksbron	42 m	1964	Reinforced concrete
KP 7+015 m	Mejeribron	30 m	1970	concrete
KP 7+400 m	Kristian II bro	42.5 m	1966	Reinforced concrete
KP 7+560 m	Ängavångsbron	30 m	2009	Steel
KP 8+400 m	Nyhemsbron	30 m	1979	Reinforced concrete
KP 10+380 m	Ludvigaskogsbron			
KP 11+025 m	E6 bron			

Note: Some data were not available, KP denotes upstream from river outlet.

CHAPTER 7- LOCAL SCOUR MAPPING AND GEOMETRIC ANALYSIS

Through a thorough study of the bathymetry of the river bed and geometry, it was possible to find several bed anomalies along the studied 12-km river reach. Considering only the most extreme conditions of hole developments, the number of holes was limited 13 for the detailed evaluation and mapping, see figure 7.1.

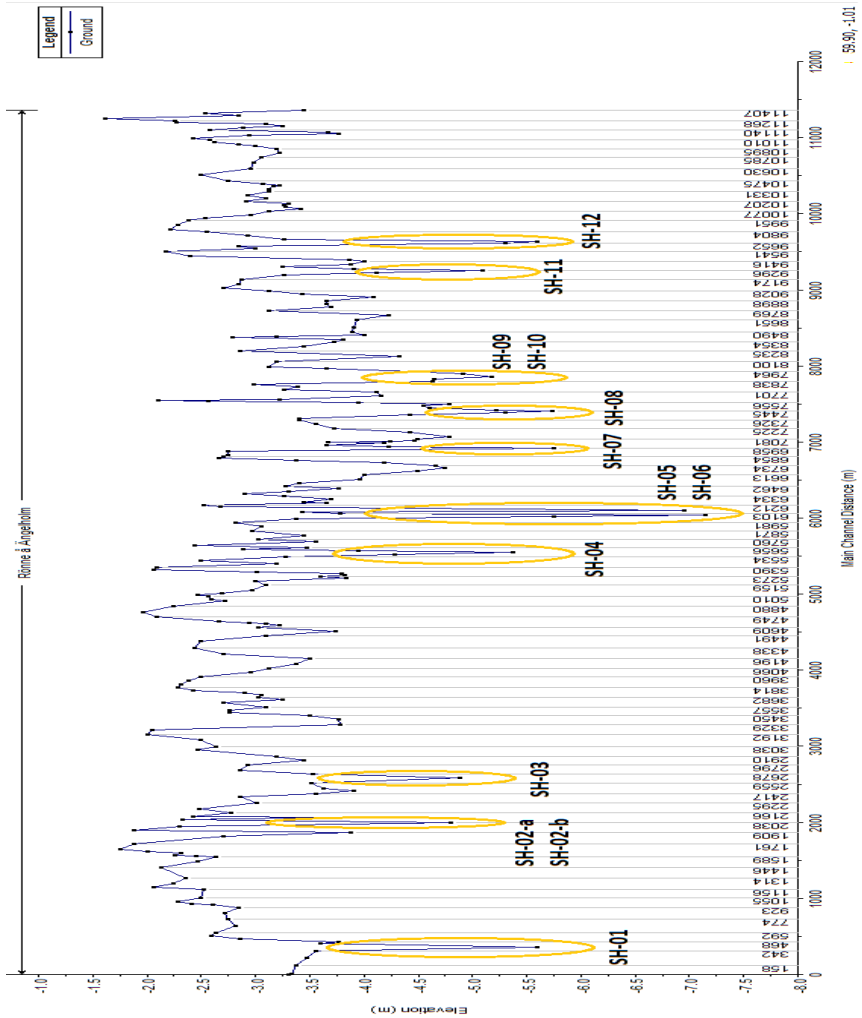

Figure 7.1.: The longitudinal river bed profile with possible scour holes along Rönne å river reach (from HEC RAS model)

The holes were characterized by the presumed controlling mechanism as bend scour, bridge scour, and general scour from abrupt changes in bed conditions (or a combination). Figure 7.2 illustrates an example of a scour hole geometry closed to Carl XV bridge; the visualization of the other holes is presented in Appendix 2. The technical evaluation of local scour holes are presented in table 7.1.

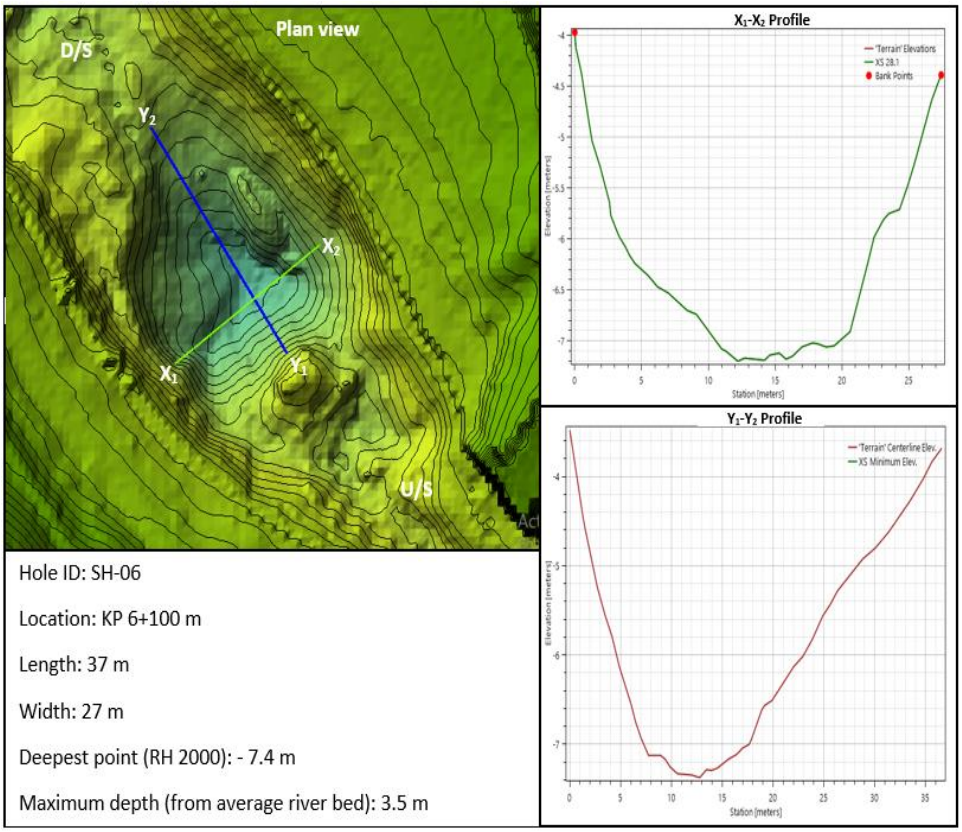

Figure 7.2: The scour hole geometry of SH-06, with sectional views, located downstream of Carl XV Bridge

Table 7.1: Technical evaluation of identified scour holes

Hole ID	Location	Deep hole geometry	General description	Possible causes
SH-01	KP 0+425 m	Length: 55 m Width: 18 m Deepest point (RH 2000): -5.6 m Maximum depth (from average river bed): 2.0 m	The scour hole is located on the concave side of the meander bend with a sinuosity 1.2. It is oriented towards the flow direction, and parallel to the banks.	High probability for bend scouring, where the deep hole is formed at the concave side where flow velocity and shear stress are high. (Refer figure 3.1 in chapter 3). A revetment was constructed at concave side that may also influence local scour conditions at the toe of the revetment. The entrance and exit points of the hole show some bed aggradation, may be due to sediment deposition, indicating possible Riffle-Pool sequences at the river bend. According to Keller (1971), the pool feature has more erosion and it can develop further by future effective flows. Thus, it requires continuous monitoring to understand its further developments, and requires geotechnical characteristics of the sediments for further conclusions.

SH-02-a	KP 2+025 m	Length: 41 m Width: 22 m Deepest point (RH 2000): - 5 m Maximum depth (from average river bed): 2.5 m	The scour hole is located middle of the flow path, directly downstream of a narrow river cross section and stretched towards the flow direction.	The narrow section at upstream of the hole is resistant for average flows and, possible for contraction scour at low flows. But the geometry of the hole shows that the upstream of the hole has steep slope compared to the downstream slope. It suggests the hole is influenced by a hard bottom feature at the entrance of the hole (upstream). A study is needed on the sediment characteristics for final conclusions on this.
SH-02-b	KP 2+025 m	Length: 16 m Width: 20 m Deepest point (RH 2000): -4.8 m Maximum depth (from average river bed): 2.3 m	The scour hole is located adjacent to SH-02-a hole in a wake region, formed by narrow section (refer to Figure 2.4.2). The hole is oriented perpendicular to the flow direction and has almost a circular planar shape.	The formation of strong wake vortices at the downstream side of the left bank embankment of the narrow section may the reason for the scour hole development. Furthermore, the lack of scouring at the upstream side of the narrow section indicates that upstream of the embankment the material is mostly cobble with consolidated rocks.
SH-03	KP 2+590 m	Length: 47 m Width: 17 m Deepest point (RH 2000): -4.9 m Maximum depth (from	The hole is located near a marshy land and centered towards left banks of the river section. The hole is	There are no bridge structures visible close to hole formation. Also, the hole is situated at a very gently curving bend; thus, is not much influenced by the bend.

		average river bed): 2.3 m	oriented towards the flow direction. In contrast to other scour holes, the downstream side of the hole has very steep slopes (V:H = 0.185) compared upstream side (V:H = 0.067).	Therefore the formation and development of this scour hole may markedly be influenced by the presence of hard non-erodible bottom down-stream of the scour hole and the geometry of hole provides some evidence for this. In addition, a small natural contraction upstream of the hole may have some influence too.
SH-04	KP 5+550 m	Length: 27 m Width: 17 m Deepest point (RH 2000): -5.83 m Maximum depth (from average river bed): 2 m	The hole is located 20m downstream from the Järnvägsbron bridge. It is centered at the concave side of the bend with a sinuosity of 1.2.	Even though the bridge creates more turbulences, the scour is possibly due to bend scouring and hard bottom features at the concave side of the bend, see the geometry in appendix 2. The bottom profile along the bridge also justifies the Järnvägsbron is not significant for long-term bridge scouring. The scour hole is located and significantly away from the bridge opening.
SH-05	KP 6+030 m	Length: 53 m Width: 30 m Deepest point (RH 2000): -7.2 m Maximum depth (from average river bed): 3.4 m	The hole is located right under Tullportsbron bridge and centered slightly towards the left bank from the middle of the river section.	In the vicinity of the bridge some sort of bridge scour is indicated, but due to lack of information on the bridge geometry it was not possible to estimate the importance of the bridge scour. The bridge embankments were placed well away

			The hole is oriented towards the flow direction. Furthermore, the upstream side of the hole has very steep slopes compared to the downstream side.	from the main river section, implying low influence from bridge scour. On the other hand, the hole geometry justifies the assumption that the bottom anomaly is due to local scouring down-stream hard bottom (low erodible rocks); see figure 3.3 and the hole geometry shown in appendix 2. It also stated in the MTE report (2020) the presence of hard rock sediments where the hole is located.
SH-06	KP 6+100 m	Length: 37 m Width: 27 m Deepest point (RH 2000): -7.4 m Maximum depth (from average river bed): 3.5 m	The hole is located 40 m downstream from the Carl XV bridge and centered in the middle of the river section. The hole is oriented towards the flow direction. The upstream side of the hole has very steep slopes (V:H = 0.5) compared to the downstream side (V:H = 0.2).	The significant distance from the bridge structure and the bed profile along the bridge indicate that the scour hole is very little influenced by the bridge structure. The formation and development of this scour hole may be heavily influenced by the presence of hard non-erodible bottom upstream the scour hole and the geometry of hole provides evidence of this. Reference is made to figure 3.3 and the hole geometry shown in appendix 2. However, further studies on sediments around the hole

				are required to make firm conclusions.
SH-07	KP 6+900 m	Length: 62 m Width: 10 m Deepest point (RH 2000): -5.95 m Maximum depth (from average river bed): 2.2 m	The scour hole is located on the concave side of the meander bend with a sinuosity of 1.4. It is extended and oriented towards the flow direction, and parallel to banks. Furthermore, the upstream side of the hole is slightly moved to the center of the section.	The hole formation is likely due to bend scouring, where the deep hole is formed at the concave side where flow velocities and shear stresses are high. (see figure 3.1 in chapter 2 and the hole geometry in appendix 2). The entrance and exit points of the hole shows some bed aggradation and therefore, possibilities for Riffle-Pool sequences at the river bend. However, it will require monitoring after several high and low flows with sediment analysis to draw firm conclusions about this. Since the center of the hole at the downstream side is moved towards the inner curve, it may be assumed that there is the presence of a hard layer, which also influences the scour hole formation together with the river bend.
SH-08	KP 7+380 m	Length: 72 m Width: 13 m Deepest point (RH 2000): -6.02 m	The scour hole is located exactly in the center of the meander bend with a	The significant distance away from the bridge structure, and the bed profile along the bridge, justifies the assumption

		Maximum depth (from average river bed): 1.5 m	sinuosity of 1.15. It is extended and oriented towards the flow direction, and parallel to banks. The downstream part of the hole is extended under Kristian II bridge and the deepest point is formed 20m away from the upstream bridge opening.	that the scour hole is little influenced by the bridge structure. The hard sediment bottom along the concave side of the bend may cause the orientation of the scour hole towards the center of the section; however, further studies about the geotechnical conditions are required at bend site.
SH-09	KP 7+740 m	Length: 57 m Width: 18 m Deepest point (RH 2000): -5.31 m Maximum depth (from average river bed): 2 m	The scour hole is located 75m downstream of a meander bend with a sinuosity of 1.2. The hole is extended and oriented towards the flow direction, and parallel to the banks. The hole is centered towards the middle of the river section with a steep slope (V:H = 0.16) at upstream side compared to the downstream side	Most likely, the hole formation is due to the hard bottom at the upstream side of the hole with a narrowing upstream section. The hole geometry justifies the hypothesized formation behavior. (See hole geometry in appendix 2).

			slope (V:H =0.065).	
SH-10	KP 7+800 m	Length: 40 m Width: 12 m Deepest point (RH 2000): -5.53 m Maximum depth (from average river bed): 1.3 m	The scour hole is located just downstream of a meander bend with a sinuosity of 1.2. The center of the hole is just 60m upstream of the hole SH-08. It is extended and oriented towards the flow direction and parallel to the banks. The hole is centered towards the middle of the river.	The hole formation is slightly offset from the high-stress area of the bend, showing some indication that the hole is not mainly influenced by the bend curve. The changes in flow direction and the erodibility of the sediments in the area may be a possible reason for the hole formation.
SH-11	KP 9+250 m	Length: 68 m Width: 12 m Deepest point (RH 2000): -5.11 m Maximum depth (from average river bed): 1.9 m	The scour hole is located at a meander bend with a sinuosity of 2.8. It is extended and oriented towards the flow direction, and parallel to the banks. The hole is centered towards the middle of the river with higher upstream slopes than downstream.	The hole formation is expected to be a results of bend scouring. The geometry of the hole shows some indication of the presence of hard rocks along the bend curve and shift the hole towards middle of the river in the river bend. (see hole geometry in appendix 2). Additional studies about geotechnical properties are required at the bend site for further conclusion.

SH-12	KP 9+600 m	Length: 88 m Width: 20 m Deepest point (RH 2000): -6.0 m Maximum depth (from average river bed): 2.9 m	The scour hole is located on the concave side of the meander bend with a sinuosity of 2.8. It is oriented towards the flow direction, and parallel to left bank. The left bank is much steeper than the right bank.	High probability for bend scour, where a deep hole is formed at the concave side where the flow velocity and shear stress are high (see figure 3.1 in chapter 3 and hole geometry in appendix 2). There are some bed aggradation at the upstream and downstream sides of the hole. It may be due to sediment deposition. There are indications that Riffle-Pool sequences are a dominant feature at the river bend. However, monitoring is required to understand its further developments.

CHAPTER 8- SIMULATIONS WITH HEC RAS

8.1 THE MODEL CALIBRATION & VALIDATION

The model was calibrated using the Magnarp sea level measurements and the Pyttebron water level measurements. It was calibrated by altering the Manning n values for selected higher flows of 2011 and 2012. The final Manning values for the main channel and the flood plains were 0.028 and 0.04 respectively. The higher flows were used because scouring is typically more critical when higher flows are encountered. Furthermore, the water level in the river is less effected by sea-level variation when the river flows are high. Later, the model was validated for higher flows of 2013 and 2014. Overall, the agreement between measured and modelled (HEC RAS) water levels was excellent for most flows. According to the calibration and validation results, particularly measured and modelled water levels for higher flows were in good agreement, see figure 8.1 and table 8.1. Besides, a flood map from SMHI for a 100-year flow and the flood map from HEC RAS for the same flow conditions were subjected to visual interpretation. The inundation areas correlated well, which

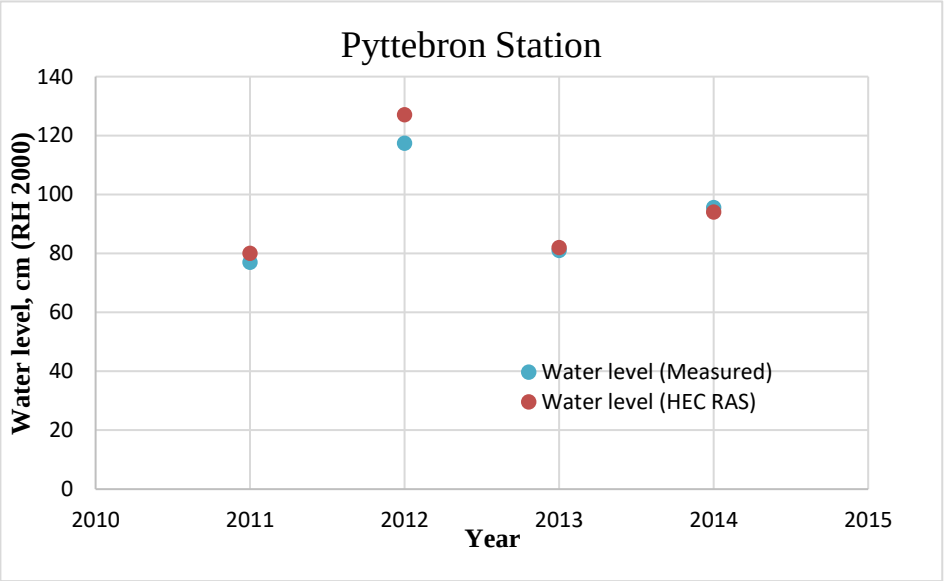

Figure 8.1.: The measured and modelled water level at Pyttebron for selected calibration and validation cases

provided extra validation to the model set up and calibration; the flood maps are presented in Appendix 2.

Year	Date	Flow-541 (m^3/s)	Flow-554 (m^3/s)	Magnarp water level(cm)	Pyttebron WL , cm (measured)	Pyttebron WL, cm (HEC-RAS calculated)	Error (cm)	Error %
2011	9/9/2011	53.6	73.2	36	77	80	3	4%
2012	6/1/2012	83.7	98.9	69	117.4	127	9.6	8%
2013	3/1/2013	57.8	72.3	34	81	82	1	1%
2014	12/1/2014	60.8	75.5	50.2	95.5	94	-1.5	-2%

Table 8.1.: The results from the calibration and validation cases

8.2 FLOOD LEVEL VARIATION

The model test run for different sea levels indicated that the water levels along the river reach were quite sensitive to sea-level variations. For the flood analysis purpose, the water levels along the river were simulated through HEC RAS steady flow model for minimum, average, and maximum sea-level conditions. Sea level measurements from the SMHI Viken station for the 2010-2019 period were used as boundary conditions. Figures 8.2, 8.3 and 8.4 illustrate how water level changes along the river stretch for different flow conditions when sea level is assumed at minimum (-1.06 m), average (0.08 m), and maximum (1.75 m) level, respectively. The figures show that for the higher flows, water levels at the upstream end of the river reach are quite stable irrespective of the sea-level variations.

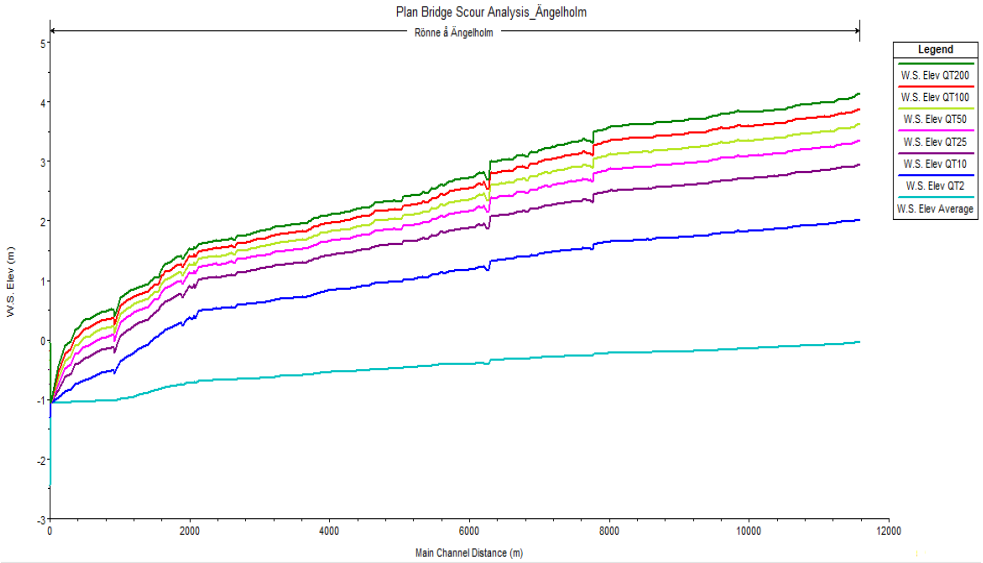

Figure 8.2.: The water level variation along Rönne å for different river flows when sea level is -1.06 m (minimum), HEC RAS.

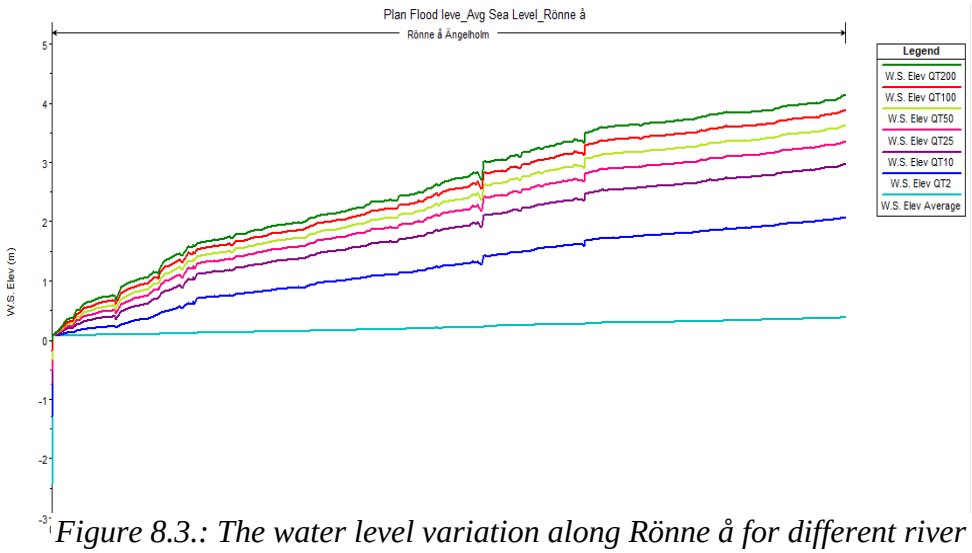

Figure 8.3.: The water level variation along Rönne å for different river flows when sea level is 0.08 m (average), HEC RAS.

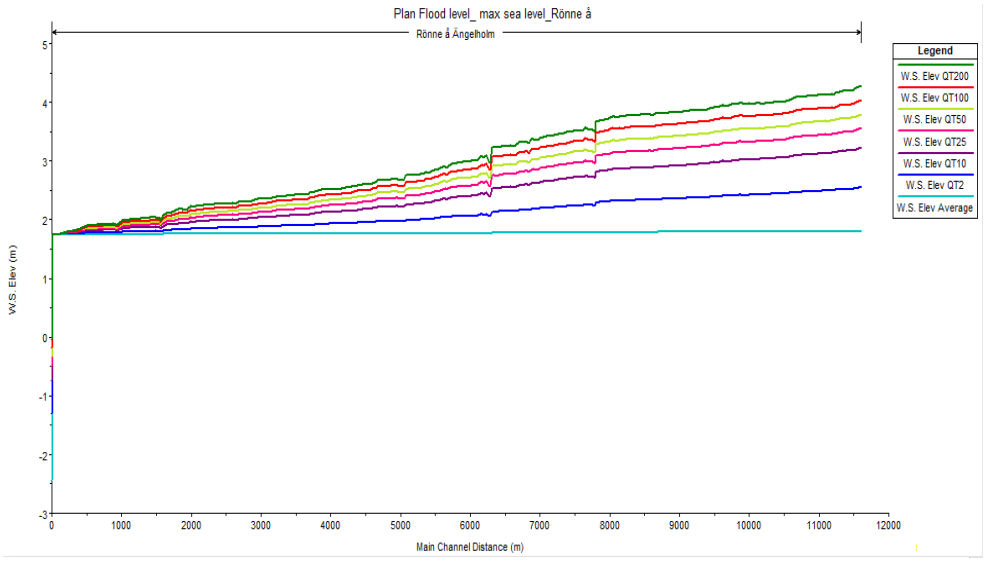

Figure 8.4.: The water level variation along Rönne å for different river flows when sea level is 1.75 m (maximum), HEC RAS.

8.3 THE HYDRAULIC CHARACTERISTICS

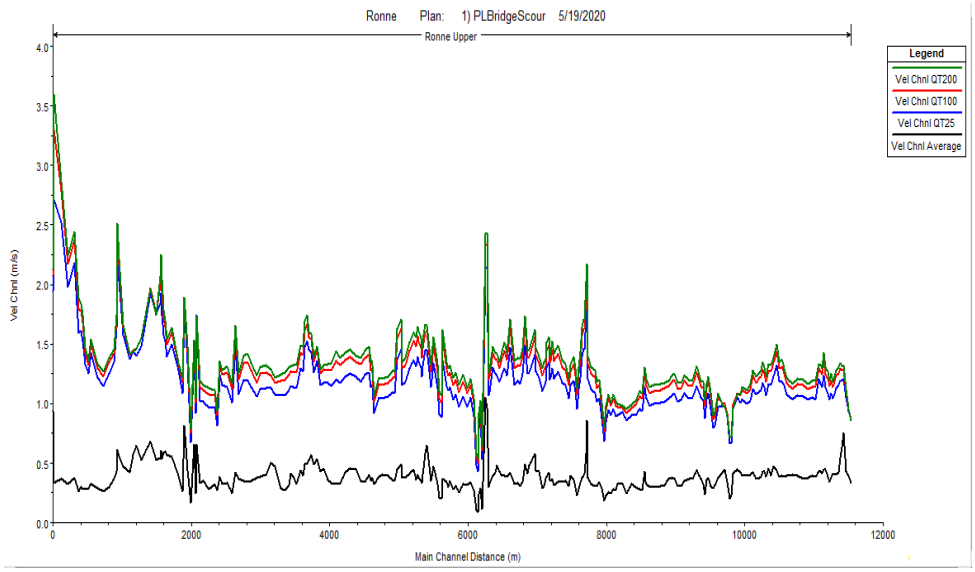

Figure 8.5.: The velocity variation along Rönne å for different river flows when sea level is -1.06 m (minimum), HEC RAS.

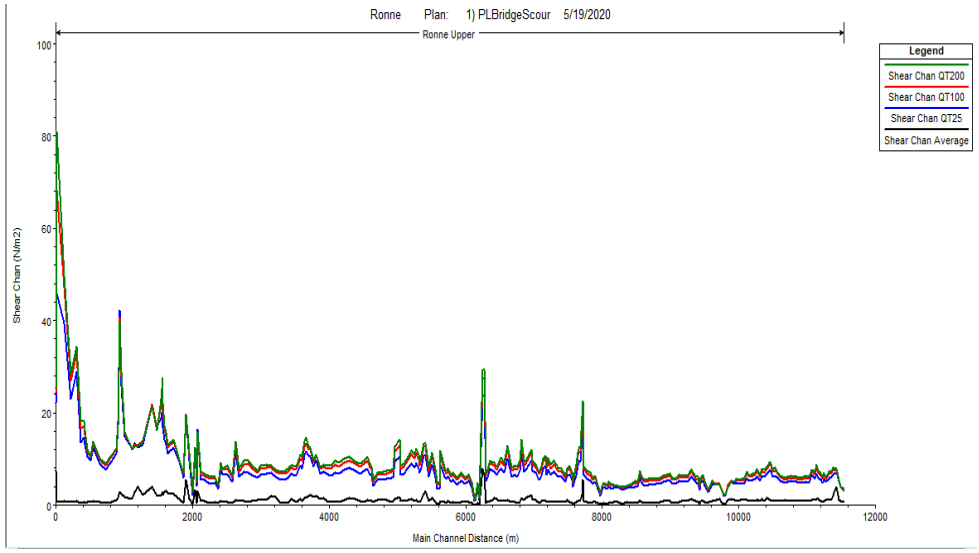

Figure 8.6.: The shear stress variation along Rönne å for different river flows when sea level is -1.06 m (minimum), HEC RAS.

The shear stress and velocity of the flows are key parameters for the sediment transport. HEC RAS model simulations were performed to obtain the flow velocity and shear stress for different return flows when sea level condition was minimum (-1.06 m), see figures 8.5 and 8.6, respectively. It is clear that higher flows increase the shear stress and velocity, enhancing the erosive power of the stream. Furthermore, minimum sea level tends to increase the velocity and the shear stress in the river, particularly in the lower part of the studied reach.

Furthermore, the shear stress and flow velocity upstream of the identified scour holes were analyzed and the results for 100-year return flow and average flow are given in table 2. The values were obtained when sea level was at the minimum (-1.06 m) condition.

Table 8.2.: The flow velocity and shear stress upstream of the scour holes

Location	Hole ID	QT100	Average flow	QT100	Average flow
		Velocity (m/s)	Velocity (m/s)	Shear Stress (N/m^2)	Shear Stress (N/m^2)

KP 0+425 m	SH-01	1.77	0.29	17.12	0.55
KP 2+025 m	SH-02-a	1.2	0.52	7.98	1.83
KP 2+025 m	SH-02-b	1.2	0.52	7.98	1.83
KP 2+590 m	SH-03	1.48	0.38	11.15	0.92
KP 5+550 m	SH-04	1.54	0.36	10.72	0.77
KP 6+030 m	SH-05	0.88	0.23	3.5	0.33
KP 6+100 m	SH-06	2.33	1.05	27.5	7.84
KP 6+900 m	SH-07	1.32	0.37	7.73	0.81
KP 7+380 m	SH-08	1.36	0.33	7.9	0.61
KP 7+740 m	SH-09	0.99	0.25	4.16	0.32
KP 7+800 m	SH-10	0.98	0.24	4.05	0.32
KP 9+250 m	SH-11	1.13	0.36	5.51	0.79
KP 9+600 m	SH-12	0.99	0.41	4.33	1.11

8.4 BRIDGE SCOUR SIMULATION FROM HEC RAS

There were six bridges (out of 16) where it was possible to analyze bridge scour using the HEC RAS model; the other bridges could not be investigated due to limited available bridge geometry data. When studying the scour holes identified in chapter 7, there were not any of analyzed bridges that seemed to have major impact on the observed scour holes. However, these six bridges were still analyzed in order to get some information regarding potential bridge scouring for high flows. This is useful in order to understand possible threats to the bridge structures. Furthermore, HEC RAS bridge scour analysis were

also carried out to estimate contraction scour and abutment scour. Among the six bridges, only bridge Järnvägsbron has piers and equations for estimating pier scour are heavily dependent on sediment characteristics. Therefore, due to lack of proper sediment information for the modeling, pier scour was not investigated through the HEC RAS analysis.

8.4.1 CONTRACTION SCOUR ESTIMATION

The HEC RAS bridge scour simulation shows that generally, abutment scour is more dominant than contraction scour at the tested bridges. Figure 8.7 illustrates the estimated contraction scour depth at the bridges for different return floods (from frequency analysis). Kristian II Bridge has a higher contraction scour problem for higher flows than the other bridges. In Appendix 2, a table is presented with the complete scour results.

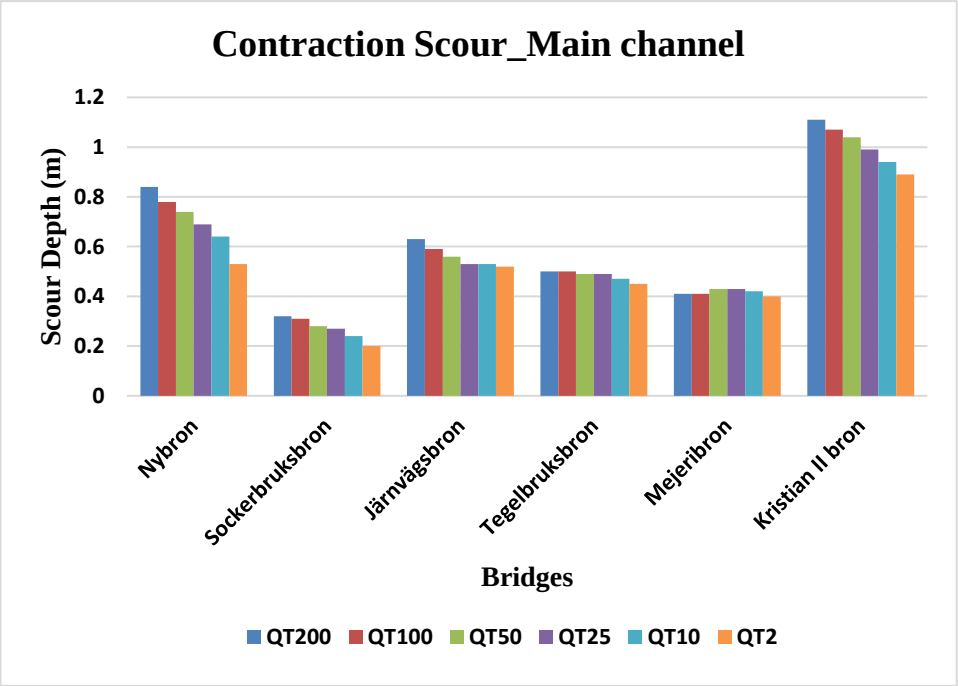

Figure 8.7.: The estimated contraction scour depth at the bridges through HEC RAS analysis

8.4.2 ABUTMENT SCOUR ESTIMATION

The abutment scour depth for the studied return year floods was estimated through the HEC RAS model for each bridge and the results are presented in figures 8.8, 8.9, 8.10, 8.11, 8.12 and 8.13. Please note that as mentioned in section 4.5.2, the Froehlich equation includes the average depth of the flow for considering a factor of safety. Therefore, the scour depths were manually adjusted for particular flood events (refer to section 4.5.2). Furthermore, in Appendix 2, a table is presented with complete scour results and an example of the output file of HEC RAS bridge scour analysis. Attached is also the input hydraulic parameters from the 1D steady flow model.

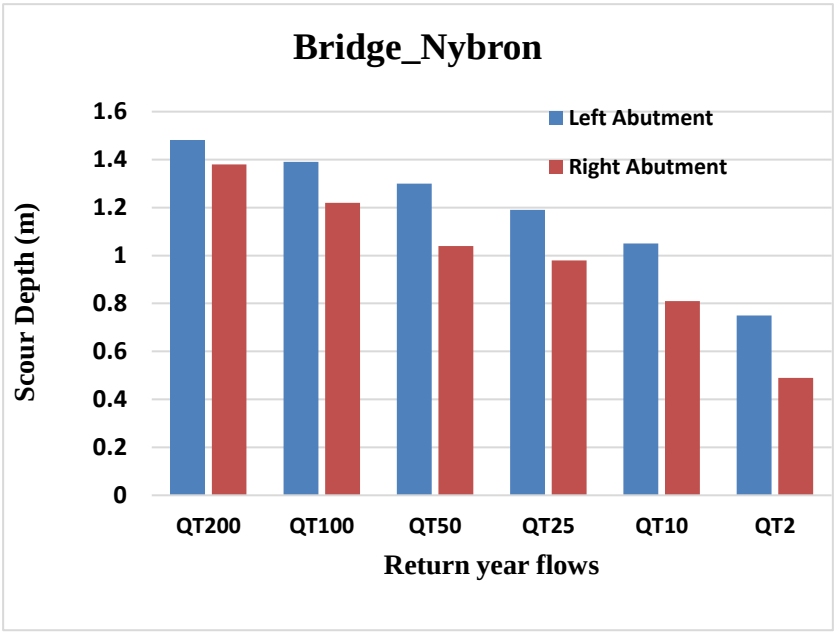

Figure 8.8.: The estimated abutment scour depth for bridge Nybron

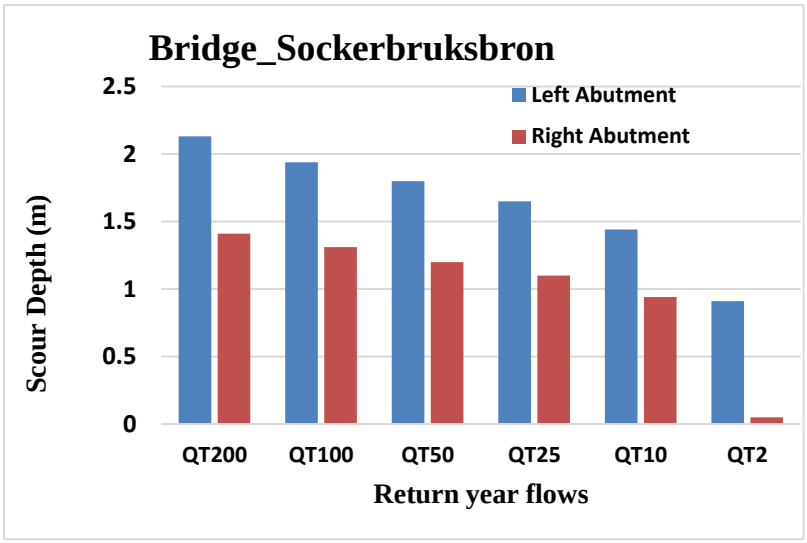

Figure 8.9.: The estimated abutment scour depth for bridge Sockerbruksbron

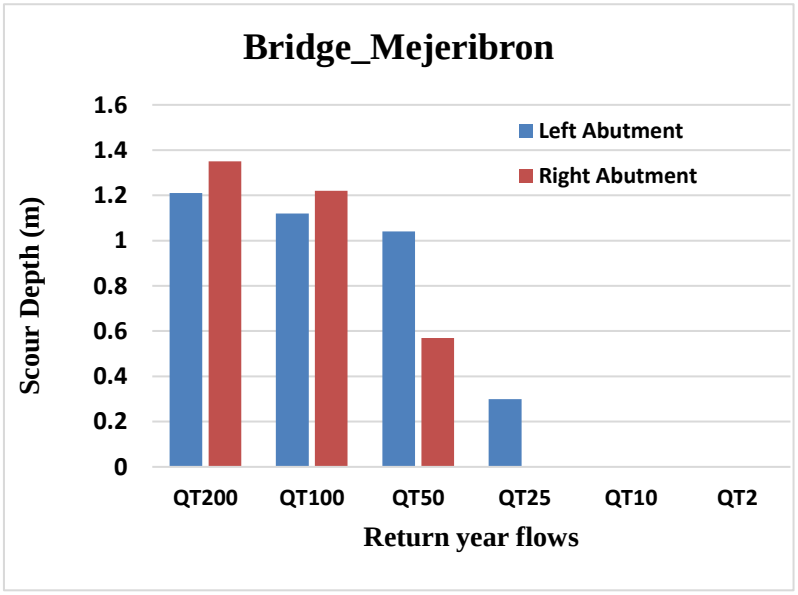

Figure 8.10.: The estimated abutment scour depth for bridge Mejeribron

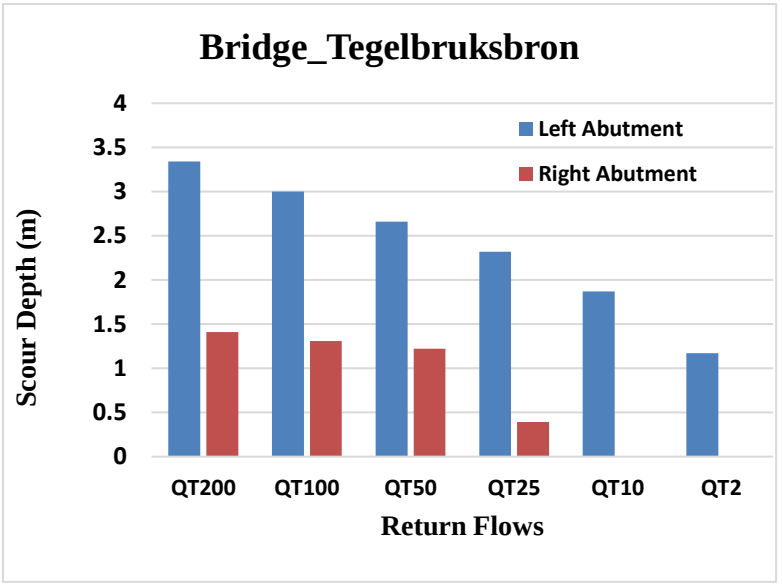

Figure 8.11.: The estimated abutment scour depth for bridge Tegelbruksbron

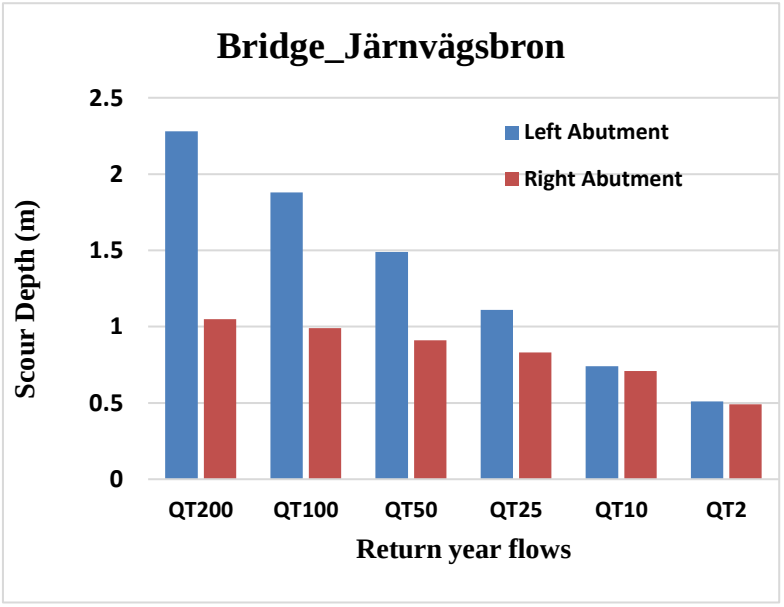

Figure 8.12.: The estimated abutment scour depth for bridge Järnvägsbron

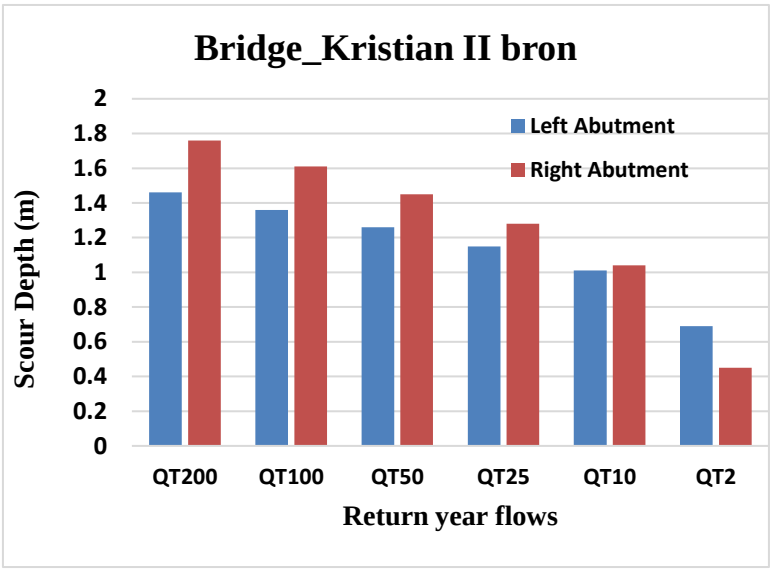

Figure 8.13.: The estimated abutment scour depth for bridge Kristian II bron

According to the figures, the bridge Tegelbruksbron has the highest vulnerability to abutment scour; in addition, the left abutment is more vulnerable than the right abutment.

CHAPTER 9- ASSESSMENT OF LOCAL SCOUR

9.1 BATHYMETRIC ANALYSIS

The bathymetric analyses revealed that the Rönne å river reach at Ängelholm experiences unusual river bed anomalies. Furthermore, there were many scour holes spread out along the river reach of different magnitudes. Even though, only 13 holes were analyzed in this study, there are many smaller scour holes that exist at different locations. In general, most of the scour holes were attached to the river bends, since the river has many meander bends. The riffle pool sequences was also a common geomorphological feature at the bends. In addition, there were several holes developed due to different sediment conditions present in the riverbed. Some hole geometries justify the hypothesis of scour holes being developed downstream of the non-erodible river bottom. However, this study found that a comprehensive sediment analysis is required at different locations for further understanding of the scour hole developments. Most of the analyzed holes are not markedly influenced by bridge structures, since the holes typically were located significant distances away from the structures.

9.2 HEC RAS SCOUR ANALYSIS

The HEC RAS hydrodynamic model results state that the sea level can significantly affect the hydraulic characteristics of the river. Therefore, the backwater flows could reduce shear stress and velocity of water in the river, and can make hindrance to sediment transport from upstream to downstream when low flow conditions (Arneson et al., 2012). Moreover, the sea-level data from Viken (2010-2019) and Magnarp (2011-2014) shows there are big fluctuations exist in water level at Skälderviken bay, and backwater flow is common for certain conditions. Therefore, it can suspect that the backwater flow causes unstable sediment transportation in the river stretch. Thus, it can assume the scouring at high flows and backfilling at low flows aren't smooth process along the river in long term considerations.

The bridge scour analyses through HEC RAS suggests that contraction scour was a smaller problem for the tested bridges compared to abutment scour. Furthermore, the bathymetric analysis around bridge structures also indicated that contraction scour was not significant at the bridges. However, a common feature at many bridges was that just inside of the upstream bridge openings

sediment aggradation occurred. These characteristics may also suggest some lower likelihood for heavy long-term contraction scour at bridges. However, a study should be performed about the flow conditions when the survey was done for further understanding of the sediment transport mechanisms.

According to the riverbed profile under the bridges, the bridge Mejeribron has around 1 m bed lowering at both the upstream and downstream end of the bridge with sediment pile up inside the bridge. However, the bridge is located in a bend, therefore it could be assumed that the severity of the particular bottom erosion probably is due to the influence of bend characteristics. Kristian II Bridge has the highest bed lowering in front of the bridge with 1.4 m. As mentioned in chapter 7, there was an identified scour hole (SH-07) located just upstream of the bridge in a bend with a sinuosity of 1.15. The deepest point of the SH-07 hole was located 20 m upstream to the bridge opening. However, HEC RAS simulation results indicated that the Kristian II Bridge has a higher contraction scour problem for high flows than the other bridges.

According to the HEC RAS results, the bridge Tegelbruksbron has the highest vulnerable to abutment scour; in addition, the left abutment is more vulnerable than the right abutment. The consultancy report by MTE (2020) also stated that there are some severe cracks obtained in the wing walls of the left abutment, see Appendix 2. Therefore, the results indicate that the cracks may have developed due to abutment scouring during previous high flows. Overall, the HEC RAS model shows that all the tested bridges have some threats from abutment scouring and that the degree of threat is larger when the flow is high. Furthermore, among six bridges only bridge Järnvägsbron has piers and due to lack of information, pier scour was not tested through HEC RAS analysis.

Overall, as mentioned in chapter 2 section 2.6, the HEC RAS results are good in the initial assessment stage to differentiate high-risk and low-risk bridges for more detailed bridge scour evaluation. However, it is good to remember that HEC RAS may overestimate the results when sediment properties are cohesive. Since there were not enough detailed information on geotechnical characteristics of the river bed available during this study, it is recommended to redo the calculations when such information has been obtained. Finally, it could have been better if site visits were conducted to observe bridges and abutments for visual evidences of scour problems. Then, it would have been possible to perform more useful comparisons with the forecasted results.

However, due to the Corona pandemic the options were rather limited regarding field visits.

9.3 UNCERTAINTIES OF RESULTS

It is useful to understand the uncertainties involved in the model study. As discussed in chapter 6, the flow data was acquired through the S-Hype model used by SMHI that includes a certain degree of uncertainty. These errors could affect the flood frequency analysis. Including the flow data, there were few options available to validate the data that were used in this study. The hydrodynamic model were calibrated against measured water levels using the high flow events; thus, the model results can with some confidence reproduce high flows. Moreover, as discussed in section 5.2, the HEC RAS 1D model includes governing equations with several assumptions and simplifications. However, the dynamic nature of the flows may in some cases be much more complex than steady-state conditions. Finally, the lack of geotechnical data was another major constraint for the study.

CHAPTER 10- CONCLUSIONS

The focus of the report was to explore the local scour in the downstream stretch of Rönne å that flows through Ängelholm municipality. The initial hypothesis was the large scour holes developed due to bridge scour problems. In contrast, this study has indicated that the available deep scour holes have developed mainly by general scour mechanisms, such as bend scour and the presence of hard non-erodible river bottom. In the study it was possible to map local scour holes and obtain a reasonable understanding of causes for the scour.

Despite many limitations, the hydrodynamic model developed in HEC RAS for Rönne å was robust and reliable for understanding the hydraulic behavior of the river. The HEC-RAS model satisfactorily simulated the water levels for the various flows within the study river reach; thus, the model simulations may provide a good estimation for local scour as well as for inundation purposes.

The HEC RAS bridge scour analyses for six bridges shows that the bridges exhibit more threats from abutment scour than contraction scour. The bridge Tegelbruksbron has the highest susceptibility to abutment scour, especially at the left abutment. Similarly, Kristian II Bridge has the highest threat from contraction scour among the tested bridges. Furthermore, the results could give a fair estimation of potential threats to bridge structures and may give initial suggestions for future investigations. Model simulations could also be used for assessing the impact due to increases in the flow caused by climate change.

Finally, as a recommendation, it would be good to perform a river bed sediment analysis along the studied river reach; especially including locations of bridges and locations of identified scour holes. It would give better background information for the detailed scour hole analysis.

REFERENCES

Almström, B., 2010. Översiktlig analys av översvämningsrisk och erosion längs Rönne å i Ängelholms kommun, SWECO (in Swedish).

Ängelholm Municipality, 2020.

Ansari S A, Kothyari U C and Ranga Raju K G 2002. Influence of cohesion on scour around bridge piers. J. Hydraul. Res. 40(6): 717–729

Arneson, L. A., Zevenbergen, L. W., Lagasse, P. F., and Clopper, P. E. (2012). Evaluating scour at bridges, 5th Ed. Hydraulic Engineering Circular No. 18 (HEC-18), Federal Highway Administration, Washington, DC.

Björn, H. and Berggreen-Clausen, S., 2016. Detaljerad översvämningskartering längs Rönne å – uppdatering, SMHI.

Briaud, J.L., H.C. Chen, K.A. Chang, S.J. Oh, S. Chen, J. Wang, Y. Li, K. Kwak, P. Nartjaho, R. Gudaralli, W. Wei, S. Pergu, Y.W. Cao, and F. Ting, 2011, "The Sricos – EFA Method" Summary Report, Texas A&M University.

Briaud J L, Chen H C, Li Y and Nurtjahyo P 2004 SRICOS EFA method for complex pier in fine-grained soil. J. Geotech. Geoenviron. Eng. 130 (11): 1180–1191

Brunner, G. W. (2016). HEC-RAS River Analysis System: User's Manual, Version 5.0, US Army Corps of Engineers, Institute for Water Resources, Hydrologic Engineering Center.

Directives.sc.egov.usda.gov. 2020. [online] Available at: <https://directives.sc.egov.usda.gov/OpenNonWebContent.aspx?content=17811.wba> [Accessed 17 April 2020].

Ettema, R., Yoon, B., Nakato, T. and Muste, M., 2004. A review of scour conditions and scour-estimation difficulties for bridge abutments. *KSCE Journal of Civil Engineering*, 8(6), pp.643-650.

Ghodsian, M. and Mousavi, S.K., 2004. Scour around a spur dike at a 90^{o} bend. In *Proceedings 2nd International Conference on Scour and Erosion (ICSE-2). November 14.–17., 2004, Singapore*.

Gilja, G., Ocvirk, E. and Kuspilić, N., 2018. Joint probability analysis of flood hazard at river confluences using bivariate copulas. *Journal of the Croatian Association of Civil Engineers,* 70(04), pp.267-275.

Google Earth. 2020. *Overview – Google Earth*. [online] Available at: <https://www.google.com/earth/> [Accessed 22 March 2020].

MTE (2020). Sjömätningsrappport, Ängelholms Kommun. Skälderviken och Rönne å. Rapport Rönne å, Ängelholms Kommun, Projektnummer 181019, MarCon Teknik AB, Malmö (in Swedish).

Keller, E.A., 1971. Areal sorting of bed-load material: the hypothesis of velocity reversal.

Kimiaghalam, N., Clark, S. and Ahmari, H., 2016. An experimental study on the effects of physical, mechanical, and electrochemical properties of natural cohesive soils on critical shear stress and erosion rate. *International Journal of Sediment Research*, 31(1), pp.1-15.

Kirby, A.; Roca, M.; Kitchen, A.; Escarameia, M.; Chesterton, O. Manual on Scour at Bridges and Other Hydraulic Structures; CIRIA: London, UK, 2015; ISBN 0860177475.

Macky, G.H. Survey of Roading Expenditure due to Scour; CR 90_09; Department of Scientific and Industrial Research, Hydrology Centre: Christchurch, New Zealand, 1990.

Melville B M and Coleman S E 2000 Bridge Scour. Water Resources Publication, Littleton, pp. 550.

Melville B W 1997 Pier and abutment scour: integrated approach. J. Hydraul. Eng. 123(2): 125–136

Melville B W 1975 Local scour at bridge sites. Ph.D. Dissertation. University of Auckland, School of Engineering, New Zealand.

Namaee, M. and Sui, J., 2019. Local scour around two side-by-side cylindrical bridge piers under ice-covered conditions. *International Journal of Sediment Research*, 34(4), pp.355-367.

Nemry, F.; Demirel, H. Impacts of Climate Change on Transport: A focus on road and rail transport infrastructures. Eur. Comm. Jt. Res. Cent. (JRC), Inst. Prospect. Technol. Stud. **2012**. Available online: ftp://s-jrcsvqpx101p.jrc.es/pub/EURdoc/JRC72217.pdf (accessed on 14 April 2020).

Park, S., Hwang, J. and Ahn, J., 2019. Physical Modeling of Spatial and Temporal Development of Local Scour at the Downstream of Bed Protection for Low Froude Number. *Water*, 11(5), p.1041.

Park, S.W. Experimental Study of Local Scouring at the Downstream of River Bed Protection. Ph.D. Thesis,

Seoul National University, Seoul, Korea, 2016.

Pizarro, A., Manfreda, S. and Tubaldi, E., 2020. The Science behind Scour at Bridge Foundations: A Review. *Water*, 12(2), p.374.

Rambabu M, Narasimha Rao S and Sundar 2003. Current induced scour around a vertical pile in cohesive soil. Ocean Eng. 30(4): 893–920

Salmela, J., Kasvi, E., Vaaja, M., Kaartinen, H., Kukko, A., Jaakkola, A. and Alho, P., 2020. *Morphological Changes And Riffle-Pool Dynamics Related To Flow In A Meandering River Channel Based On A 5-Year Monitoring Period Using Close-Range Remote Sensing*.

Scalgo.com. 2020. *SCALGO Live Global*. [online] Available at: <http://scalgo.com/live/> [Accessed 2 April 2020].

Sgu.se. 2020. *Geologiska Data*. [online] Available at: <https://www.sgu.se/produkter/geologiska-data/> [Accessed 30 April 2020].

Shafai-Bejestan, M., Mahmoodi, S. and Soozepour, A., 2016. Floating vanes for bend scour control. *River Flow 2016*,.

Shen H W, Schneider V R and Karaki S 1969 Local scour around bridge piers. J. Hydraul. Div. ASCE 96(6): 1919–1940

Smhi.se. 2020. *Ladda Ner Oceanografiska Observationer | SMHI*. [online] Available at: <https://www.smhi.se/data/oceanografi/ladda-ner-oceanografiska-observationer#param=seatemperature,stations=all> [Accessed 10 April 2020].

Smhi.se. 2020. *Ladda Ner Oceanografiska Observationer | SMHI*. [online] Available at: <https://www.smhi.se/data/oceanografi/ladda-ner-oceanografiska observationer#param=seatemperature,stations=all> [Accessed 10 April 2020].

Soulsby, R., 1997. Dynamics of Marine Sands. London: Thomas Telford, pp.99-108.

STATE OF FLORIDA DEPARTMENT OF TRANSPORTATION (FDOT) (2005) "Bridge Scour Manual.", FLORIDA.

Vattenatlas.se. 2020. *Vattenatlas.Se*. [online] Available at: <https://vattenatlas.se/> [Accessed 25 April 2020].

Vattenwebb.smhi.se. 2020. *Vattenwebb - Modelldata Per Område*. [online] Available at: <https://vattenwebb.smhi.se/modelarea/> [Accessed 15 March 2020].

Zhang, G., Hsu, S., Guo, T., Zhao, X., Augustine, A. and Zhang, L., 2013. Evaluation of Design Methods to Determine Scour Depths for Bridge Structures. pp.28-32.

Appendix 1

1.1 The geological map of Ängelholm

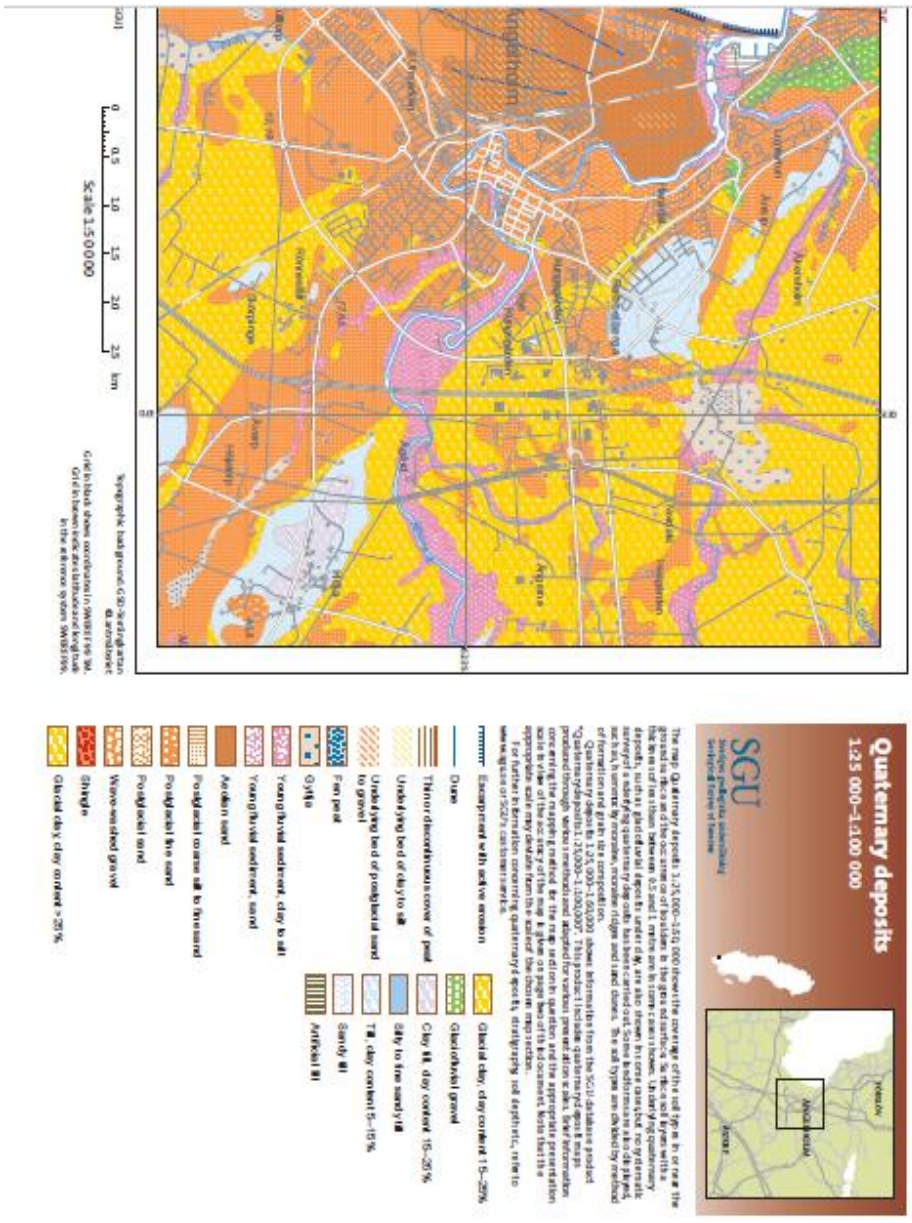

Figure 1.1: The geological map of Ängelholm (from SGU)

1.2 Flood Frequency Analysis (FFA)

FFA was performed using Gumbel distribution with a flood frequency factor using the Powell method. Following equations are used to determine the statistical factors.

$QT = Qav + KT\ SQ$

Where : QT = Value corresponding to T-year flood
Qav = average value of the data series (maximum value series)
SQ = standard deviation of the data series (maximum value series)
KT = frequency factor

$KT = -0.7797\ \{\ \Gamma + \ln [\ln (T/(T-1))]\}$ (Powell method)

$\Gamma = 0.5772$ (Euler's constant)

$KT = -0.7797\ \{0.5772 + \ln [\ln (T/(T-1))]\}$

Table 1.1: The maximum flow data obtained through the S-Hype model and FFA for sub-catchment 541

Date	Max Flow (m^3/s)
2009-11-20	39.9
2013-01-02	57.8
2008-03-07	59.1
2016-01-31	62.2
2010-03-23	64.9
2018-01-04	67.1
2019-03-18	84.0
2014-12-23	89.2

Sub Catchment 541

T (years)	K_T	Qav	S_Q	Q_T (m^3/s)
2.0	-0.164	87.3	30.5	82.3
10.0	1.305	87.3	30.5	127.1
25.0	2.044	87.3	30.5	149.6
50.0	2.592	87.3	30.5	166.3
100.0	3.137	87.3	30.5	182.9
200.0	3.679	87.3	30.5	199.4

2017-12-16	91.1	
2015-12-29	92.0	
2012-02-24	94.0	
2011-02-06	98.9	
2005-01-10	101	
2004-02-06	112	
2006-12-16	115	
2007-07-07	169	

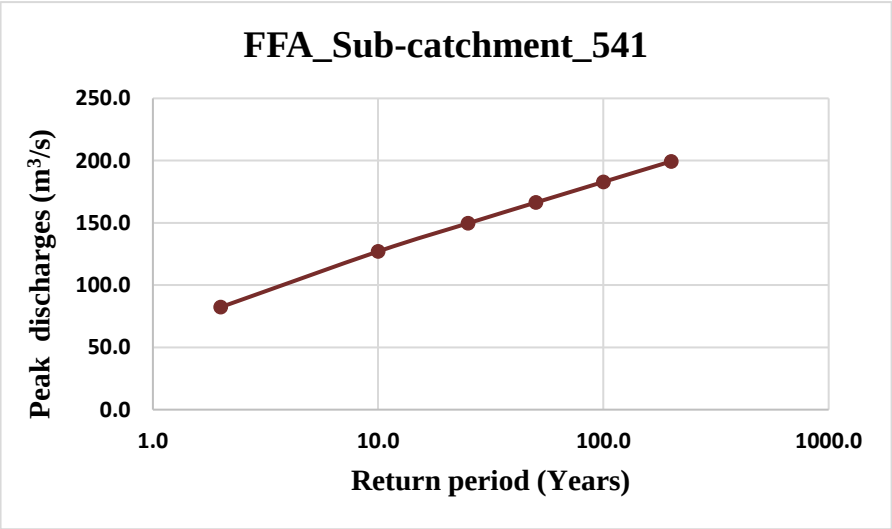

Figure 1.2: Gumbel distribution flood frequency analysis for sub-catchment 541 flows

Table 1.2: The maximum flow data obtained through the S-Hype model and FFA for sub-catchment 554

Date	Max Flow (m^3/s)	
2009-11-19	47.7	**Sub Catchment 554**
2008-10-27	69.9	

2013-01-03	72.3
2016-01-30	77.5
2010-03-22	78.0
2018-01-04	82.0
2014-12-23	105
2019-03-17	106
2015-12-28	109
2017-12-16	110
2012-02-24	114
2005-01-10	118
2011-02-06	118
2006-12-16	133
2004-02-05	140
2007-07-07	207

T (years)	K_T	Qav	S_Q	Q_T (m^3/s)
2.0	-0.164	105.5	36.9	99.4
10.0	1.305	105.5	36.9	153.7
25.0	2.044	105.5	36.9	181.0
50.0	2.592	105.5	36.9	201.2
100.0	3.137	105.5	36.9	221.3
200.0	3.679	105.5	36.9	241.4

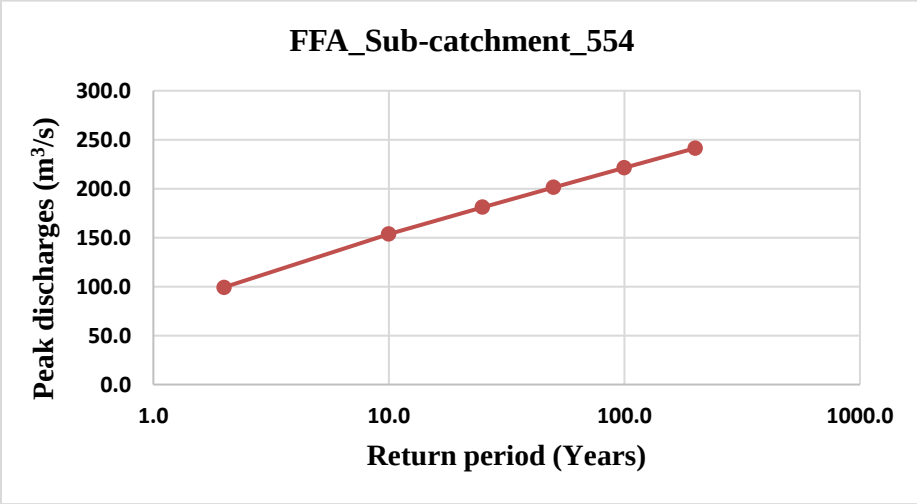

Figure 1.3: Gumbel distribution flood frequency analysis for sub-catchment 554 flows

Table 1.3: The maximum flow data obtained through the S-Hype model and FFA for sub-catchment 564

Date	Max Flow (m^3/s)	**Sub Catchment 564**				
2009-12-26	11.7					
2016-01-27	16.1					
2013-01-01	17.0					
2018-01-01	19.0	T (years)	K_T	Qav	S_Q	Q_T (m^3/s)
2005-03-18	20.4	2.0	-0.164	23.5	6.8	22.4
2006-12-14	20.5	10.0	1.305	23.5	6.8	32.4
2014-12-22	21.1	25.0	2.044	23.5	6.8	37.4
2015-12-27	21.5	50.0	2.592	23.5	6.8	41.2
2010-11-23	22.6	100.0	3.137	23.5	6.8	44.9
2019-03-17	24.3	200.0	3.679	23.5	6.8	48.6
2008-08-05	25.9					
2017-12-25	26.0					
2012-02-23	29.2					
2004-02-05	29.7					
2011-01-17	32.4					
2007-07-06	39.2					

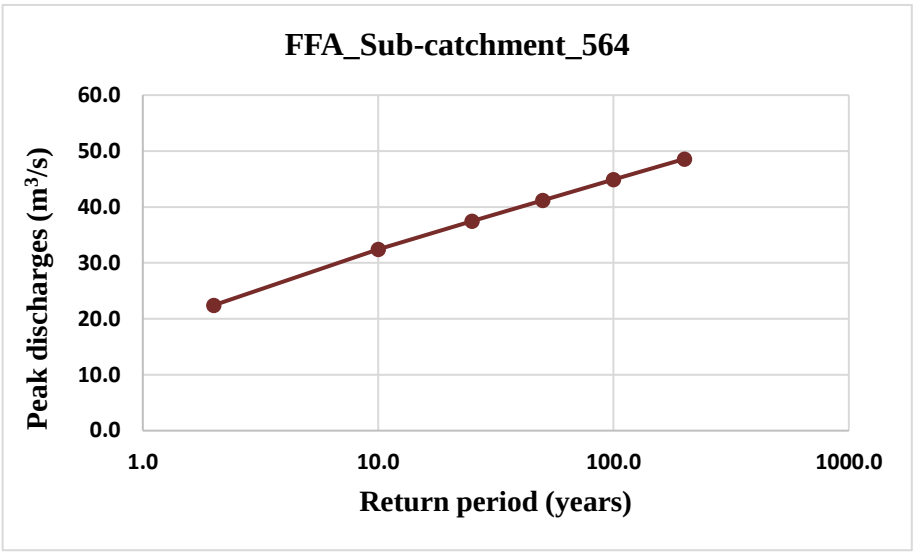

Figure 1.4: Gumbel distribution flood frequency analysis for sub-catchment 564 flows

The flood exceedance probability for the above mentioned return years in N years is calculated by following equation and the results given in table below.

$P_N = 1- (1-P_a)^N$

Where: P_N = Probability of exceedance in N years
Pa = Annual probability of exceedance (1/T)
N = Number of years
T = Flood event frequency of exceedance

Table 1.4: The flood exceedance probability for various return floods

Probability of Flood Exceedance of Various Return Floods						
Flood Frequency	Probability of Exceedance in N Years,(or Assumed Bridge Design Life)					
Years	N = 1	N = 5	N = 10	N = 25	N = 50	N = 75
2	50.00%	96.9%	99.9%	100.0%	100.0%	100.0%

10	10.00%	41.0%	65.1%	92.8%	99.5%	100.0%
25	4.00%	18.5%	33.5%	64.0%	87.0%	95.3%
50	2.00%	9.6%	18.3%	39.7%	63.6%	78.0%
100	1.00%	4.9%	9.6%	22.2%	39.5%	52.9%
200	0.50%	2.5%	4.9%	11.8%	22.2%	31.3%
500	0.20%	1.0%	2.0%	4.9%	9.5%	13.9%

Appendix 2

2.1 Geometric Analysis of the Scour Holes

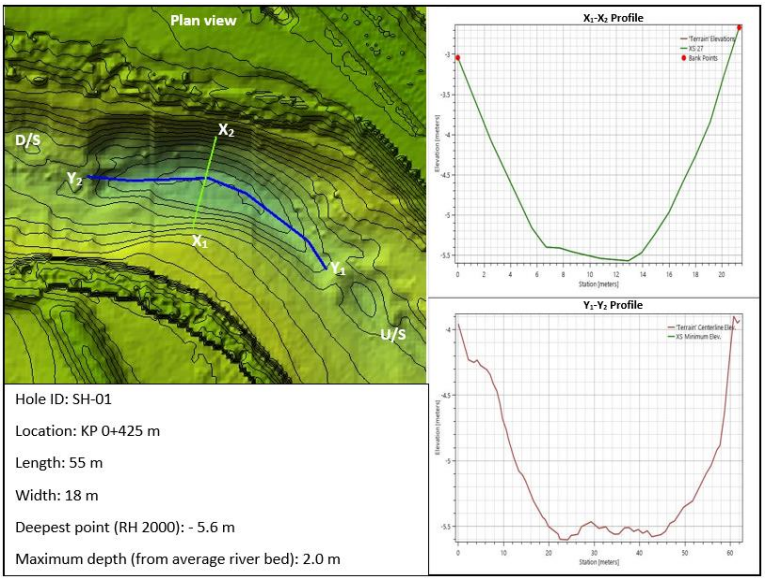

Figure 2.1: The scour hole geometry of SH-01 with sectional views

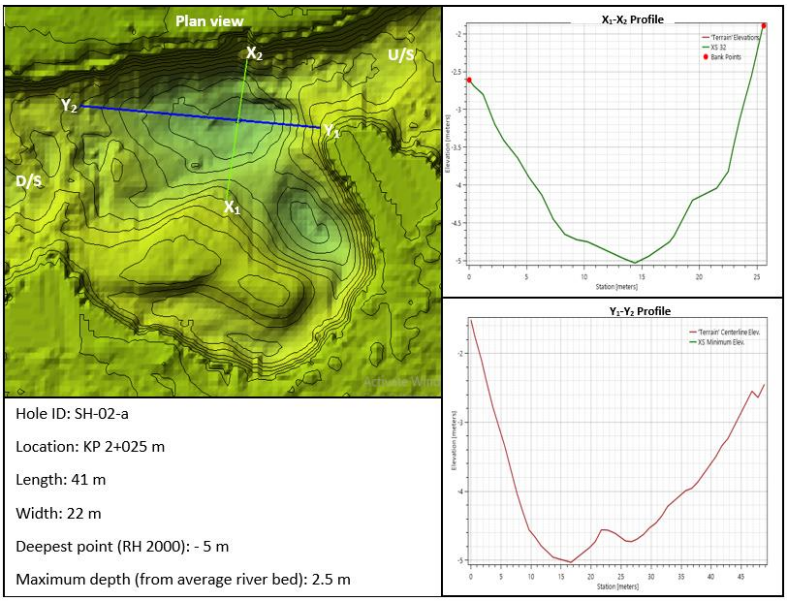

Figure 2.2: The scour hole geometry of SH-02-a with sectional views

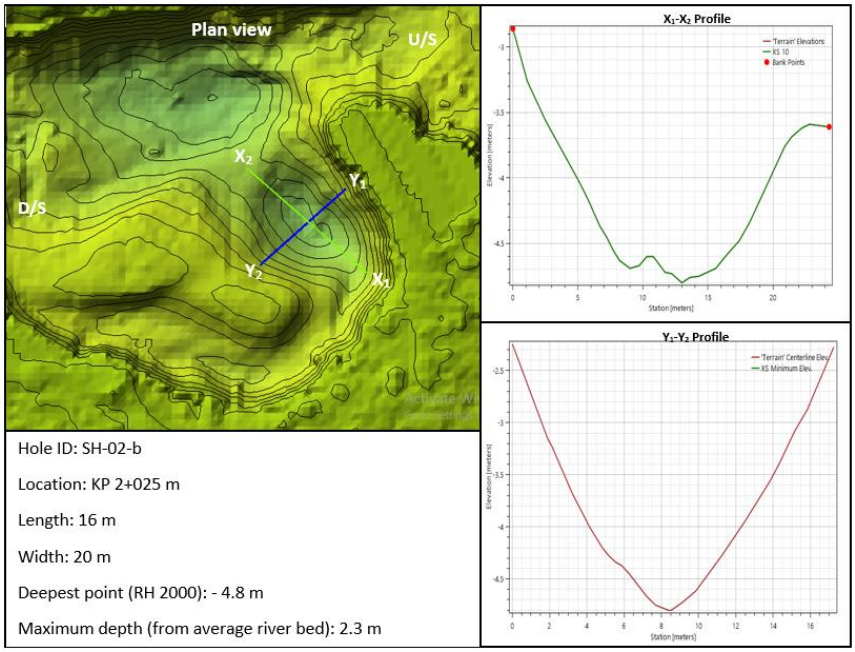

Figure 2.3: The scour hole geometry of SH-02-b with sectional views

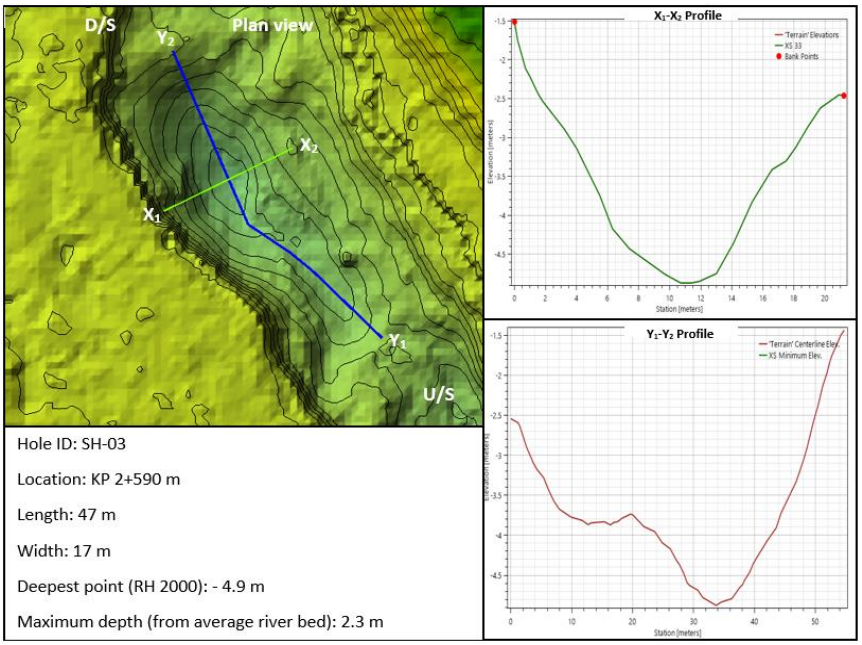

Figure 2.4: The scour hole geometry of SH-03 with sectional views

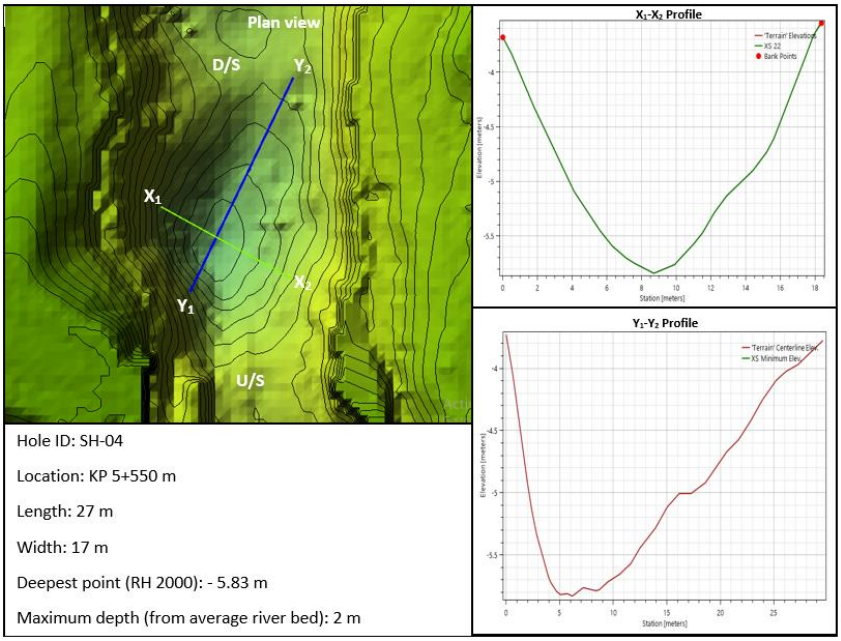

Figure 2.5: The scour hole geometry of SH-04 with sectional views

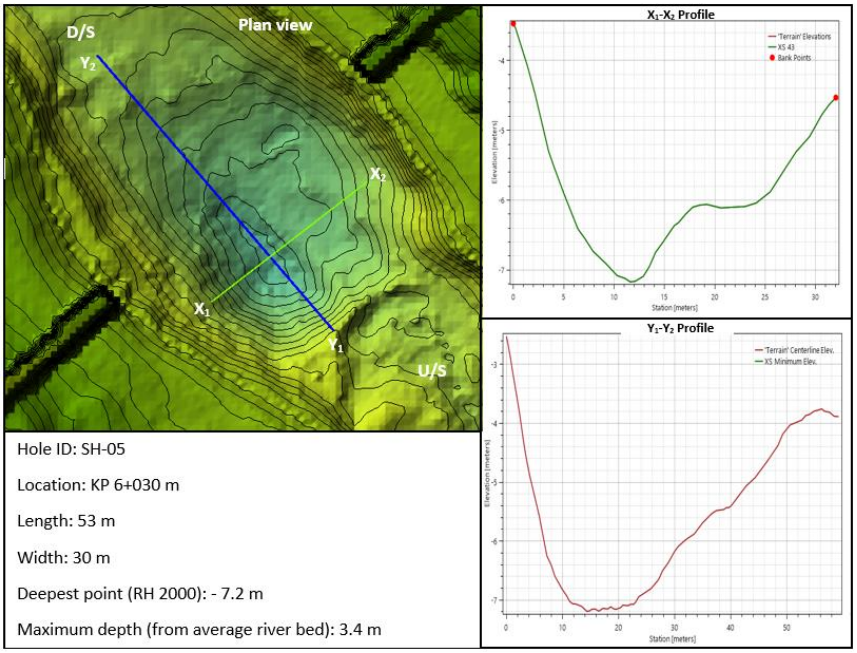

Figure 2.6: The scour hole geometry of SH-05 with sectional views

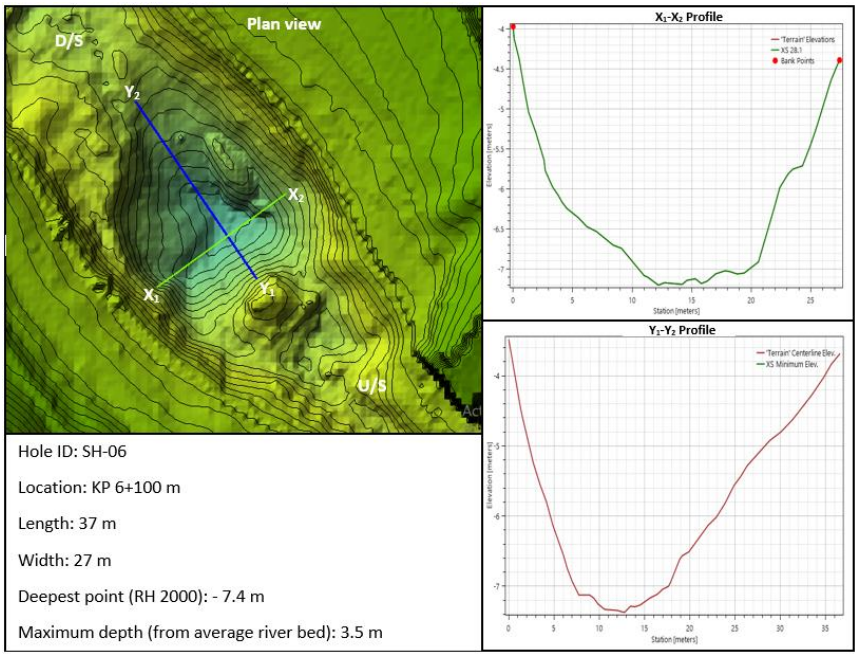

Figure 2.7: The scour hole geometry of SH-06 with sectional views

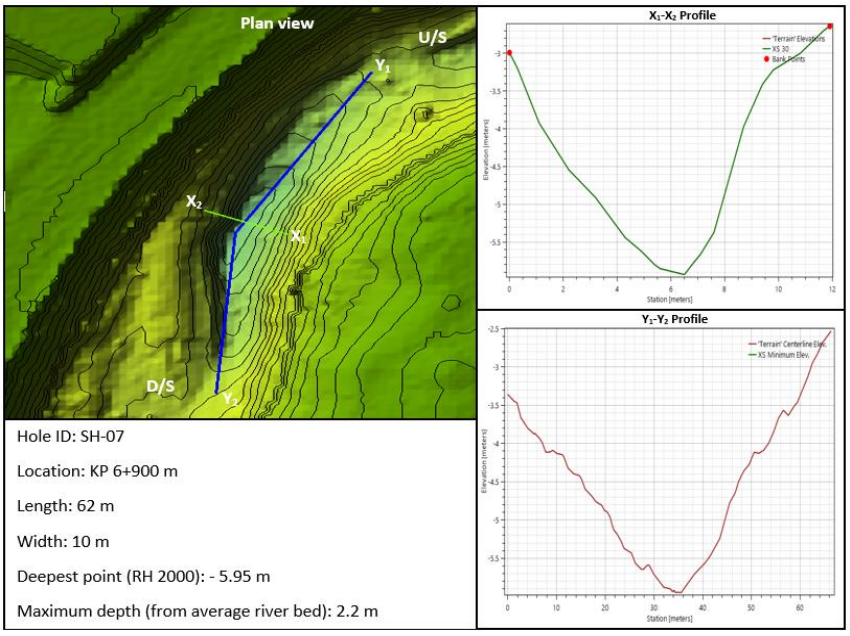

Figure 2.8: The scour hole geometry of SH-07 with sectional views

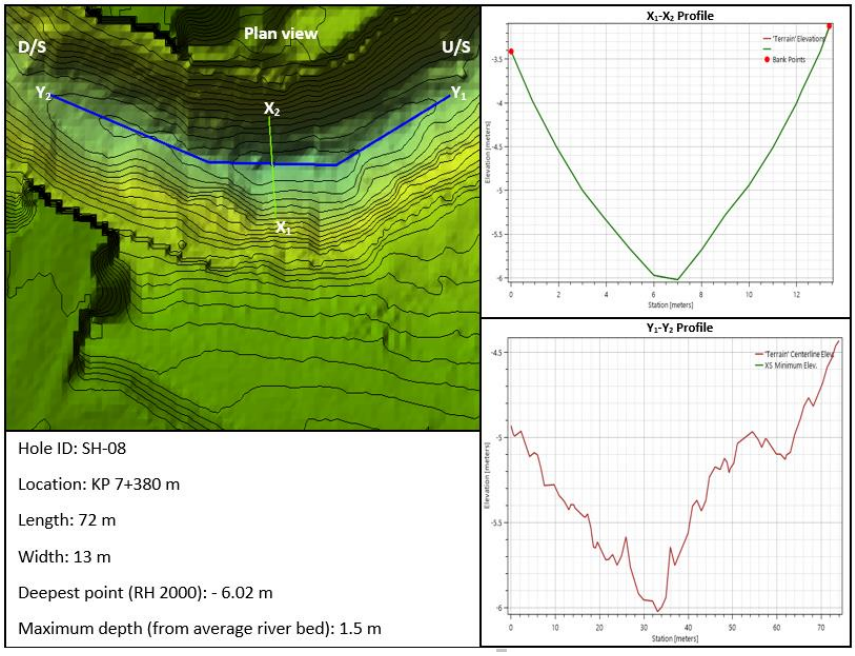

Figure 2.9: The scour hole geometry of SH-08 with sectional views

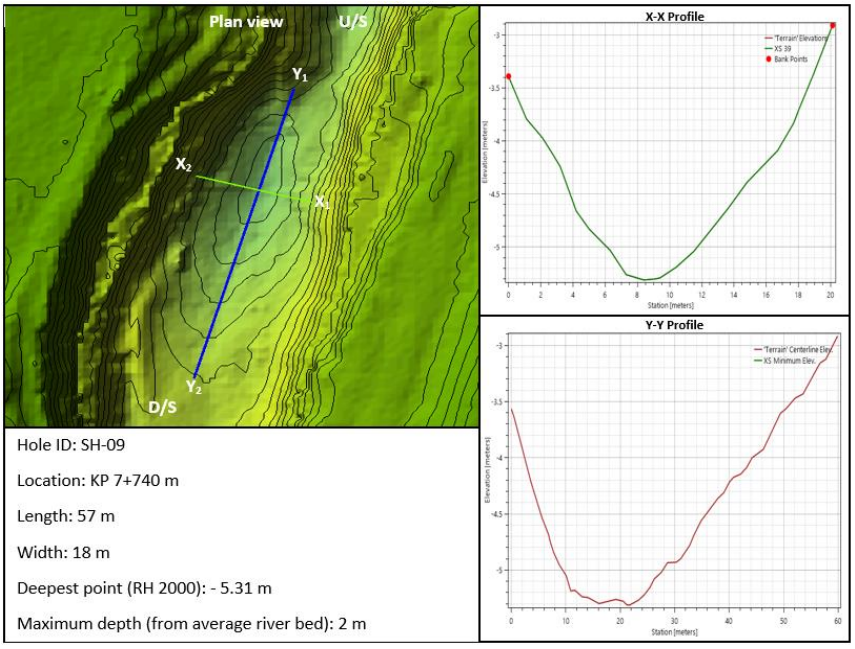

Figure 2.10: The scour hole geometry of SH-09 with sectional views

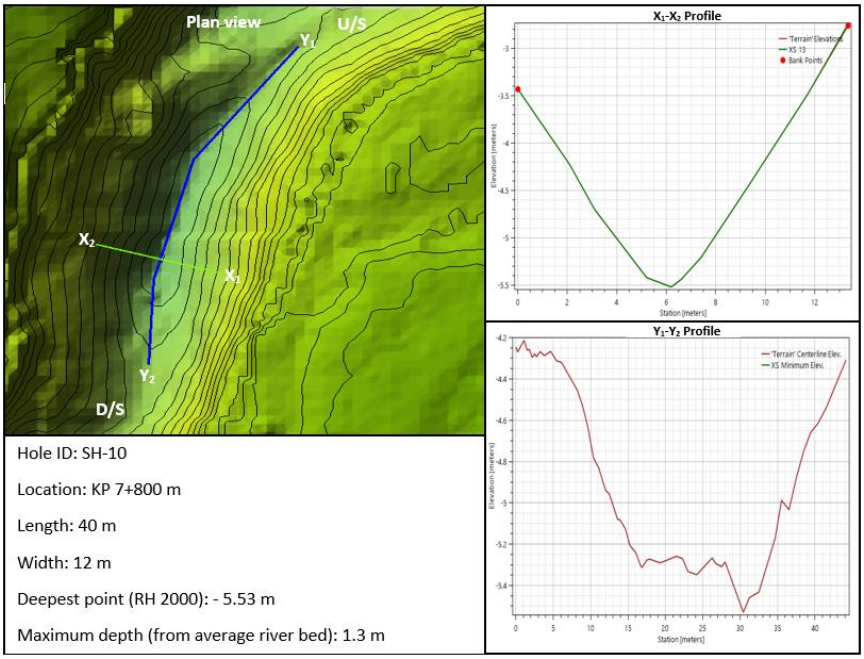

Hole ID: SH-10

Location: KP 7+800 m

Length: 40 m

Width: 12 m

Deepest point (RH 2000): - 5.53 m

Maximum depth (from average river bed): 1.3 m

Figure 2.11: The scour hole geometry of SH-10 with sectional views

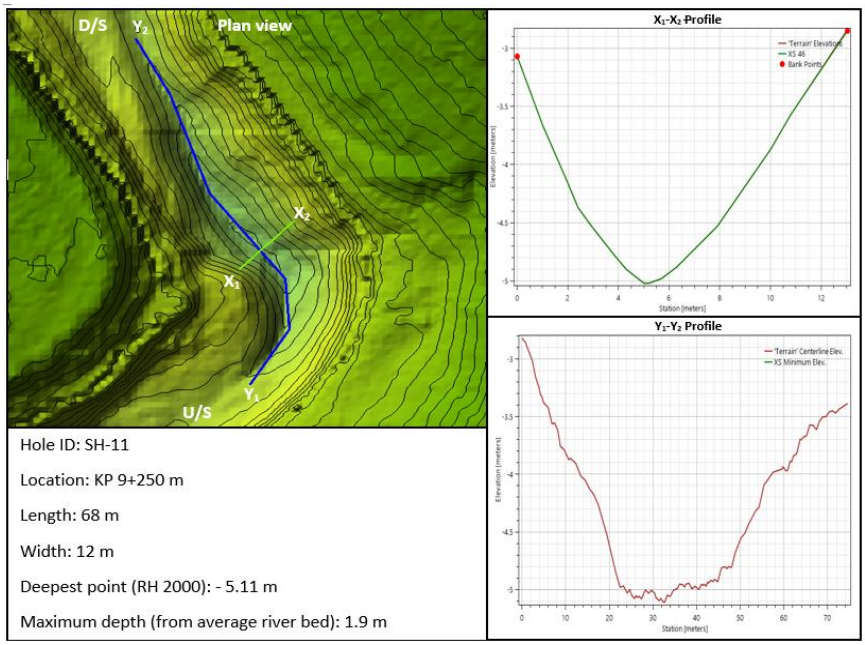

Hole ID: SH-11

Location: KP 9+250 m

Length: 68 m

Width: 12 m

Deepest point (RH 2000): - 5.11 m

Maximum depth (from average river bed): 1.9 m

Figure 2.12: The scour hole geometry of SH-11 with sectional views

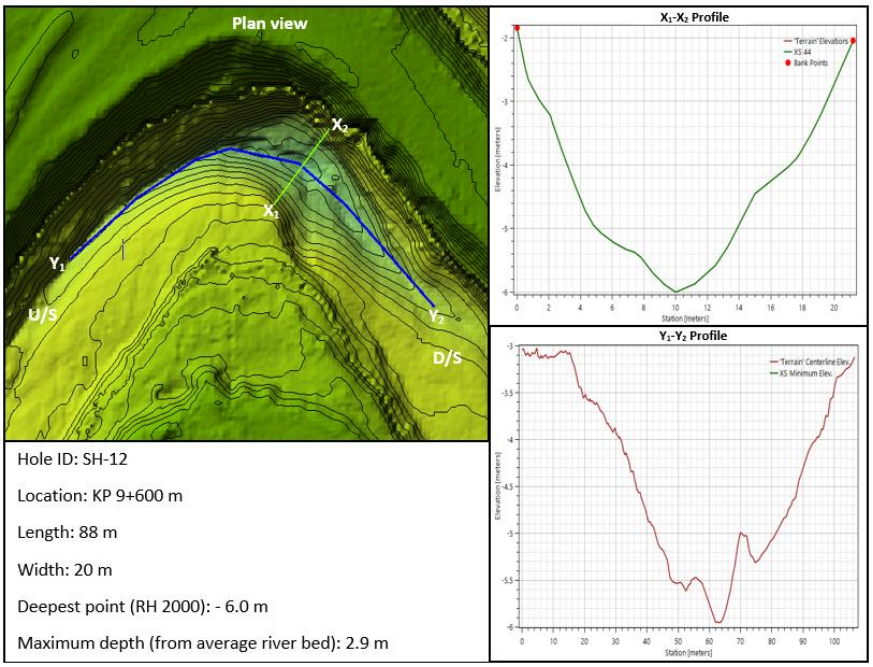

Figure 2.13: The scour hole geometry of SH-12 with sectional views

2.2 Bridge Scour Analysis by HEC RAS

Table 2.1: The Contraction scour estimation for different flows by HEC RAS

Location	Bridge	QT200	QT100	QT50	QT25	QT10	QT2	Average
KP 5,000	Nybron	0.84	0.78	0.74	0.69	0.64	0.53	0
KP 5,275	Sockerbruksbron	0.32	0.31	0.28	0.27	0.24	0.2	0
KP 5,600	Järnvägsbron	0.63	0.59	0.56	0.53	0.53	0.52	0
KP 6,825	Tegelbruksbron	0.5	0.5	0.49	0.49	0.47	0.45	0

KP 7,015	Mejeribron	0.41	0.41	0.43	0.43	0.42	0.4	0
KP 7,400	Kristian II bron	1.11	1.07	1.04	0.99	0.94	0.89	0

*All values are in m. * all values are from Live-Bed scour Equation

Table 2.2: The Abutment scour estimation for different flows by HEC RAS

Bridge	QT200		QT100		QT50		QT25		QT10		QT2	
	LB	RB	LB	RB	LB	RB	LB	RB	LB	RB	LB	RB
Nybron	1.48	1.38	1.39	1.22	1.3	1.04	1.19	0.98	1.05	0.81	0.75	0.49
Sockerbruksbron	2.13	1.41	1.94	1.31	1.8	1.2	1.65	1.1	1.44	0.94	0.91	0.05
Järnvägsbron	2.28	1.05	1.88	0.99	1.49	0.91	1.11	0.83	0.74	0.71	0.51	0.49
Tegelbruksbron	3.34	1.41	3	1.31	2.66	1.22	2.32	0.39	1.87	0	1.17	0
Mejeribron	1.21	1.35	1.12	1.22	1.04	0.57	0.3	0	0	0	0	0
Kristian II bron	1.46	1.76	1.36	1.61	1.26	1.45	1.15	1.28	1.01	1.04	0.69	0.45

*All values are in m. The highlighted zones values are calculated by HIRE equation and others are by the Froehlich equation. HEC RAS chooses equations automatically based on some hydraulic parameters (for more information, see HEC RAS model chapter)

* LB-Left Abutment; RB-Right Abutment

Figure 2.14.: Severe cracks in wing wall of the left abutment at Tegelbruksbron Bridge (MTE, 2020)

Table 2.3: An example of output file of HEC RAS Bridge scour analysis

Hydraulic Design Data				
Contraction Scour		Left	Channel	Right
Input Data				
	Average Depth (m):	1.96	7.18	1.73
	Approach Velocity (m/s):	0.31	1.07	0.3
	Br Average Depth (m):	2.69	6.28	2.71
	BR Opening Flow (m3/s):	4.83	174.54	3.54
	BR Top WD (m):	4.43	22	3.43

	Grain Size D50 (mm):	0.5	0.5	0.5
	Approach Flow (m3/s):	5.18	170.36	7.36
	Approach Top WD (m):	8.63	22.1	14.17
	K1 Coefficient:	0.64	0.64	0.64
Results				
	Scour Depth Ys (m):	0	1.07	0
	Critical Velocity (m/s):	0.55	0.68	0.54
	Equation:	Clear	Live	Clear
Abutment Scour				
		Left	Right	
Input Data				
	Station at Toe (m):	38.03	67.98	
	Toe Sta at appr (m):	44.93	74.98	
	Abutment Length (m):	8.63	14.17	
	Depth at Toe (m):	1.87	2.11	
	K1 Shape Coef:	0.82 - Vert. with wing walls		
	Degree of Skew (degrees):	90	90	
	K2 Skew Coef:	1	1	
	Projected Length L' (m):	8.63	14.17	
	Avg Depth Obstructed Ya (m):	1.96	1.73	
	Flow Obstructed Qe (m3/s):	5.18	7.36	
	Area Obstructed Ae (m2):	16.89	24.47	
Results				
	Scour Depth Ys (m):	3.32	3.34	
	Qe/Ae = Ve:	0.31	0.3	
	Froude #:	0.07	0.07	

	Equation:	Froehlich	Froehlich	
Combined Scour Depths				
	Left abutment scour + contraction scour (m):	3.32		
	Right abutment scour + contraction scour (m):	3.34		

2.3 Flood Map comparison

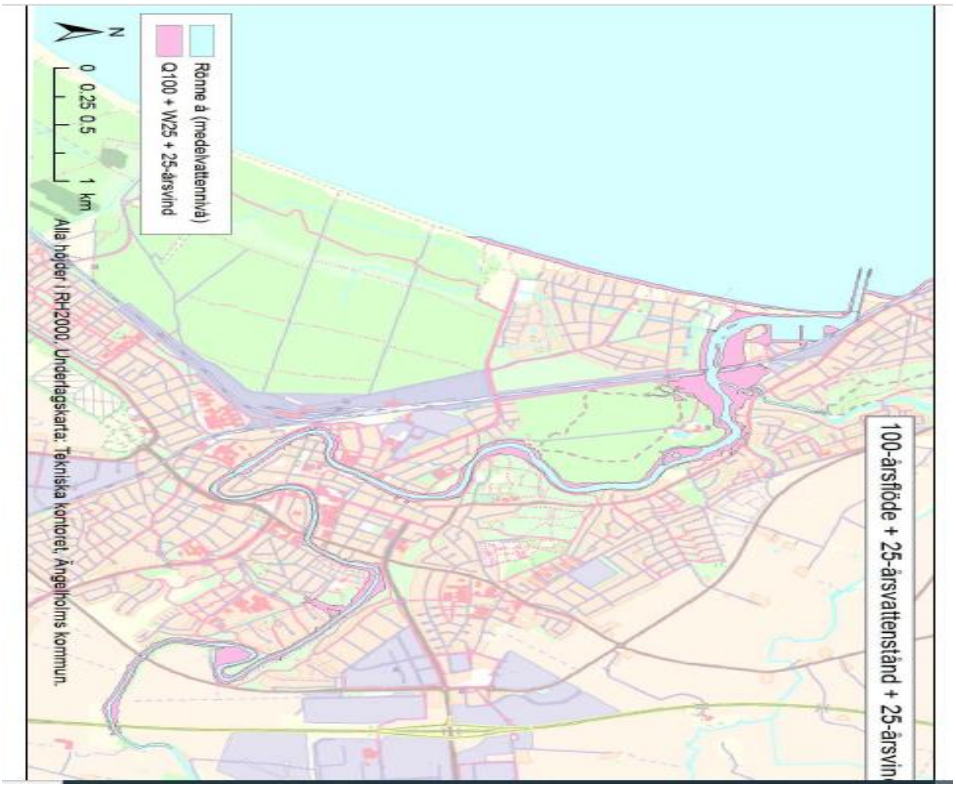

Figure 2.15: A flood map for 100-year flow by SMHI, 2016.

Figure 2.16: A flood map for 100-year flow from SMHI by the HEC RAS model